

# Resonant amplified seismic response within a hill or mountain

Armand Wirgin\*

February 4, 2020

## Abstract

We show theoretically what is meant by the term '(surface shape) resonance' in connection with the seismic response of a protuberance (emerging from flat ground) such as a hill or mountain of arbitrary shape. We address the specific problem of cylindrical protuberances of rectangular shape submitted to a SH plane wave. We find that the principal (i.e., qualitative) characteristics of the seismic response of a mountain are quite similar to those of a hill, and that the occurrence of significative amplification of the displacement field within these structures is due to the coupling of the incident wave to (surface shape) resonances.

Keywords: seismic response, surface shape resonances, field amplification,.

Abbreviated title: Seismic motion within a hill or mountain

Corresponding author: Armand Wirgin,  
e-mail: [wirgin@lma.cnrs-mrs.fr](mailto:wirgin@lma.cnrs-mrs.fr)

---

\*LMA, CNRS, UPR 7051, Aix-Marseille Univ, Centrale Marseille, F-13453 Marseille Cedex 13, France, ([wirgin@lma.cnrs-mrs.fr](mailto:wirgin@lma.cnrs-mrs.fr))

# Contents

<b>1</b>	<b>Introduction</b>	<b>4</b>
<b>2</b>	<b>Description of what is meant here by the seismic response of a protuberance</b>	<b>6</b>
<b>3</b>	<b>Boundary-value problem for the bilayer protuberance whose boundary is of arbitrary shape</b>	<b>8</b>
<b>4</b>	<b>Case of a bilayer protuberance of rectangular shape</b>	<b>9</b>
4.1	Description of the configuration . . . . .	9
4.2	Boundary-value problem . . . . .	10
4.3	Field representations via separation of variables (SOV) . . . . .	10
<b>5</b>	<b>Employment of the SOV field representations in the remaining boundary and continuity conditions</b>	<b>11</b>
<b>6</b>	<b>Some mathematical properties of the solution for <math>d_m</math></b>	<b>12</b>
6.1	General properties of $I_{lm}^\pm$ and their incidence on $J_{lm}$ and $E_{lm}$ . . . . .	13
6.2	Linear systems of equations for even and odd orders of $\mathcal{F}_m$ . . . . .	13
6.3	Normal incidence . . . . .	13
6.3.1	The odd-order diffraction coefficients . . . . .	13
6.4	Iterative approach for the obtention of the even-order diffraction coefficients . . . . .	14
6.4.1	Closed-form solution for $d_{2p}$ by the iterative scheme in a very special (VS) case	14
6.4.2	VS case: expressions of the fields and demonstration that the continuity conditions are satisfied . . . . .	15
6.5	Coping with $J_{lm}$ . . . . .	16
<b>7</b>	<b>On the origin of building, hill and mountain resonances</b>	<b>19</b>
7.1	Introductory remarks . . . . .	19
7.2	A first definition of (surface shape) resonances . . . . .	20
7.3	A second definition of (surface shape) resonances . . . . .	20
7.4	An alternate system of equations . . . . .	21
7.5	The issue of the infinite dimensions of the matrix equation for the diffraction amplitudes	21
7.6	Resonances from the point of view of the $M = 0$ approximation . . . . .	22
7.6.1	Origin of the so-called shear-wall resonance (SWR) . . . . .	22
7.6.2	Coupling to a HSWR resonance . . . . .	24
7.6.3	Coupling to resonances when the $k^{[0]}w \rightarrow 0$ asymptoticity is not assumed . .	25
7.7	Resonances from the point of view of the $M = 1$ approximation . . . . .	26
7.8	Resonances from the point of view of the $M > 1$ approximations . . . . .	27
<b>8</b>	<b>Numerical resolution of the linear system of equations</b>	<b>27</b>
<b>9</b>	<b>Seismic response from stress-free boundary irregularities in the sense of Sills and beyond</b>	<b>28</b>
9.1	Comparison with the numerical results of Sills . . . . .	28
9.1.1	Our computed transfer functions and $1/D$ for $\theta^i = 0^\circ$ . . . . .	31

9.1.2	Our computed transfer functions and $1/D$ for $\theta^i = 30^\circ$ . . . . .	34
9.1.3	Our computed transfer functions and $1/D$ for $\theta^i = 60^\circ$ . . . . .	37
9.1.4	Discussion . . . . .	38
9.2	Beyond Sills: seismic response within the rectangular version of Sills' hill at the first five resonant frequencies . . . . .	38
9.2.1	Displacement field graphs for $\theta^i = 0^\circ$ . . . . .	38
9.2.2	Displacement field graphs for $\theta^i = 30^\circ$ . . . . .	42
9.2.3	Displacement field graphs for $\theta^i = 60^\circ$ . . . . .	45
9.2.4	Displacement field graphs for $\theta^i = 80^\circ$ . . . . .	48
<b>10</b>	<b>Simulation of the seismic response of the Civita di Bagnoregio hill</b>	<b>49</b>
10.1	First model results . . . . .	50
10.2	Second model results . . . . .	53
10.3	Alternative (third) model results . . . . .	56
<b>11</b>	<b>On the possibility of very-strong seismic response in a hill</b>	<b>60</b>
11.1	Without attenuation . . . . .	60
11.1.1	Search for the first four resonant frequencies . . . . .	61
11.1.2	Resonant coupling at $f = 2.44 \text{ Hz}$ . . . . .	64
11.1.3	Resonant coupling at $f = 3.3374 \text{ Hz}$ . . . . .	66
11.2	With attenuation . . . . .	68
11.2.1	Search for the third and fourth resonant frequencies . . . . .	68
11.2.2	Coupling at the third resonance frequency . . . . .	70
11.2.3	Coupling at the fourth resonant frequency . . . . .	72
<b>12</b>	<b>Seismic response in a small, hard-rock mountain</b>	<b>74</b>
12.1	Search for the resonances . . . . .	74
12.2	Response within the mountain at the resonant frequencies and two angles of incidence	77
12.2.1	Response at the first resonant frequency . . . . .	77
12.2.2	Response at the second resonant frequency . . . . .	78
12.2.3	Response at the third resonant frequency . . . . .	79
12.3	Response within the mountain at an off-resonant frequency . . . . .	80
<b>13</b>	<b>Conclusion</b>	<b>81</b>

# 1 Introduction

This investigation is concerned with a problem of determining the response of an object to an incident wave [263, 166], the object being such that its interior is accessible to the incident wave.

The wavefield in the interior of the object, as well in its (external) vicinity can be qualified as its 'near-field response' [76, 134, 145, 203, 204, 206, 242, 261, 294]. The wavefield in the exterior of the object, and rather far from the latter can be qualified as its 'far-field response' [134, 200, 219, 224, 250, 253, 272, 280]. The term 'scattering' is usually associated with the far-field response, but since the distinction between the near and far fields is not always clear, 'scattering' [306, 263, 325, 349] is often employed to qualify the global response of the object to a dynamical solicitation. Nevertheless, there is an intimate connection between the the near- and far-field response, as well as between the interior and exterior response, as is illustrated in two recent publications [359, 358].

Herein, we shall be particularly interested in the internal response of an isolated feature (loosely-termed 'structure' [67, 92, 117, 154, 157, 158, 214, 284, 288, 291]) located near or on the earth's nominally-flat boundary to an elastic wave (more precisely, seismic wave) whose sources are within the earth. The social and economic implications of this problem are considerable since they have to do with the disasters [141] provoked by earthquakes: destruction of the natural [103] and built environment [20, 29, 34, 40, 61, 84, 92, 120, 130, 243, 244, 245, 251, 254, 289] often resulting in considerable harm to the population.

The feature of the earth's boundary that first comes to mind is the above-ground structure (AGS), often termed topography [56, 21, 19, 14, 4, 16, 20, 24, 25, 27, 32, 34, 42, 43, 47, 48, 57, 64, 65, 73, 75, 79, 111, 118, 119, 135, 171, 181, 183, 195, 216, 265, 279, 282, 283, 305, 322, 325, 344, 371, 383, 227, 228, 229, 327, 285, 270, 215, 85, 106, 225, 26, 22, 12, 233, 33, 181, 233, 235, 247, 259, 264, 271, 292, 304, 309, 327, 343, 148, 374], convex surface irregularity [25, 212, 209, 255, 306, 334, 383, 5, 13, 346, 85, 291, 334, 163] or slope [256, 304, 322, 19, 48, 58, 165, 12, 166, 167, 217, 237, 273], roughness [147, 150, 220, 221, 250, 280, 338, 351, 38, 2, 231, 272, 324, 348, 186, 201, 202, 224, 258], cliff [23, 217, 255], ridge [36, 183, 260, 380], protuberance [358], or bump [232].

The AGS's affected by seismic waves can be divided into two classes: i) a 'natural' AGS such as a hill [14, 25, 46, 55, 71, 73, 118, 131, 159, 181, 191, 193, 194, 197, 205, 241, 251, 256, 264, 268, 255, 278, 307, 376, 378, 85, 87, 153, 46, 212, 269, 106, 375, 326, 376, 325, 333, 264], volcano [296, 282, 307, 219, 60, 219, 296], mountain [177, 178, 351, 352, 353, 363, 364, 58, 58, 119, 216, 79, 308, 273, 141, 194, 189, 227] and ii) a 'manmade' AGS such as a building (composed or not of a limited number of smaller units) [120, 50, 206, 209, 356, 361, 362, 373, 382, 330, 317, 267, 318, 156, 157, 236, 130, 233, 109, 8, 9, 41, 62, 66, 82, 83, 146, 151, 152, 156, 179, 190, 243, 244, 287, 320, 342], industrial facility such as a nuclear power plant [95, 249, 377, 368, 389, 143, 110, 248, 126], dike [138, 329, 86, 86, 375], dam [43, 174, 175, 124, 125], town or city [120, 254, 109, 49, 50, 61, 63, 72, 74, 82, 88, 98, 109, 113, 123, 126, 127, 128, 129, 151, 152, 160, 169, 182, 185, 206, 208, 233, 252, 286, 290, 297, 298, 300, 301, 302, 312, 313, 314, 315, 330, 336, 356, 360, 361, 362, 373], or layer of some sort (such as landfill [226, 379, 202, 323, 334]).

Other structures affected by seismic waves are the below-ground structures (BGS's) which can also be divided into two classes: 1) 'natural' such as a cavity, canyon [131, 341, 326, 69, 132], unfilled valley [31, 45, 183, 89, 153, 100, 183], basin or sediment-filled valley [53, 354, 44, 184, 266, 279, 290, 301, 303, 319, 379, 226, 300, 144, 30, 31, 161, 163, 3, 11, 384, 385, 386, 388, 341, 335, 101, 281, 52, 359, 291, 100, 104, 68, 109, 100, 162, 169, 170, 234, 302, 308, 336, 372], or other underground layer of some sort [15, 369, 28, 35, 39, 91, 155, 164, 168, 173, 192, 196, 213, 218, 303, 310, 311, 323, 339,

341, 374, 387], and 2) 'manmade' such as a pipeline [78], tunnel [176, 132], or mine [115].

From the practical point of view all these structures have in common that their seismic response is marked by augmented duration of the shaking [321, 360, 361, 362, 120, 123, 126] as well as amplification of the wavefield [16, 120, 79, 119, 364, 385] in their interiors and in their neighborhood relative to this response on flat ground overlying a homogeneous underground. This is known, or thought, to be the principal causal agent of: damage or destruction of buildings in cities (often located on flat ground underlain by a soft soil layer) [84, 102, 161, 279, 315], landslides on hills and mountains [165, 257, 390, 304, 237, 136, 137, 103, 99, 273], damage or destruction of dikes [138, 329, 86] and dams [174, 175, 304] resulting in massive flooding, damage of towns built near or on hill and mountain summits, the liberation of poisonous gases in landfills [226, 379] and even the triggering of volcanic eruptions [296, 219].

From the theoretical point of view, there are obvious connections between the seismic response of 'natural' AGS's and that of both 'natural' and 'manmade' BGS's, but since this general subject is vast, we shall be more-specifically interested in the seismic response of an isolated 'natural' AGS, which we assume to be entirely located above, and attached to, the (flat) ground. Nevertheless, we offer some bibliographic references and evoke the issue of resonances in connection with the seismic response of 'manmade' AGS's and 'natural' as well as 'manmade' BGS's.

It so happens that similar problems are of great interest in other fields of physics such as electrodynamics (e.g. optics and microwaves) [37, 211, 240, 210, 220, 77, 223, 365, 108, 316, 295, 6, 366, 367, 203, 345, 294, 112, 134, 204, 76, 81, 198, 199, 238, 114, 180, 276, 59, 90, 230, 250, 253, 261, 262, 272, 280, 294, 324, 338, 346, 347, 348, 349, 355], acoustics [338, 331, 236, 337, 121, 122, 357, 147, 221, 224, 231], hydrodynamics [391] and atomic physics [140, 96, 107, 149, 250, 276, 277], even though what was traditionally-important in these contexts was the far-field response of the scattering structures usually termed periodically-rough surfaces, corrugations and gratings [93, 94, 186, 202, 258, 18, 199, 210, 262, 276, 277, 347], or irregular surfaces [147, 150, 221, 250, 280, 338, 38, 2, 220, 231, 272, 324, 348, 150, 346, 350, 355]), rather than their near-field response.

In recent years, research in these fields has largely switched to the near-field, stimulated by the discovery of such spectacular effects as SERS (Surface-Enhanced Raman Scattering)[211, 240, 315, 345, 365], enhanced frequency-selective (total) absorption (as applied notably to energy harvesting [172, 198] or noise reduction [121, 122, 357, 198]), and negative refraction [180, 207] in media (recently dubbed metamaterials [368, 381]) bounded by, or including, periodic structures [90, 211, 210, 220, 77, 222, 365, 108, 316, 295, 6, 366, 367, 203, 345, 294, 112, 134, 204, 76, 81, 198, 199, 54, 80, 97, 134, 207, 261].

The core of the present contribution is the notion of 'resonance' and its connection with wavefield amplification [274, 116, 339, 155, 351, 352, 353, 133, 213, 222, 221, 223, 102, 331, 332, 246, 51, 385, 188, 369, 31, 89, 142, 201, 208, 209, 210, 211, 236, 337, 354, 366, 367, 391, 80, 81, 91, 120, 124, 125, 126, 158, 159, 171, 177, 182, 185, 187, 198, 199, 201, 209, 230, 238, 242, 255, 274, 275, 294, 295, 299, 310, 311, 342, 351, 364, 365]. This notion has often been invoked, but, in our opinion not well-understood, in connection with scattering of a seismic wave by one or several protuberances. The reason for this may be linked to the fact that the majority of previous studies on the seismic response of structures on or below the earth's surface were purely-numerical (e.g., [105, 340, 7, 8, 10, 11, 48, 62, 83, 117, 128, 170, 283, 300, 335, 344, 379, 138, 44, 374, 306, 45, 85, 87, 131, 334, 153, 179, 195, 215, 209, 234, 327, 235, 252, 255, 256, 259, 278, 281, 282, 283, 292, 293, 299, 300, 301, 302, 303, 312, 313, 314, 320, 327, 334, 336, 344, 349, 371, 372, 375, 376, 378, 380]).

In optics, the topic has been dubbed 'surface shape resonances' [91, 262, 220, 77, 221, 222,

223, 351, 353, 354, 211, 210, 210, 240], and appears to be well-understood at present, notably from the theoretical viewpoint, so that it is opportune to make use of this knowledge in the present investigation.

## 2 Description of what is meant here by the seismic response of a protuberance

The general problem is identical to the one studied in our recent contribution [358]. In the first approximation, the earth's surface is considered to be (horizontally-) flat (termed "ground" for short) and to separate the vacuum (above) from a linear, isotropic, homogeneous (LIH) solid (below), so as to be stress-free. In the second approximation the flat ground is locally deformed so as to penetrate into what was formerly the vacuum half space. We now define the protuberance as the region between the locally-deformed stress-free surface and what was formerly a portion of the flat ground. This protuberance is underlain by the same LIH solid as previously, but the solid material within the protuberance is now assumed to be only linear and isotropic (i.e., not homogeneous). In fact, we consider the specific case in which the material within the protuberance is in the form of a horizontal bilayer so as to be able to account for various empirically-observed effects that are thought to be due to inhomogeneity of the protuberance material. Furthermore, we assume that: the protuberance is of infinite extent along one ( $z$ ) of the cartesian ( $xyz$ ) coordinates, and its stress-free boundary to be of arbitrary shape (in its  $xy$  cross-section plane). The underlying problem of much of what follows is the prediction of the seismic wave response of this earth model.

The earthquake sources are assumed to be located in the lower half-space and to be infinitely-distant from the ground so that the seismic (pulse-like) solicitation takes the form of a body (plane) wave in the neighborhood of the protuberance. This plane wavefield is assumed to be of the shear-horizontal ( $SH$ ) variety, which means that: only one (i.e., the cartesian coordinate  $z$ ) component of the incident displacement field is non-nil and this field does not depend on  $z$ .

We assume, not only that the protuberance boundary does not depend on  $z$  but also, that the (often relatively-soft) medium filling the protuberance as well as the (usually relatively-hard) medium below the protuberance are both linear and isotropic. Furthermore the medium of the below-ground half space is assumed to be homogeneous, whereas that of the protuberance to be piecewise homogeneous (however, this heterogeneity is such as to not depend on  $z$ ). It ensues that the scattered and total displacement fields within and outside the protuberance do not depend on  $z$ . Thus, the problem we are faced with is 2D ( $z$  being the ignorable coordinate), and it is sufficient to search for the  $z$ -component of the scattered displacement field, designated by  $u_z^s(\mathbf{x}; \omega)$  in the sagittal (i.e.,  $x - y$ ) plane, when  $u_z^i(\mathbf{x}; \omega)$  designates the incident displacement field, with  $\mathbf{x} = (x, y)$  and  $\omega = 2\pi f$  the angular frequency,  $f$  the frequency. Since we now know that only the  $z$  component of the field is non-nil, we drop the index  $z$  in the incident, scattered, and total displacement fields. The temporal version of the displacement field is  $u_z(\mathbf{x}; t) = 2\Re \int_0^\infty u_z^i(\mathbf{x}; \omega) \exp(-i\omega t) d\omega$  wherein  $t$  is the temporal variable. Since we now know that only the  $z$  component of the field is non-nil, we drop the index  $z$  in the incident, scattered, and total displacement fields in all that follows.

Fig. 1 describes the scattering configuration in the sagittal ( $xy$ ) plane. In this figure,  $\mathbf{k}^i = \mathbf{k}^i(\theta^i, \omega)$  is the incident wavevector oriented so that its  $z$  component is nil, and  $\theta^i$  is the angle of incidence.

The portion of the ground outside the protuberance is stress-free but since the protuberance





### 3 Boundary-value problem for the bilayer protuberance whose boundary is of arbitrary shape

The protuberance occupies (in the sagittal plane (SP)) the finite-sized region  $\Omega_1 \cup \Omega_2$  (see fig. 1). The below-ground half-space occupies the region  $\Omega_0$ .  $\Omega_0$  is entirely filled with  $M^{[0]}$  whereas  $\Omega_1$  is filled with  $M^{[1]}$  and  $\Omega_2$  with  $M^{[2]}$ .

Always in the sagittal plane, the flat ground is described by  $\Gamma_G$ , with  $x, y$  the cartesian coordinates in the SP) and is composed of three segments;  $\Gamma_l$ ,  $\Gamma_m$ , and  $\Gamma_r$ , which designate the left-hand, middle, and right-hand portions respectively of  $\Gamma_G$ . The protuberance is an above-ground structure whose upper and lower boundaries (in the SP) are  $\Gamma_p$  and  $\Gamma_m$ , the latter being a plane segment of width  $w$ .

The analysis takes place in the space-frequency framework, so that all constitutive and field variables depend on the frequency  $f$ . This dependence will henceforth be implicit (e.g.,  $u(\mathbf{x}; f)$ , with  $\mathbf{x} = (x, y)$ , will be denoted by  $u(\mathbf{x})$ ).

The seismic solicitation is a shear-horizontal (SH) plane wave field of the form

$$u^i(\mathbf{x}) = a^i \exp(i\mathbf{k}^i \cdot \mathbf{x}) = a^i \exp[i(k_x^i x + k_y^i y)] , \quad (1)$$

wherein  $a^i = a^i(\omega)$  is the spectral amplitude of the seismic pulse,  $\mathbf{k}^i = (k_x^i, k_y^i)$ ,  $k_x^i = k^{[0]} \sin \theta^i$ ,  $k_y^i = k^{[0]} \cos \theta^i$ ,  $k^{[l]} = \omega / \beta^{[l]}$  ;  $l = 0, 1, 2$ .

Owing to the fact that the configuration comprises three distinct regions, each in which the elastic parameters are constants as a function of the space variables, it is opportune to employ domain decomposition and (later on separation of variables). Thus, we decompose the total field  $u$  as:

$$u(\mathbf{x}) = u^{[l]}(\mathbf{x}) ; \forall \mathbf{x} \in \Omega_l, \quad l = 0, 1, 2 , \quad (2)$$

with the understanding that these fields satisfy the 2D SH frequency domain elastic wave equation (i.e., Helmholtz equation)

$$\left( \Delta + (k^{[l]})^2 \right) u^{[l]}(\mathbf{x}) = 0 ; \forall \mathbf{x} \in \Omega_l, \quad l = 0, 1, 2 , \quad (3)$$

with the notations  $\Delta = \frac{\partial^2}{\partial x^2} + \frac{\partial^2}{\partial y^2}$  in the cartesian coordinate system of the sagittal plane.

In addition, the field  $u^{[0]}$  satisfies the radiation condition

$$u^{[0]}(\mathbf{x}) - u^i(\mathbf{x}) \sim \text{outgoing wave} ; \|\mathbf{x}\| \rightarrow \infty . \quad (4)$$

due to the fact that  $\Omega_0$  is unbounded (i.e., a semi-infinite domain).

The stress-free nature of the boundaries  $\Gamma_l$ ,  $\Gamma_p$ ,  $\Gamma_r$ , entail the boundary conditions:

$$\mu^{[0]} u_{,y}^{[0]}(\mathbf{x}) = 0 ; \forall \mathbf{x} \in \Gamma_l + \Gamma_r , \quad (5)$$

$$\mu^{[2]} u_{,y}^{[2]}(\mathbf{x}) = 0 ; \forall \mathbf{x} \in \Gamma_p , \quad (6)$$

wherein  $u_{,\zeta}$  denotes the first partial derivative of  $u$  with respect to  $\zeta$ .

The fact, that the horizontal segment  $\Gamma_{12}$  between the two media filling the protuberance is assumed to be an interface across which two media are in welded contact, entails the continuity conditions:

$$u^{[2]}(\mathbf{x}) - u^{[1]}(\mathbf{x}) = 0 ; \forall \mathbf{x} \in \Gamma_{12} , \quad (7)$$



$$\mu^{[2]}u_{,y}^{[2]}(\mathbf{x}) - \mu^{[1]}u_{,y}^{[1]}(\mathbf{x}) = 0 ; \forall \mathbf{x} \in \Gamma_{12} . \quad (8)$$

Finally, the fact, that  $\Gamma_m$  was assumed to be an interface across which two media are in welded contact, entails the continuity conditions:

$$u^{[0]}(\mathbf{x}) - u^{[1]}(\mathbf{x}) = 0 ; \forall \mathbf{x} \in \Gamma_m , \quad (9)$$

$$\mu^{[0]}u_{,y}^{[0]}(\mathbf{x}) - \mu^{[1]}u_{,y}^{[1]}(\mathbf{x}) = 0 ; \forall \mathbf{x} \in \Gamma_m , \quad (10)$$

The purpose of addressing such a boundary-value (direct) problem is to determine  $u^{[l]}(\mathbf{x})$ ;  $l = 0, 1, 2$  for various solicitations and parameters relative to the various geometries of, and media filling,  $\Omega_l$  ;  $l = 0, 1, 2$ . Rather than carry out this too-ambitious program, we shall treat only one specific configuration: a protuberance of rectangular shape.

Before doing this, it is opportune to recall some consequences, brought to fore in [358], of the above-evoked boundary-value problem for bilayer protuberances of general shape. In this publication, we show that the wavefield is constrained by the following conservation law:

$$-\frac{\mu^{[1]}}{\mu^{[0]}} \Im \int_{\Gamma_m} u^{[1]*}(\mathbf{x}) \boldsymbol{\nu}_1 \cdot \nabla u^{[1]}(\mathbf{x}) + \Im \int_{\Gamma_\infty} u^{[0]*}(\mathbf{x}) \boldsymbol{\nu}_0 \cdot \nabla u^{[0]}(\mathbf{x}) d\Gamma = 0 , \quad (11)$$

or

$$\Im \int_{\Gamma_\infty} u^{[0]*}(\mathbf{x}) \boldsymbol{\nu}_0 \cdot \nabla u^{[0]}(\mathbf{x}) d\Gamma + \frac{\mu^{[2]}}{\mu^{[0]}} \Im [(k^{[2]})^2] \int_{\Omega_2} \|u^{[2]}(\mathbf{x})\|^2 d\Omega + \frac{\mu^{[1]}}{\mu^{[0]}} \Im [(k^{[1]})^2] \int_{\Omega_1} \|u^{[1]}(\mathbf{x})\|^2 d\Omega = 0 . \quad (12)$$

The term 'constrained' means that the solution (for the wavefield) of the equations in the boundary-value problem must be such as to satisfy either (11) or (12), this being a necessary but not sufficient condition for this solution to be qualified as 'correct'. Thus, either of these two equations furnish a useful, although not foolproof, means of testing a method for solving a scattering problem such as the one we are about to evoke.

## 4 Case of a bilayer protuberance of rectangular shape

### 4.1 Description of the configuration

From now on, the option is to completely solve the forward scattering problem for the configuration depicted in fig.2. The important feature thereof is the rectangular shape (in the sagittal plane) of the protuberance. Note that we could just as well have chosen a feature of triangular shape as is done in e.g., [178] and thus obtain essentially the same results (notably as concerns the resonant nature of the response) as in the present study.

The choice of protuberances with such simple shapes is dictated by the fact that key aspects of their seismic response can be unveiled in a relatively-simple manner, both from the theoretical and numerical angles, the latter (numerical) feature being very useful in a parametric study such as the one undertaken in the last part (i.e., starting with sect. 9) of the present investigation.

As previously, the width of the protuberance is  $w$ , and its other characteristic dimensions are the bottom ( $h_1$ ) and top ( $h_2$ ) layer thicknesses, with  $h = h_1 + h_2$  being the height of the protuberance. What was formerly  $\Gamma_p$  is now  $\Gamma_g \cup \Gamma_s \cup \Gamma_d$ , wherein  $\Gamma_g$  is the leftmost vertical segment of height  $h$ ,  $\Gamma_s$  is the top segment of width  $w$  (located between  $x = -w/2$  and  $x = w/2$ ) and  $\Gamma_d$  is the rightmost vertical segment of height  $h$ . Everything else is as in fig.1.

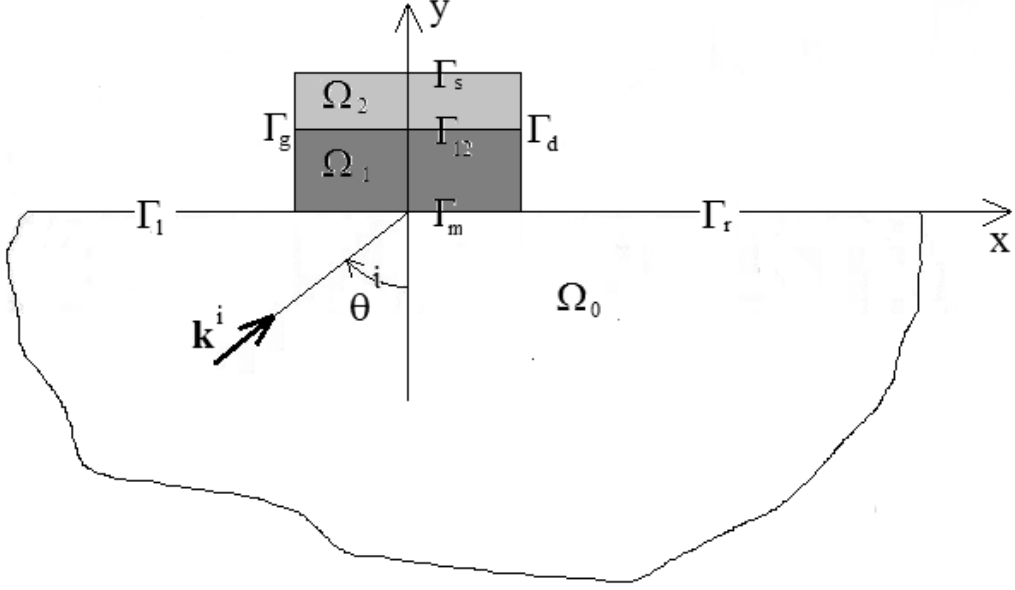


Figure 2: Sagittal plane view of the 2D rectangular protuberance scattering configuration. Note that now the boundary  $\Gamma_p$  of the above-ground feature is composed of three connected portions,  $\Gamma_g$ ,  $\Gamma_s$  and  $\Gamma_d$ .

## 4.2 Boundary-value problem

Owing to the fact that the configuration comprises three distinct regions, each in which the elastic parameters are constants as a function of the space variables, it is opportune to employ domain decomposition and separation of variables (DD-SOV). Thus, as previously, we decompose the total field  $u$  as:

$$u(\mathbf{x}) = u^{[l]}(\mathbf{x}) ; \forall \mathbf{x} \in \Omega_l, l = 0, 1, 2 , \quad (13)$$

with the understanding that these fields satisfy the 2D SH frequency domain elastic wave equation (i.e., Helmholtz equation),  $u^{[0]}$  the radiation condition  $u^{[0]}$ , the stress-free boundary conditions on  $\Gamma_g$ ,  $\Gamma_d$ , and  $\Gamma_p$ , as well as the continuity conditions across  $\Gamma_m$  and  $\Gamma_{12}$ .

## 4.3 Field representations via separation of variables (SOV)

As in the case of arbitrarily-shaped protuberances, the SOV technique gives rise to the field representation [358]

$$u^{[0]}(\mathbf{x}) = u^i(\mathbf{x}) + u^r(\mathbf{x}) + u^s(\mathbf{x}) \quad (14)$$

wherein  $u^r(x, y) = u^i(x, -y)$  and

$$u^s(\mathbf{x}) = \int_{-\infty}^{\infty} \mathcal{B}(k_x) f(k_x, x) \exp(-ik_y y) \frac{dk_x}{k_y^{[0]}} , \quad (15)$$

with:

$$f(k_x, x) = \exp(ik_x x) \quad , \quad k_y^{[0]} = \sqrt{(k^{[0]})^2 - (k_x)^2} \quad ; \quad \Re k_y^{[0]} \geq 0 \quad , \quad \Im k_y^{[0]} \geq 0 \quad ; \quad \text{for } \omega \geq 0 \quad . \quad (16)$$

Note that the scattered field  $u^s$  satisfies the radiation condition and is expressed as a sum of plane waves, some of which are propagative (for real  $k_y^{[0]}$ ) and the others evanescent (for imaginary  $k_y^{[0]}$ ).

Within the rectangular protuberance, the same SOV technique, together with the stress-free boundary conditions on  $\Gamma_p$  give rise to the field representations:

$$u^{[1]}(\mathbf{x}) = \sum_{m=0}^{\infty} \left[ a_m \exp(ik_{ym}^{[1]}y) + b_m \exp(-ik_{ym}^{[1]}y) \right] f_m(x) \quad , \quad (17)$$

$$u^{[2]}(\mathbf{x}) = \sum_{m=0}^{\infty} d_m \cos[k_{ym}^{[2]}(y-h)] g_m(x) \quad , \quad (18)$$

wherein:

$$f_m(x) = \exp(ik_{xm}x) \quad , \quad g_m(x) = \cos[k_{xm}(x+w/2)] \quad , \quad (19)$$

$$k_{xm} = \frac{m\pi}{w} \quad , \quad k_{ym}^{[l]} = \sqrt{(k^{[l]})^2 - (k_{xm})^2} \quad , \quad \Re k_{ym}^{[l]} \geq 0 \quad , \quad \Im k_{ym}^{[l]} \geq 0 \quad ; \quad \omega \geq 0 \quad , \quad l = 1, 2 \quad . \quad (20)$$

## 5 Employment of the SOV field representations in the remaining boundary and continuity conditions

As shown in [358], the stress-free boundary condition on the flanks of the protuberance , the continuity condition across  $\Gamma_m$ , as well as the orthogonality conditions of  $g_m(x)$  and  $f(k_x, x)$  give rise to the following two coupled sets of equations:

$$d_l \frac{\kappa_l}{\epsilon_l} = 2a^i I_l^+(k_x^i) + \int_{-\infty}^{\infty} \mathcal{B}(k_x) I_l^+(k_x) \frac{dk_x}{k_y^{[0]}} \quad ; \quad l = 0, 1, 2, \dots \quad , \quad (21)$$

$$\mathcal{B}(k_x) = \frac{iw}{2\pi} \frac{\mu^{[1]}}{\mu^{[0]}} \sum_{m=0}^{\infty} d_m^{(M)} \sigma_m k_{ym}^{[1]} I_m^-(k_x) \quad ; \quad \forall k_x \in \mathbb{R} \quad , \quad (22)$$

as well as to the relations connecting  $a_l$ ,  $b_l$  to  $d_l$ :

$$a_l = d_l \left( \frac{\exp(-ik_{yl}^{[1]}h_1)}{2i\mu^{[1]}k_{yl}^{[1]}} \right) \left[ i\mu^{[1]}k_{yl}^{[1]} \cos(k_{yl}^{[2]}h_2) + \mu^{[2]}k_{yl}^{[2]} \sin(k_{yl}^{[2]}h_2) \right] \quad , \quad (23)$$

$$b_l = d_l \left( \frac{\exp(ik_{yl}^{[1]}h_1)}{2i\mu^{[1]}k_{yl}^{[1]}} \right) \left[ i\mu^{[1]}k_{yl}^{[1]} \cos(k_{yl}^{[2]}h_2) - \mu^{[2]}k_{yl}^{[2]} \sin(k_{yl}^{[2]}h_2) \right] \quad , \quad (24)$$

in which:

$$I_m^\pm(k_x) = \int_{-w/2}^{w/2} \exp(\pm i k_x x) \cos[k_{xm}(x + w/2)] \frac{dx}{w} = \frac{i^m}{2} \text{sinc}\left[(\pm k_x + k_{xm}) \frac{w}{2}\right] + \frac{(-i)^m}{2} \text{sinc}\left[(\pm k_x - k_{xm}) \frac{w}{2}\right] \quad (25)$$

(with  $\text{sinc}(\zeta) = \sin(\zeta)/\zeta$  and  $\text{sinc}(0) = 1$ ) ,

$$\kappa_l = \cos(k_{yl}^{[1]} h_1) \cos(k_{yl}^{[2]} h_2) - \frac{\mu^{[2]} k_{yl}^{[2]}}{\mu^{[1]} k_{yl}^{[1]}} \sin(k_{yl}^{[1]} h_1) \sin(k_{yl}^{[2]} h_2) , \quad (26)$$

$$\sigma_l = \sin(k_{yl}^{[1]} h_1) \cos(k_{yl}^{[2]} h_2) + \frac{\mu^{[2]} k_{yl}^{[2]}}{\mu^{[1]} k_{yl}^{[1]}} \cos(k_{yl}^{[1]} h_1) \sin(k_{yl}^{[2]} h_2) . \quad (27)$$

Plugging (22) into (27) finally yields the single system of linear equations

$$\sum_{m=0}^{\infty} E_{lm}^{(M)} d_m^{(M)} = c_l ; \quad l = 0, 1, 2, \dots , \quad (28)$$

in which:

$$E_{lm}^{(M)} = \delta_{lm} \frac{\kappa_l}{\epsilon_l} - \frac{i w \mu^{[1]}}{2\pi \mu^{[0]}} k_{ym}^{[1]} \sigma_m J_{lm} , \quad c_l = 2a^i I_l^+(k_x^i) , \quad J_{lm} = \int_{-\infty}^{\infty} I_l^+(k_x) I_m^-(k_x) \frac{dk_x}{k_y^{[0]}} , \quad (29)$$

with  $\{d_m\}$  the to-be-determined set of wavefield coefficients.

Until now everything has been rigorous provided the equations in the statement of the boundary-value problem are accepted as the true expression of what is involved in the seismic response of the rectangular protuberance and certain summation interchanges (involved in the the obtention of the linear system) are valid. In order to actually solve for the sets  $\{d_m\}$ , and then for  $\{a_m\}$ ,  $\{b_m\}$ ,  $\{\mathcal{B}(k_x)\}$  (each of whose populations is considered to be infinite at this stage) we should usually resort to numerics. This is explained further on.

But before doing this we must evoke an encouraging result obtained in [358]: the formal solution to the scattering problem for  $\{d_m\}$ , and then for  $\{a_m\}$ ,  $\{b_m\}$ ,  $\{\mathcal{B}(k_x)\}$  (the term formal meaning implicit, because at this stage we have not solved explicitly for these quantities) turns out to be such as to wholly satisfy the conservation of flux law.

## 6 Some mathematical properties of the solution for $d_m$

Before going into the details of numerics it is of considerable interest to evoke some mathematical properties of the solution of the scattering problem.

## 6.1 General properties of $I_{lm}^\pm$ and their incidence on $J_{lm}$ and $E_{lm}$

Eq. (25) tells us that

$$I_{2p+1}^\pm(k_x) = i \frac{(-1)^p}{2} [\text{sinc}[(\pm k_x + k_{x2p+1})w/2] - \text{sinc}[(\pm k_x - k_{x2p+1})w/2]] ; m = 0, 1, 2, \dots , \quad (30)$$

from which we find

$$I_{2p+1}^\pm(-k_x) = -I_{2p+1}^\pm(k_x) ; m = 0, 1, 2, \dots . \quad (31)$$

Eq. (25) also tells us that

$$I_{2p}^\pm(k_x) = \frac{(-1)^p}{2} [\text{sinc}[(\pm k_x + k_{x2p})w/2] + \text{sinc}[(\pm k_x - k_{x2p})w/2]] ; m = 0, 1, 2, \dots , \quad (32)$$

from which we find

$$I_{2p}^\pm(-k_x) = I_{2p}^\pm(k_x) ; m = 0, 1, 2, \dots . \quad (33)$$

It follows that

$$J_{2p,2q+1} = J_{2p+1,2q} = 0 ; p, q = 0, 1, 2, \dots , \quad (34)$$

whence

$$E_{2p,2q+1} = E_{2p+1,2q} = 0 ; p, q = 0, 1, 2, \dots . \quad (35)$$

## 6.2 Linear systems of equations for even and odd orders of $\mathcal{F}_m$

We had:

$$\begin{aligned} \sum_{q=0}^{\infty} [E_{2p,2q}d_{2q} + E_{2p,2q+1}d_{2q+1}] &= c_{2p} \\ \sum_{q=0}^{\infty} [E_{2p+1,2q}d_{2q} + E_{2p+1,2q+1}d_{2q+1}] &= c_{2p+1} \end{aligned} ; p = 0, 1, 2, \dots , \quad (36)$$

so that

$$\begin{aligned} \sum_{q=0}^{\infty} E_{2p,2q}d_{2q} &= c_{2p} \\ \sum_{q=0}^{\infty} E_{2p+1,2q+1}d_{2q+1} &= c_{2p+1} \end{aligned} ; p = 0, 1, 2, \dots , \quad (37)$$

which shows that the equations for the odd order  $d_m$  are decoupled from those for the even order  $d_m$ .

## 6.3 Normal incidence

Normal incidence means that  $\theta^i = 0^\circ$ .

### 6.3.1 The odd-order diffraction coefficients

Eq. (30) tells us that, for  $k_x = k_x^i$ , and normal incidence,  $k_x^i = 0$ ,

$$I_{2p+1}^\pm(k_x^i) = I_{2p+1}^\pm(0) = 0 ; p = 0, 1, 2, \dots . \quad (38)$$

whereas (32) indicates

$$I_{2p}^\pm(k_x^i) = I_{2p}^\pm(0) = (-1)^p \text{sinc}(p\pi) = \delta_{p0} ; p = 0, 1, 2, \dots . \quad (39)$$

It follows that:

$$c_{2p} = 2a^i \delta_{p0} , \quad c_{2p+1} = 0 ; p = 0, 1, 2, \dots , \quad (40)$$

whence the linear system of equations for the odd  $d_m$  becomes

$$\sum_{q=0}^{\infty} E_{2p+1,2q+1} d_{2q+1} = 0 ; p = 0, 1, 2, \dots , \quad (41)$$

whose solution is necessarily

$$d_{2q+1} = 0 ; q = 0, 1, 2, \dots , \quad (42)$$

which means that, for normal incidence plane-wave solicitation, the odd-order diffraction coefficients are nil.

#### 6.4 Iterative approach for the obtention of the even-order diffraction coefficients

We can write  $E_{lm}$  as  $E_{lm} = \delta_{lm}\chi_l - F_{lm}$  so that the first equation of (42) becomes

$$d_{2p}\chi_{2p} = c_{2p} + \sum_{q=0}^{\infty} F_{2p,2q} d_{2q} ; p = 0, 1, 2, \dots , \quad (43)$$

which suggests solving for  $d_{2p}$  by the iterative scheme:

$$d_{2p}^{(0)} = \frac{c_{2p}}{\chi_{2p}} , \quad d_{2p}^{(j)} = d_{2p}^{(0)} + \sum_{q=0}^{\infty} \frac{F_{2p,2q}}{\chi_{2p}} d_{2q}^{(j-1)} ; p = 0, 1, 2, \dots , \quad (44)$$

##### 6.4.1 Closed-form solution for $d_{2p}$ by the iterative scheme in a very special (VS) case

We first note that  $c_{2p} = 2a^i I_{2p}^+(0) = 2a^i \delta_{p0}$  so that  $d_{2p}^{(0)} = \frac{2a^i \delta_{p0}}{\chi_0}$ ,

$$d_{2p}^{(1)} = d_{2p}^{(0)} + \frac{F_{2p,0}}{\chi_{2p}} \frac{2a^i}{\chi_0} ; p = 0, 1, 2, \dots , \quad (45)$$

and so on. Before going to higher-order iterates, first consider the first one, in which

$$F_{2p,0} = \frac{iw}{2\pi} \frac{\mu^{[1]}}{\mu^{[0]}} k_{y0}^{[1]} \sigma_0 J_{2p,0} . \quad (46)$$

Secondly, we note that  $\chi_0 = \kappa_0$ , and by means of (26)-(27)

$$\kappa_0 = \cos(k^{[1]}h_1 + k^{[2]}h_2) + \left( \frac{\mu^{[2]}k^{[2]}}{\mu^{[1]}k^{[1]}} - 1 \right) \sin(k^{[1]}h_1) \sin(k^{[2]}h_2) , \quad (47)$$

$$\sigma_0 = \sin(k^{[1]}h_1 + k^{[2]}h_2) + \left( \frac{\mu^{[2]}k^{[2]}}{\mu^{[1]}k^{[1]}} - 1 \right) \cos(k^{[1]}h_1) \sin(k^{[2]}h_2) , \quad (48)$$

from which we find

$$\sigma_0 = 0 , \quad \kappa_0 = \cos N\pi = (-1)^N , \quad (49)$$

in the very special (VS) case (recall that we are still assuming that  $\theta^i = 0^\circ$ ) in which:

$$k^{[1]}h_1 + k^{[2]}h_2 = N\pi \quad , \quad \mu^{[2]}k^{[2]} = \mu^{[1]}k^{[1]} \quad ; \quad N = 0, 1, 2, \dots \quad . \quad (50)$$

It follows (in this VS case) that  $F_{2p,0} = 0$  so that

$$d_{2p}^{(1)} = d_{2p}^{(0)} \quad ; \quad p = 0, 1, 2, \dots \quad , \quad (51)$$

and, in the same manner, we find that the higher-order iterates are equal to the zeroth-order iterate, so that, in the very special case (recall that  $\theta^i = 0^\circ$  was also assumed) defined by (50), the closed-form solution for the (even-order) diffraction coefficients is:

$$d_{2p}^{(0)} = a^i(-1)^N \delta_{p0} \quad ; \quad p = 0, 1, 2, \dots, N = 0, 1, 2, \dots \quad , \quad (52)$$

it being recalled (always in the case  $\theta^i = 0^\circ$ ) that  $d_{2p+1} = 0 \quad ; \quad p = 0, 1, 2, \dots$

#### 6.4.2 VS case: expressions of the fields and demonstration that the continuity conditions are satisfied

Inserting (52) into (99) gives

$$u^{[2]}(\mathbf{x}) = 2a^i(-1)^N \cos(k^{[2]}(y-h)) \quad ; \quad N = 0, 1, 2, \dots \quad , \quad (53)$$

whence

$$u^{[2]}(x, h_1) = 2a^i(-1)^N \cos(k^{[2]}h_2) \quad , \quad u_{,y}^{[2]}(x, h_1) = 2a^i(-1)^N k^{[2]} \sin(k^{[2]}h_2) \quad ; \quad N = 0, 1, 2, \dots \quad . \quad (54)$$

Eqs. (97) and (26)-(27) lead to

$$u^{[1]}(\mathbf{x}) = \sum_{m=0}^{\infty} d_m \left[ \kappa_m \cos(k_{ym}^{[1]}y) + \sigma_m \sin(k_{ym}^{[1]}y) \right] \exp(ik_{xm}x) \quad , \quad (55)$$

which, by means of (52) (and the fact that the odd-order  $d_m$  are nil), gives rise to

$$u^{[1]}(\mathbf{x}) = 2a^i \cos(k^{[1]}y) \quad ; \quad N = 0, 1, 2, \dots \quad , \quad (56)$$

whence

$$u_{,y}^{[1]}(\mathbf{x}) = -2a^i k^{[1]} \sin(k^{[1]}y) \quad ; \quad N = 0, 1, 2, \dots \quad , \quad (57)$$

$$u^{[1]}(x, h_1) = 2a^i(-1)^N \cos(k^{[2]}h_2) \quad , \quad u_{,y}^{[1]}(x, h_1) = 2a^i(-1)^N k^{[1]} \sin(k^{[2]}h_2) \quad ; \quad N = 0, 1, 2, \dots \quad . \quad (58)$$

Consequently

$$u^{[1]}(x, h_1) - u^{[2]}(x, h_1) = 0 \quad ; \quad \forall N = 0, 1, 2, \dots \quad , \quad (59)$$

$$\mu^{[1]}u_{,y}^{[1]}(x, h_1) - \mu^{[2]}u_{,y}^{[2]}(x, h_1) = 2a^i(-1)^N [\mu^{[1]}k^{[1]} - \mu^{[2]}k^{[2]}] \sin(k^{[2]}h_2) \quad , \quad (60)$$

of, on account of the second VS condition

$$\mu^{[1]}u_{,y}^{[1]}(x, h_1) - \mu^{[2]}u_{,y}^{[2]}(x, h_1) = 0 \quad ; \quad \forall N = 0, 1, 2, \dots \quad , \quad (61)$$



which shows that the continuity conditions on the segment of separation at  $y = h_1$  are satisfied by the VS case solution for the diffraction coefficients.

Introducing the fact that the odd-order  $d_m$  are nil into (22) gives

$$\mathcal{B}(k_x) = \frac{iw}{2\pi} \frac{\mu^{[1]}}{\mu^{[0]}} \sum_{p=0}^{\infty} d_{2p} \sigma_{2p} k_{y2p}^{[1]} I_{2p}^-(K_x) ; \forall k_x \in \mathbb{R} , \quad (62)$$

so that, due to (52)

$$\mathcal{B}(k_x) = a^i (-1)^N \frac{iw}{\pi} \frac{\mu^{[1]}}{\mu^{[0]}} \sigma_0 k_{y0}^{[1]} I_0^-(K_x) ; \forall k_x \in \mathbb{R} , N = 0, 1, 2, \dots , \quad (63)$$

or, on account of (49),

$$\mathcal{B}(k_x) = 0 . \quad (64)$$

Consequently,

$$u^d(\mathbf{x}) = 0 \Rightarrow u^{[0]}(\mathbf{x}) = u^i(x, y) + u^i(x, -y) = 2a^i \cos(k_y^{[0]}) , \quad (65)$$

so that

$$u_{,y}^{[0]}(\mathbf{x}) = -2a^i k^{[0]} \sin(k_y^{[0]}) . \quad (66)$$

From (65) and (56) we find  $u^{[0]}(x, 0) = 2a^i$  and  $u^{[1]}(x, 0) = 2a^i$  respectively, so that the continuity condition across the base segment of the convex rectangular feature

$$u^{[0]}(x, 0) - u^{[1]}(x, 0) = 0 , \quad (67)$$

is satisfied. Moreover, (68) and (57) indicate that  $u_{,y}^{[1]}(x, 0) = 0$  and  $u_{,y}^{[0]}(x, 0) = 0$  respectively, so that the continuity condition across the base segment of the convex rectangular feature

$$\mu^{[0]} u_{,y}^{[0]}(x, 0) - \mu^{[1]} u_{,y}^{[1]}(x, 0) = 0 , \quad (68)$$

is satisfied, whatever be the relation of  $\mu^{[0]}$  to  $\mu^{[1]}$ .

Thus, in the VS case, i.e., when the parameters of the scattering configuration obey  $\theta^i = 0^\circ$  and (50), the field admits the closed-form expressions: (53) for  $u^{[2]}(\mathbf{x})$ , (56) for  $u^{[1]}(\mathbf{x})$ , and (65) for  $u^{[0]}(\mathbf{x})$ , which are such as to satisfy the four continuity conditions across the various interfaces and the stress-free boundary conditions along the stress-free boundary of the scatterer.

A last remark: the VS case provides a useful testing ground for the numerical methods and solutions described and offered further on in sect. 7.4. This is demonstrated, e.g. in fig. 59.

## 6.5 Coping with $J_{lm}$

Anticipating the issue of numerics we can expect that the principal problem will be how to cope with  $J_{lm}$ . If, for the moment, we exclude resorting to a purely-numerical double-integral quadrature scheme, we must dispose of another more-mathematical method. The one we devised (see also [349]) for a brief description) enables the reduction of the evaluation of the double integral to that of at most three single-integrals.

Inserting the expressions (25) for  $I_{lm}^\pm$  into (29) gives rise, after interchanges of the orders of integration:

$$J_{lm} = \frac{\pi}{w^2} \int_{-w/2}^{w/2} dx' \cos[k_{xl}(x' + w/2)] \int_{-w/2}^{w/2} dx \cos[k_{xm}(x + w/2)] \int_{-\infty}^{\infty} \frac{dk_x}{\pi k_y} \exp[ik_x(x' - x)] , \quad (69)$$

or, using the fact [239] that

$$\int_{-\infty}^{\infty} \frac{dk_x}{\pi k_y} \exp[ik_x(x' - x)] = H_0^{(1)}(k^{(0)}|x' - x|) , \quad (70)$$

wherein  $H_j^{(1)}(\cdot)$  is the  $j$ th-order Hankel function of the first kind, we find

$$J_{lm} = \frac{\pi}{w^2} \int_{-w/2}^{w/2} dx' \cos[k_{xl}(x' + w/2)] \int_{-w/2}^{w/2} dx \cos[k_{xm}(x + w/2)] H_0^{(1)}(k^{[0]}|x' - x|) , \quad (71)$$

which becomes, with the changes of variables  $\eta' = k^{[0]}(x' + w/2)$ ,  $\eta = k^{[0]}(x + w/2)$ ,  $\alpha_l = k_{xl}/k^{[0]}$

$$J_{lm} = \frac{\pi}{(k^{[0]}w)^2} \int_0^{k^{[0]}w} d\eta' \cos(\alpha_l \eta') \int_0^{k^{[0]}w} d\eta \cos(\alpha_m \eta) H_0^{(1)}(|\eta' - \eta|) . \quad (72)$$

From the fact that

$$\cos(\alpha_l \eta') \cos(\alpha_m \eta) = \frac{1}{2} \{ \cos[\alpha_{-l}(\eta' - \eta) + (\alpha_m + \alpha_{-l})\eta] + \cos[\alpha_l(\eta' - \eta) + (\alpha_m + \alpha_l)\eta] \} . \quad (73)$$

we obtain

$$\frac{(k^{[0]}w)^2}{\pi} J_{lm} = \mathcal{J}_{-lm} + \mathcal{J}_{lm} , \quad (74)$$

wherein

$$\mathcal{J}_{lm} = \frac{1}{2} \int_0^{k^{[0]}w} d\eta' \int_0^{k^{[0]}w} d\eta H_0^{(1)}(|\eta' - \eta|) \cos[\alpha_l(\eta' - \eta) + (\alpha_m + \alpha_l)\eta] . \quad (75)$$

We make the change of variables  $\mu = \eta$  and  $\nu = \eta' - \eta$  so as to convert the original rectangular  $\eta' - \eta$  integration domain into a parallelogram  $\mu - \nu$  domain which is decomposable into a triangular domain for negative  $\nu$  and another triangular domain for positive  $\nu$ , both of which correspond to positive  $\mu$ . Consequently

$$\mathcal{J}_{lm} = \int_0^\kappa d\nu \int_0^{\kappa-\nu} d\mu \mathcal{P}(\mu, \nu) + \int_{-\kappa}^0 d\nu \int_{-\nu}^\kappa d\mu \mathcal{P}(\mu, \nu) = \mathcal{J}_{lm}^+ + \mathcal{J}_{lm}^- , \quad (76)$$

wherein:

$$\mathcal{P}(\mu, \nu) = \frac{1}{2} H_0^{(1)}(|\nu|) \cos[\alpha_l \nu + (\alpha_m + \alpha_l)\mu] , \quad \kappa = k^{[0]}w , \quad (77)$$

$$\mathcal{J}_{lm}^+ = \int_0^\kappa d\nu \int_0^{\kappa-\nu} d\mu \mathcal{P}(\mu, \nu) , \quad \mathcal{J}_{lm}^- = \int_{-\kappa}^0 d\nu \int_{-\nu}^\kappa d\mu \mathcal{P}(\mu, \nu) . \quad (78)$$

We easily find

$$\mathcal{J}_{lm}^+ = \frac{\sin[(\alpha_l + \alpha_m)\kappa]}{2(\alpha_m + \alpha_l)} \int_0^\kappa d\nu H_0^{(1)}(|\nu|) \cos(\alpha_m \nu) - \frac{\cos[(\alpha_l + \alpha_m)\kappa]}{2(\alpha_m + \alpha_l)} \int_0^\kappa d\nu H_0^{(1)}(|\nu|) \sin(\alpha_m \nu) - \frac{1}{2(\alpha_m + \alpha_l)} \int_0^\kappa d\nu H_0^{(1)}(|\nu|) \sin(\alpha_l \nu) . \quad (79)$$

$$\mathcal{J}_{lm}^- = -\frac{\cos[(\alpha_l + \alpha_m)\kappa]}{2(\alpha_m + \alpha_l)} \int_0^\kappa d\nu H_0^{(1)}(|\nu|) \sin(\alpha_l \nu) + \frac{\sin[(\alpha_l + \alpha_m)\kappa]}{2(\alpha_m + \alpha_l)} \int_0^\kappa d\nu H_0^{(1)}(|\nu|) \cos(\alpha_l \nu) - \frac{1}{2(\alpha_m + \alpha_l)} \int_0^\kappa d\nu H_0^{(1)}(|\nu|) \sin(\alpha_m \nu) , \quad (80)$$

whence

$$\mathcal{J}_{lm} = \frac{\kappa}{2} \text{sinc}[(\alpha_l + \alpha_m)\kappa] \int_0^\kappa d\nu H_0^{(1)}(|\nu|) [\cos(\alpha_m \nu) + \cos(\alpha_l \nu)] - \frac{[1 + \cos[(\alpha_l + \alpha_m)\kappa]]}{2(\alpha_m + \alpha_l)} \int_0^\kappa d\nu H_0^{(1)}(|\nu|) [\sin(\alpha_m \nu) + \sin(\alpha_l \nu)] , \quad (81)$$

or

$$\mathcal{J}_{lm} = \frac{\kappa}{2} \delta_{l,-m} \int_0^\kappa d\nu H_0^{(1)}(|\nu|) [\cos(\alpha_m \nu) + \cos(\alpha_l \nu)] - \frac{[1 + \cos[(\alpha_l + \alpha_m)\kappa]]}{2} \int_0^\kappa d\nu H_0^{(1)}(|\nu|) \nu \text{sinc}[(\alpha_m + \alpha_l)\nu/2] \cos[(\alpha_m - \alpha_l)\nu/2] . \quad (82)$$

In the same way we find

$$\mathcal{J}_{-l,m} = \mathcal{J}_{l,-m} = \frac{\kappa}{2} \delta_{l,m} \int_0^\kappa d\nu H_0^{(1)}(|\nu|) [\cos(\alpha_m \nu) + \cos(\alpha_l \nu)] - \frac{[1 + \cos[(\alpha_l - \alpha_m)\kappa]]}{2} \int_0^\kappa d\nu H_0^{(1)}(|\nu|) \nu \text{sinc}[(\alpha_m - \alpha_l)\nu/2] \cos[(\alpha_m + \alpha_l)\nu/2] , \quad (83)$$

so that

$$\begin{aligned} \frac{\kappa^2}{\pi} J_{lm} &= \mathcal{J}_{l,m} + \mathcal{J}_{-l,m} + \frac{\kappa}{2} (\delta_{l,-m} + \delta_{l,-m}) \int_0^\kappa d\nu H_0^{(1)}(|\nu|) [\cos(\alpha_m \nu) + \cos(\alpha_l \nu)] - \\ &\quad \frac{[1 + \cos[(\alpha_l + \alpha_m)\kappa]]}{2} \int_0^\kappa d\nu H_0^{(1)}(|\nu|) \nu \text{sinc}[(\alpha_m + \alpha_l)\nu/2] \cos[(\alpha_m - \alpha_l)\nu/2] + \\ &\quad \frac{[1 + \cos[(\alpha_l - \alpha_m)\kappa]]}{2} \int_0^\kappa d\nu H_0^{(1)}(|\nu|) \nu \text{sinc}[(\alpha_m - \alpha_l)\nu/2] \cos[(\alpha_m + \alpha_l)\nu/2] , \end{aligned} \quad (84)$$

from which we deduce, recalling that  $l, m = 0, 1, 2, \dots$ :

$$\frac{\kappa^2}{\pi} J_{l,m \neq \pm l} = \left( \frac{1 + (-1)^{l+m}}{2} \right) \left[ \frac{\alpha_m \mathcal{S}_m(\kappa) - \alpha_l \mathcal{S}_l(\kappa)}{(\alpha_l)^2 - (\alpha_m)^2} \right] , \quad (85)$$

$$\frac{\kappa^2}{\pi} J_{l,l \neq 0} = \kappa \mathcal{C}_l(\kappa) - \frac{1}{\alpha_l} \mathcal{S}_l(\kappa) - \mathcal{A}_l(\kappa) , \quad (86)$$

$$\frac{\kappa^2}{\pi} J_{0,0} = 2\kappa \mathcal{C}_0(\kappa) - 2\mathcal{A}_0(\kappa) , \quad (87)$$

with:

$$\begin{aligned} \mathcal{S}_l(\kappa) &= \int_0^\kappa H_0^{(1)}(\nu) \sin(\alpha_l \nu) d\nu , \\ \mathcal{C}_l(\kappa) &= \int_0^\kappa H_0^{(1)}(\nu) \cos(\alpha_l \nu) d\nu , \\ \mathcal{A}_l(\kappa) &= \int_0^\kappa H_0^{(1)}(\nu) \nu \cos(\alpha_l \nu) d\nu . \end{aligned} \quad (88)$$

Thus, we have reduced the evaluation of the double-integrals in the primitive form of  $J_{lm}$ , for each  $l, m$ , to that of three single-integrals (i.e.,  $\mathcal{S}_l$ ,  $\mathcal{C}_l$  and  $\mathcal{A}_l$ ).

## 7 On the origin of building, hill and mountain resonances

The issue that must be discussed, in theoretical terms before going into the numerics, is that of resonances, which, as stated in the Introduction, is at the core of our contribution.

### 7.1 Introductory remarks

We saw that the problem of the response of a convex, rectangular-shaped feature emerging from flat ground leads to a matrix equation (see (28))

$$\mathbf{E} \mathbf{d} = \mathbf{c} , \quad (89)$$

wherein the elements of the square, infinite-order matrix  $\mathbf{E}$  are the  $E_{lm}$ , and the elements of the infinite-order vectors  $\mathbf{d}$  and  $\mathbf{c}$  are  $d_m$  and  $c_l$  respectively. An important feature of this equation is that the amplitude  $a^i$  and incident angle  $\theta^i$  of the plane-wave solicitation do not appear in  $\mathbf{E}$  but only in  $\mathbf{c}$ .

The formal solution of the matrix equation is

$$\mathbf{d} = \mathbf{E}^{-1} \mathbf{c} , \quad (90)$$

wherein  $\mathbf{E}^{-1}$  designates the (formal) inverse of  $\mathbf{E}$ .

Lest it be forgotten, the principal motivation of this study is to find out, as is suggested by empirical evidence and other, former theoretical and numerical studies, why the response at locations within and on a building or mountain (this list could just as well include a building) to a seismic wave can be larger, or even much larger, than the so-called free-field response (i.e., the response on, and below, the ground in the absence of the convex free-surface feature). Our working hypothesis is that such amplifications are due to *resonances*.

Loosely-speaking, a resonance designates the moment at which all the parameters of the scattering configuration except  $a^i$  and  $\theta^i$  are such that one or several terms in  $\mathbf{d}$  are large, the consequence of which is (due to the fact that  $\mathbf{d}$  is what largely conditions the amplitude of the displacement field

in the convex rectangular feature) that at resonance the displacement field might become large in certain subregions within or below the rectangular region occupied by the convex feature.

Note that in the seismic engineering community, one often speaks of resonances (typically of a site with flat stress-free boundary underlain by one or several media arranged as layers) and even of a (convex) topographic feature (in [46] the authors speak of a "transverse oscillatory resonance mode of a hill from 3 to 5  $H_z$ "), but the physical origin of these convex topographic resonances are not really explained. They are rather named 'resonances' because they occur (both empirically and in numerical studies) in rather narrow ranges of frequencies and are characterized by response peaks, often qualified as 'amplifications', particularly at the top of the convex surface feature. Some authors [225] also underline (but do not explain) the fact that the ('resonance') frequencies of occurrence of these amplifications do not seem to vary with the solicitation (notably the distance and azimuth of the source), but the level of amplifications depend on the shape (notably aspect ratio) and composition of the convex surface feature.

## 7.2 A first definition of (surface shape) resonances

Let  $D = \det \mathbf{E}$  denote the formal, complex determinant of  $\mathbf{E}$ . At (or near) resonance,  $D$  is equal (or nearly-) equal to zero since this is what makes  $\mathbf{E}^{-1}$ , and thus one or several elements of  $\mathbf{d}$ , large. Since there exist attenuation mechanisms in the scattering problem at hand, such as radiation damping (energy that escapes to the outer confines of the bottom half-space [370]) and material damping related to the lossy nature of the material(s) within the convex feature, the real and imaginary parts of  $D$  will not vanish entirely and simultaneously (at real frequencies). Thus, we modify our definition of resonance as the moment when  $\|D\|$  is very small or  $1/\|D\|$  is very large (large meaning compared to the off-resonance situations). Note that the resonances are easily spotted when the attenuations are small, but possibly hard to spot when the attenuations are large (this will be demonstrated further on in the computed transfer functions, and will, in fact constitute the method by which we shall determine the resonance frequencies). Again, note that our definition of resonance is independent of  $a^i$  and  $\theta^i$ , whatever be the degree of attenuation.

We shall define the term 'coupling to a resonance' as the moment (for fixed  $h_1$ ,  $h_2$ ,  $w$ ,  $\mu^{[0]}$ ,  $\mu^{[1]}$ ,  $\mu^{[2]}$ ,  $\beta^{[0]}$ ,  $\beta^{[1]}$ ,  $\beta^{[2]}$ ,  $a^i$ ,  $\theta^i$ ) at which the frequency  $f$  of the seismic solicitation equals a resonant frequency (whose meaning will emerge in what follows).

As we shall see in the numerical results, coupling to a resonance results in a large value of at least one term in the SOV representations of the field within the protuberance, which fact should not be interpreted as the amplification of the field *at all locations within the protuberance*. The configuration of the field, within and outside the protuberance, at a resonance frequency is termed the mode at this frequency.

## 7.3 A second definition of (surface shape) resonances

Consider the determinant  $D(\omega)$  (which we have written as a function of  $\omega = 2\pi f$  instead of  $f$ ), with  $\omega$  now thought of as being a complex variable. In the complex  $\omega$  plane, a zero of  $D(\omega)$  occurs at that (generally-complex) value  $\omega^R$  of  $\omega$  for which

$$D(\omega) = 0. \quad (91)$$

To this zero corresponds a pole, synonymous with infinite  $1/D$  and infinite  $\mathbf{d}$ . As we know that the zero generally does not occur for real  $\omega^R$  we write  $\omega^R = \omega^{R'} - i\omega^{R''}$  wherein  $\omega^{R'} \geq 0$  and

$\omega^{R''} \geq 0$ . The 'physical' angular frequency is  $\omega'$  so that we can expect  $\|1/D(\omega')\|$  to be largest when  $\omega' \simeq \omega^{R'}$ , which fact can be seen as follows. By means of a Taylor series expansion in the neighborhood of  $\omega = \omega^R$  we find

$$\|D(\omega)\|^{-2} \simeq \|D_{,\omega}(\omega^R)\|^{-2} \|\omega - \omega^R\|^{-2} = \|D_{,\omega}(\omega^R)\|^{-2} \left[ \|\omega\|^2 + \|\omega\|^2 - 2\Re(\omega^R \omega^*) \right]^{-1}, \quad (92)$$

so that

$$\|D(\omega')\|^{-2} \simeq \|D_{,\omega}(\omega^R)\|^{-2} \left[ (\omega' - \omega^{R'})^2 + (\omega^{R''})^2 \right]^{-1}. \quad (93)$$

This function (as well as  $\|D(\omega')\|^{-1}$  which we shall depict in many of our numerical results hereafter), has the shape of a lorentzian, indicative of *resonant response*, whose maximum is situated at  $\omega' = \omega^{R'}$ , which is called the 'resonance frequency', and whose width at half height is  $2\omega^{R''}$ . Note that more than one resonance can occur in the function  $\|D(\omega')\|^{-1}$  in which case what was offered until now remains true for each such resonance as long as the various resonance frequencies are well-separated in the complex  $\omega$  plane. This constitutes our second definition of surface shape resonances.

This definition of (surface shape) resonances applies equally-well to the seismic response of a below-ground structure (BGS), and, in fact, to the vibratory or wave-like (electromagnetic, acoustic, elastic, hydrodynamic, etc.) response of any (including inhomogeneous, such as multilayered) object [91, 349, 262, 220, 77, 221, 222, 223, 351, 353, 354, 211, 210, 391].

#### 7.4 An alternate system of equations

As it stands, the matrix equation  $\mathbf{E}\mathbf{d} = \mathbf{c}$  is not particularly-appropriate for the determination of the diffraction coefficients  $\mathbf{d}$ , particularly as concerns the issue of the dependence of the resonances on  $h_1$ ,  $h_2$  on the one hand, and on  $w$  on the other hand. The reason for this is that the matrix  $\mathbf{E}$  is the sum of two matrices both of which involve all the configurational parameters  $h_1$ ,  $h_2$ ,  $w$ .

The way to resolve this problem is actually quite simple: in (28), divide  $E_{lm}$  by  $\sigma_m$  and multiply  $d_m$  by  $\sigma_m$  so as to obtain

$$\sum_{m=0}^{\infty} \mathcal{E}_{lm} \mathcal{F}_m = \mathcal{G}_l; \quad l = 0, 1, 2, \dots, \quad (94)$$

in which:

$$\mathcal{E}_{lm} = E_{lm} \frac{\epsilon_l}{\sigma_m} = \delta_{lm} \frac{\kappa_l}{\sigma_l} - \epsilon_l \frac{iw}{2\pi} \frac{\mu^{[1]}}{\mu^{[0]}} k_{ym}^{[1]} J_{lm} \quad , \quad \mathcal{G}_l = c_l \epsilon_l = 2a^i \epsilon_l I_l^+(k_x^i) \quad , \quad \mathcal{F}_m = d_m \sigma_m. \quad (95)$$

As expected, only the first term (i.e., the one with  $\delta_{lm}$ ) involves  $h_1$ ,  $h_2$ , and only the second term (i.e., the one with  $J_{lm}$ ) involves  $w$ .

#### 7.5 The issue of the infinite dimensions of the matrix equation for the diffraction amplitudes

The matrix equation (94) can be written symbolically as  $\mathcal{E}\mathcal{F} = \mathcal{G}$ . An issue that should not be avoided, notably in connection with resonances, is that of the infinite dimensions of the matrix  $\mathcal{E}$ . In any numerical study (such as the one undertaken in sect. 7.4 hereafter),  $\mathcal{E}$  must be treated as if it had finite dimensions, i.e.,  $\mathcal{E}$  being an  $M$ -by  $M$  matrix, with  $M$  a finite integer. Similarly to

the matrix equation  $\mathbf{E}\mathbf{d} = \mathbf{c}$  in which we denoted the determinant of  $\mathbf{E}$  by  $D$ , now we denote the determinant of  $\mathcal{E}$  by  $\mathcal{D}$ .

The first point to underline is that if the resonance is to occur in the  $n$ -th coefficient of  $\mathcal{F}$ , but  $M$  is chosen to be inferior  $n$ , it will be impossible to detect the said resonance. Thus, for instance, if  $M$  is chosen to be 0, then only an approximation of the resonant coupling to  $\mathcal{F}_0$  is possible, this meaning that accounting for the possible resonant coupling to  $\mathcal{F}_{m>0}$  is impossible by this means.

Since it has been hypothesized in previous publications that coupling to the so-called fundamental  $m = 0$  component (called 'fundamental mode') of the field in the topographic feature is the dominant mechanism for explaining the seismic response of the said feature, we shall first pay attention to this component, as well as to the  $M = 0$  approximation of this response, notably to find out whether it can really be of resonant nature.

## 7.6 Resonances from the point of view of the $M = 0$ approximation

What the last line of the preceding section means is that we first examine the equation

$$\mathcal{E}_{00}\mathcal{F}_0^{(0)} = \mathcal{G}_0 \iff E_{00}d_0^{(0)} = c_0 , \quad (96)$$

wherein the superscript (0) means the zeroth-order approximation, from which it is immediately-evident (as underlined previously in the  $M \rightarrow \infty$  context) that  $d_0^{(0)}$  is all the larger, the smaller is  $D^{(0)} = E_{00}$ . So let us take a close look at  $\mathcal{E}_{00}$  via (76) and the fact that  $k_{y0}^{[1]} = k^{[1]} = 2\pi f/\beta^{[1]}$ ,

$$\mathcal{D}^{(0)} = \mathcal{E}_{00} = \frac{\kappa_0}{\sigma_0} - i \frac{\mu^{[1]}\beta^{[0]}}{\mu^{[0]}\beta^{[1]}} \frac{k^{[0]}w}{2\pi} J_{00} . \quad (97)$$

whose first term depends only on  $h_1, h_2$  and whose second term depends only on  $k^{[0]}w$  since (see (87))

$$K_{00}(k^{[0]}w) = \frac{k^{[0]}w}{2\pi} J_{00}(k^{[0]}w) = \mathcal{C}_0(k^{[0]}w) - \frac{1}{k^{[0]}w} \mathcal{D}_0(k^{[0]}w) . \quad (98)$$

We are now in a position to find out, especially when  $k^{[0]}w$  is small (which affects only  $\frac{k^{[0]}w}{2\pi} J_{00}$ ), for what frequencies (i.e., the resonant frequencies)  $\|\mathcal{E}_{00}\|$  can be small.

### 7.6.1 Origin of the so-called shear-wall resonance (SWR)

Employing (11.3.20) and (11.3.24) in [1] gives

$$\mathcal{A}_0(k^{[0]}w) = k^{[0]}w_1 H^{(1)}(k^{[0]}w) + \frac{2i}{\pi} , \quad (99)$$

so that

$$K_{00}(k^{[0]}w) = \mathcal{C}_0(k^{[0]}w) - H^{(1)}(k^{[0]}w) - \frac{1}{k^{[0]}w} \frac{2i}{\pi} , \quad (100)$$

In [1], p. 360 we find the asymptotic forms:

$$H_0^{(1)}(\zeta) \sim \frac{2}{i\pi} \ln \zeta , \quad H_1^{(1)}(\zeta) \sim \frac{2}{i\pi\zeta} ; \quad \zeta \rightarrow 0, \quad (101)$$



so that  $-H_1^{(1)}(k^{[0]}w) - \frac{1}{k^{[0]}w} \frac{2i}{\pi} \sim 0$  ;  $k^{[0]}w \rightarrow 0$ . On the other hand,

$$\mathcal{C}_0(k^{[0]}w) = \int_0^{k^{[0]}w} H_0^{(1)}(\zeta) d\zeta \sim \frac{2}{i\pi} \int_0^{k^{[0]}w} \ln \zeta d\zeta = k^{[0]}w \ln(k^{[0]}w) - k^{[0]}w = 0 ; k^{[0]}w \rightarrow 0 , \quad (102)$$

so that

$$K_{00}(k^{[0]}w) = 0 ; k^{[0]}w \rightarrow 0 , \quad (103)$$

whence

$$\mathcal{E}_{00} \sim \frac{\kappa_0}{\sigma_0} ; k^{[0]}w \rightarrow 0 . \quad (104)$$

Recall, via (47)-(48), that:

$$\kappa_0 = \cos(k^{[1]}h_1 + k^{[2]}h_2) + \left( \frac{\mu^{[2]}\beta^{[1]}}{\mu^{[1]}\beta^{[2]}} - 1 \right) \sin(k^{[1]}h_1) \sin(k^{[2]}h_2) , \quad (105)$$

$$\sigma_0 = \sin(k^{[1]}h_1 + k^{[2]}h_2) + \left( \frac{\mu^{[2]}\beta^{[1]}}{\mu^{[1]}\beta^{[2]}} - 1 \right) \cos(k^{[1]}h_1) \sin(k^{[2]}h_2) , \quad (106)$$

and assume that

$$\left\| \frac{\mu^{[2]}\beta^{[1]}}{\mu^{[1]}\beta^{[2]}} - 1 \right\| << 1 , \quad (107)$$

whence

$$\kappa_0 \approx \cos(k^{[1]}h_1 + k^{[2]}h_2) , \quad \sigma_0 \approx \sin(k^{[1]}h_1 + k^{[2]}h_2) . \quad (108)$$

Thus,  $\mathcal{E}_{00}$  is minimal when  $\cos(k^{[1]}h_1 + k^{[2]}h_2) = 0$  which occurs for

$$k^{[1]}h_1 + k^{[2]}h_2 = (2L + 1)\frac{\pi}{2} ; L = 0, 1, 2, \dots , \quad (109)$$

or for

$$f_L = \frac{2L + 1}{4 \left( \frac{h_1}{\beta^{[1]}} + \frac{h_2}{\beta^{[2]}} \right)} ; L = 0, 1, 2, \dots , \quad (110)$$

which are the  $M = 0$  approximation of the resonance frequencies for the scattering configuration: (a) under the assumption (107), and (b) at low driving frequency (i.e.,  $2\pi f/\beta^{[0]} << 1$ ) and/or narrow AGS's (i.e.,  $w << 1$ ). The condition  $w << 1$  means that the convex rectangular protuberance resembles a (thin) wall, and since we are dealing with shear motion, the  $f_L$  are often termed the shear wall resonance frequencies, usually, in connection with a homogeneous (with respect to the wavespeed and shear modulus) feature such that  $\frac{h_1}{\beta^{[1]}} + \frac{h_2}{\beta^{[2]}} = \frac{h}{\beta^{[1]}}$  and  $\frac{\mu^{[2]}\beta^{[1]}}{\mu^{[1]}\beta^{[2]}} - 1 = 0$  whose consequences are

$$f_L^{SWR} = \frac{(2L + 1)\beta^{[1]}}{4h} ; L = 0, 1, 2, \dots , \quad (111)$$

which are more properly termed the 'homogeneous shear wall resonance (HSWR) frequencies'. Finally,  $f_0 = \frac{\beta^{[1]}}{4h}$  is often termed the fundamental resonance frequency (or just the fundamental frequency) of the protuberance.

Some comments are in order concerning these resonances. Strictly speaking, they can occur only when the media in the protuberance are non-lossy (i.e., the wavespeeds therein are real), in

which case  $\mathcal{E}_{00}$  is strictly  $=0$  at  $f = f_L$ , this meaning that  $\mathcal{F}_0$ , and therefore  $d_0$  blow up at the resonance frequencies  $f = f_L$ . There are two reasons why this never occurs. The first is that all real materials are lossy, even slightly-so, so that  $\mathcal{E}_{00} \neq 0$  at  $f = f_L$  or even near  $f_L$ . The second reason is that the diffraction coefficient  $\mathcal{F}_0^{(0)}$  defined in (96), with  $\mathcal{E}_{00}$  therein replaced by its asymptotic form  $\kappa_0/\sigma_0$ , is only an approximation of  $\mathcal{F}_0$  that takes no account of radiation damping. In fact, the replacement of  $\mathcal{E}_{00}$  by its  $k^{[0]}w \rightarrow 0$  asymptotic form has (as we shall see further on in the numerical results) important consequences, notably concerning the location of the resonance frequencies. The reason why we invoked the asymptotic analysis was simply to establish the connection of our investigation with the more-traditional ones based on shear-wall, or mass-spring type resonator paradigms [320, 156, 373, 318, 157]. This means, that the correct equation for finding the zeroth-order approximation of the resonance frequencies is  $D^{(0)}(\omega) = 0$  (for complex  $\omega$ ) or  $\omega = \arg \min D^{(0)}$  (for real  $\omega$ ) wherein  $E_{00}$  is given by its exact expression  $E_{00} = \kappa_0 - \frac{iw}{2\pi} \frac{\mu^{[1]}}{\mu^{[0]}} k_{y0}^{[1]} \sigma_0 J_{00}$ .

Moreover, the same principle holds for higher-order (i.e.,  $M > 0$ ) approximations of the resonance frequencies: the matrix equation to deal with is  $\mathcal{E}^{(M)} \mathcal{F}^{(M)} = \mathcal{G}$  with the understanding that the  $M$ -th order approximation of the resonance frequencies are those that correspond to minima of  $D^{(M)} = \det \mathbf{E}^{(M)}$ . As stated briefly previously, by taking  $M > 0$ , we expect to find a whole new set of resonances that might show up as large values of the diffraction coefficients of order greater than zero. This will be demonstrated numerically further on, after treating in more detail the issue of coupling to a resonance.

### 7.6.2 Coupling to a HSWR resonance

Coupling to a resonance means: (a) obtaining the vector  $\mathbf{d}$  of diffraction coefficients at the resonance frequency and (b) determining the field in and on the convex surface feature (and eventually on and beneath the flat portions of ground) from  $\mathbf{d}$  at the resonant frequency. We shall first examine coupling to the HSWR resonance because it encompasses some of the features of coupling to more complicated resonances.

The point of departure is the relation  $\mathcal{F}_0^{(0)}(f) = \frac{\mathcal{G}(f)}{\mathcal{E}_{00}(f)}$ , and because  $\mathcal{F}_0^{(0)}(f) = d_0^{(0)}(f)\sigma_0$

$$d_0^{(0)}(f) = \frac{\mathcal{G}(f)}{\sigma_0(f)\mathcal{E}_{00}(f)} . \quad (112)$$

We found previously that  $\sigma_0(f)\mathcal{E}_{00}(f) \sim \kappa_0(f)$ ;  $k^{[0]}w \rightarrow 0$  and  $\mathcal{G}(f) = 2a^i I_0^+(k_x^i) = 2a^i \text{sinc}(k_x^i w/2) \sim 2a^i$ ;  $k^{[0]}w \rightarrow 0$ , so that

$$d_0^{(0)}(f) \sim \frac{2a^i(f)}{\kappa_0(f)} = \frac{2a^i(f)}{\cos\left(\frac{2\pi fh}{\beta^{[1]}}\right)} ; k^{[0]}w \rightarrow 0 , \quad (113)$$

which shows that the diffraction amplitude  $d_0^{(0)}(f)$  is not only conditioned by the resonant factor  $1/\cos\left(\frac{2\pi fh}{\beta^{[1]}}\right)$ , but also by the spectral amplitude  $a^i(f)$  of the solicitation, so that

$$d_0^{(0)}(f_L^{HSWR}) = \frac{2a^i(f_L^{HSWR})}{\cos\left((2L+1)\pi/2\right)} ; L = 0, 1, 2, \dots , \quad (114)$$

which is all the larger (it is infinite as it stands, but, because of the material losses and/or radiation damping, actually finite) the larger is  $a^i(f_L^{HSWR})$ . Thus, coupling to the HSWR resonance is conditioned by the spectral amplitude  $a_i(f)$  at the resonant frequency.

We now examine coupling to the fields at resonance. Within the rectangular-shape protuberance the zeroth-order approximation to the field is

$$u^{[1](0)}(x, y; f) = d_0^{(0)}(f) \cos\left(\frac{2\pi f}{\beta^{[1]}}(y - h)\right), \quad (115)$$

which shows that: (1) the field does not depend on  $x$  within the protuberance whatever the frequency  $f$ , and (2) the field is maximal at the top ( $z = h$ ) of the surface feature whatever be  $f$ . It follows that

$$u^{[1](0)}(x, 0; f) = d_0^{(0)}(f) \kappa_0 \sim 2a^i(f); \quad k^{[0]}w/2 \rightarrow 0, \quad (116)$$

which shows that the field at the base of the protuberance is asymptotically the same as what it would be in the absence of the said feature, this being true for all (low frequency)  $f$ . This result is paradoxical because if the base of the protuberance is impervious to the incident wave, it is impossible for it to penetrate into the said surface feature. As we shall see hereafter, this paradox disappears as soon as the asymptotic analysis is dropped. In any case, with the adoption of the approximations embodied in (116), we see that

$$\|u^{[1](0)}(x, h; f_L^{HSWR})\| = \|2a_i(f_L^{HSWR})\|; \quad L = 0, 1, 2, \dots, \quad (117)$$

which tells us that coupling to the HSWR does not result in any amplification or deamplification of the top displacement field of the convex rectangular-shape surface feature. This also means that the field (actually its modulus) within the homogeneous shear wall is not amplified at the HSWR resonance frequency since this field is inferior or equal to the field at the top of the HSW.

### 7.6.3 Coupling to resonances when the $k^{[0]}w \rightarrow 0$ asymptoticity is not assumed

The first task is to determine  $d_0^{(0)}(f)$  at, or near resonance, starting from (96):

$$d_0^{(0)}(f) = \frac{\mathcal{G}_0(f)}{\mathcal{E}_{00}(f)\sigma_0(f)} = \frac{c_0(f)}{E_{00}(f)}, \quad (118)$$

$$\mathcal{E}_{00}(f) = \frac{\kappa_0(f)}{\sigma_0(f)} - i \frac{\mu^{[1]\beta^{[0]}}}{\mu^{[0]\beta^{[1]}}} \left[ C_0(k^{[0]}w) - \frac{1}{k^{[0]}w} \mathcal{A}_0(k^{[0]}w) \right], \quad (119)$$

$$\mathcal{G}_0(f) = 2a^i(f)I_0^+(k_x^i) = 2a^i(f)\text{sinc}(k_x^i w/2). \quad (119)$$

As stated previously, the resonance frequencies  $f_L$  are those frequencies for which  $\|E_{00}(f)\|$  is minimal. These frequencies are all the closer to  $f_L^{SWR}$  the smaller (in absolute value) is the second term  $i \frac{\mu^{[1]\beta^{[0]}}}{\mu^{[0]\beta^{[1]}}} \left[ C_0(k^{[0]}w) - \frac{1}{k^{[0]}w} \mathcal{A}_0(k^{[0]}w) \right]$  relative to the first term  $\frac{\kappa_0(f)}{\sigma_0(f)}$  in  $\mathcal{E}_{00}$ . Moreover, the presence of this second term (which is complex) in  $\mathcal{E}_{00}$  is the reason why the so-obtained  $d_0^{(0)}(f_L)$ ;  $L = 0, 1, \dots$  are not infinite. Thus, resonant coupling of  $d_0^{(0)}(f)$  manifests itself by a relatively-large, but finite, value of this diffraction coefficient at the resonant frequency  $f_L$ . We note also that not only is this coupling more efficient, due to the proximity of the resonance frequency to the frequency of the maximum of  $a^i(f)$ , but also to the proximity of  $f_L$  to  $f = 0$  (due to the fact that the sinc function is maximum when its argument is nil).

The second aspect of resonant coupling has to do with the field at resonance within the protuberance. As previously, we have

$$u^{[1](0)}(x, y; f) = d_0^{(0)}(f) \cos\left(\frac{2\pi f}{\beta^{[1]}}(y - h)\right), \quad (120)$$

which again shows that: (1) the field does not depend on  $x$  within the protuberance whatever the frequency  $f$ , and (2) the field is maximal at the top ( $z = h$ ) of the protuberance whatever be  $f$ . It follows that

$$u^{[1](0)}(x, 0; f) = d_0^{(0)}(f) \kappa_0, \quad (121)$$

which indicates that the field at the base of the protuberance is no longer the same as what it would be in the absence of the said protuberance, this being true for all  $f$  including the resonant frequencies. This result means, as one would expect, that the base segment of the protuberance is no longer impervious to the incident wave, thus making it possible for the incident wave to penetrate into the said protuberance.

The last, all-important, feature of (120), is that

$$\|u^{[1](0)}(x, h; f_L)\| \geq \|2a_i(f_L)\|; \quad L = 0, 1, 2, \dots, \quad (122)$$

due to the fact that  $\|d_0^{(0)}(f_L)\| \geq \|2a^i(f_L)\|$ . This means that coupling to a resonance generally results in amplification of the top displacement field of the rectangular-shape protuberance (with respect to its value on flat ground). However, this amplification does not necessarily occur at other heights within the protuberance due to the presence of the  $\cos$  term in (120).

## 7.7 Resonances from the point of view of the $M = 1$ approximation

The  $M = 1$  approximation of the diffraction coefficient vectors  $\mathcal{F}$  and  $\mathbf{d}$  originates in the linear system(s):

$$\begin{aligned} \mathcal{E}_{00}\mathcal{F}_0^{(1)} + \mathcal{E}_{01}\mathcal{F}_1^{(1)} &= \mathcal{G}_0 \\ \mathcal{E}_{10}\mathcal{F}_0^{(1)} + \mathcal{E}_{11}\mathcal{F}_1^{(1)} &= \mathcal{G}_1 \end{aligned} \iff \begin{aligned} E_{00}d_0^{(1)} + E_{01}d_1^{(1)} &= c_0 \\ E_{10}d_0^{(1)} + E_{11}d_1^{(1)} &= c_1 \end{aligned}, \quad (123)$$

the latter of whose solution is

$$d_0^{(1)} = \frac{c_0 E_{11} - c_1 E_{01}}{E_{00} E_{11} - E_{10} E_{01}}, \quad d_1^{(1)} = \frac{c_1 E_{00} - c_0 E_{10}}{E_{00} E_{11} - E_{10} E_{01}}, \quad (124)$$

from which we see that resonant coupling to two diffraction coefficients is possible due to the fact that both are affected by the resonances(s) resulting from the minima of the function  $\|D^{(1)}\|$  wherein

$$D^{(1)} = E_{00} E_{11} - E_{10} E_{01}. \quad (125)$$

However, the fact that the numerators in (124) are different, the coupling to  $d_0^{(1)}$  is not necessarily as efficient as the coupling to  $d_1^{(1)}$ , which means that one or the other, or even both, of these coefficients are not necessarily large at resonance. Another feature of (124), which will be demonstrated numerically further on, is that due to the fact that  $D^{(1)}$  is a more complicated function than  $D^{(0)} = E_{00}$ , notably at relatively-high frequencies, the number of resonant frequencies associated with  $D^{(1)}$  is larger than those associated with  $D^{(0)}$ . Finally, (even) the lower-frequency resonances associated with  $D^{(1)}$  occur at frequencies that are different from the resonant frequencies associated

with  $D^{(0)}$ , which fact shows that generally, *one cannot correctly describe the resonances of the configuration by basing the description on the sole  $M = 0$  approximation.*

Another important aspect of resonant coupling to  $\mathbf{d}^{(1)}$  is the fact that it depends not only on the driving term  $c_0$  but also on  $c_1$ . Both of these are functions of  $a^i(f)$  so that the previous comments concerning the influence of this factor remain true, but they also depend on the sinc functions contained in  $I_l^+(k_x^i)$  and it is possible, for non-normal incidence, that  $\|I_1^+(k_x^i)\| > \|I_0^+(k_x^i)\|$  so as to make the coupling to  $\mathbf{d}^{(1)}$  become larger at non-normal incidence than at normal incidence, contrary to the case of resonant coupling to  $\mathbf{d}^{(0)}$  in which the envelope of  $\|I_0^+(k_x^i)\|$  diminishes with increasing incident angle. This possibility will be illustrated numerically further on.

Next, consider the resonant coupling to the field within the protuberance. To simplify the message that we want to bring across, we choose the case of a homogeneous protuberance, i.e.,  $M^{[2]} = M^{[1]}$ . The  $M = 1$  approximation of the field within the protuberance is then

$$u^{[2](1)}(x, y; f) = d_0^{(1)}(f) \cos(k_{y0}(y - h)) + d_1^{(1)}(f) \cos(k_{x1}(x + w/2)) \cos(k_{y1}(y - h)) , \quad (126)$$

from which we observe that, contrary to what occurs in the zeroth-order approximation of the field, now the  $M = 1$  approximation thereof: (1) depends on the  $x$  coordinate, 2) is not necessarily-maximal at  $y = h$ , and 3) the  $x - y$  pattern of resonant response can be dominated by the second term in (126) if, as is possible (see the comments a few lines back),  $d_1(f)$  dominates  $d_0(f)$  at a resonant frequency. The  $x - y$  pattern of response can be even more involved when both  $d_1(f)$  and  $d_0(f)$  are influential at a resonant frequency and even be such that the field is not amplified at most of the locations within the protuberance. These observations, which will be illustrated by the numerical results offered further on, again underline the absolute necessity of going beyond  $M = 0$  to correctly predict the seismic response of the hill or mountain, this being especially so if one wants to account for coupling to other than the fundamental mode resonance (i.e., the one that occurs at the lowest frequency, corresponding to the  $L = 0$  HSWR when the convex feature resembles a homogeneous shear wall).

## 7.8 Resonances from the point of view of the $M > 1$ approximations

Needless to say, essentially everything that was written for the  $M = 1$  approximation holds for the  $M > 1$  approximations of resonant response. This will be illustrated in the numerical examples which follow. The latter will show that the possibility of a resonance, manifested by a small value of  $\|D(f)\|$  at a so-called resonant frequency  $f^R$ , does not guarantee that the response will be amplified considerably and/or at all locations of the hill or mountain because of the interplay of the resonant diffraction coefficients (themselves depending on the spectrum of the solicitation) with the geometric factors (i.e., that depend on the  $x, y$  coordinates) contained in the SOV representation of the displacement field. In other words: significant amplification of this field at  $f^R$  requires (i.e., is a necessary condition for) the existence of a resonance at  $f^R$ , but is not a sufficient condition for this amplification to manifest itself (this manifestation depending heavily on the spectral attributes and incident angle of the solicitation, as well as on the location at which the field is sensed).

## 8 Numerical resolution of the linear system of equations

The first task is to obtain numerically the set  $\{\mathcal{F}_m\}$  from the linear system of equations (94). Once this set is found, it is introduced into  $d_m = \frac{\mathcal{F}_m}{\sigma_m}$  to get  $\{d_m\}$ , and into (22), (23), (24) to

obtain the sets  $\{a_m\}$ ,  $\{b_m\}$ ,  $\{\mathcal{B}(k_x)\}$ . When all these coefficients (we mean those whose values depart significantly from zero) are found, they enable the computation of the seismic response (i.e., the displacement field) in all the subdomains of the site and city via (90), (92), (97) and (99) (in the last two expressions, the sums are taken from  $m = 0$  to  $m = M$ ,  $M$  a finite, relatively-small integer defined hereafter).

Concerning the resolution of the infinite system of linear equations (94), the approach is basically to replace it by the finite system of linear equations

$$\sum_{m=0}^M \mathcal{E}_{lm} \mathcal{F}_m^{(M)} = \mathcal{G}_l ; \quad l = 0, 1, 2, \dots, M , \quad (127)$$

in which the superscript  $(M)$  signifies the  $M$ -th order approximation of  $\mathcal{F}_m$  obtained via (127), the procedure being to increase  $M$  so as to generate the sequence of numerical solutions  $\{F_0^{(0)}\}$ ,  $\{F_0^{(1)}, F_1^{(1)}\}, \dots$  until the values of the first few members of these sets stabilize and the remaining members become very small. This is usually obtained for reasonably-small values of  $M$ , especially in the low frequency regime of interest in our seismic response problem.

The so-obtained numerical solutions (which are henceforth based on the assumption  $a^i(\omega) = 1 ; \forall \omega \geq 0$ ) were found to: i) reproduce the theoretical solution for VS configurations, ii) satisfy the conservation of flux relation [358] with an error of less than a half percent for all  $M \geq 0$ , and iii) be in agreement with numerical results obtained by a finite element method [120, 126], so that they can be considered, for all practical purposes, to be 'exact'. This issue will benefit from supplementary comments further on.

## 9 Seismic response from stress-free boundary irregularities in the sense of Sills and beyond

### 9.1 Comparison with the numerical results of Sills

The publication [306] represents one of the earliest efforts to compute, as exactly as possible, the seismic response of a hill, assumed by Sills to be of semi-circular shape, radius  $h$  and (homogeneous) composition identical to that of the underlying half space. This was achieved by a boundary integral equation numerical scheme to show that the so-obtained amplifications are the result of stress-free boundary irregularities. Due to their quasi-rigorous nature, these numerical results provide a means of comparison with our own results, especially by giving evidence of the universal nature of the fundamental hill resonance (in the sense that it occurs for a variety of hill shapes).

It is interesting to cite what is written by Sills in [306] about these graphs (our figs. 3 and 4 corresponding to his figs. 13 and 11 respectively), the first of which applies to the responses, for  $\theta^i = 30^\circ, 60^\circ, 90^\circ$ , at the midpoint of the top segment of the hill ( $x = 0, y = h$  in our notation) and the second to the responses, for the same incident angles, at the bottom left-hand corner of the protuberance ( $x = -h, y = 0$  in our notation):

"The rapidly varying displacement amplitude indicates a complex constructive and destructive interference pattern which results from the presence of the irregularity.... On the other hand, for vertical incidence the energy appears to have been focused toward the top of the hill (Fig. 13) resulting in rather high amplifications. In particular, for a frequency of approximately 1, the

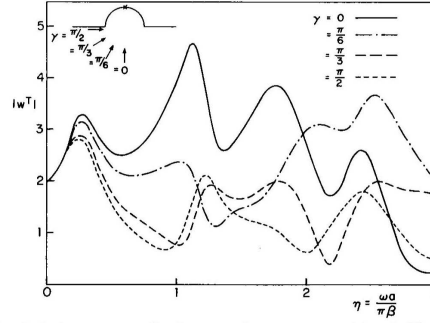


Figure 13. Graph of displacement amplitude versus frequency at position 4 (Fig. 8,  $\theta = \pi/2$ ) for the semicircular hill; four angles of incidence:  $\gamma = 0, \pi/6, \pi/3, \pi/2$ .

Figure 3: Sills' results for the total displacement field  $\|u\|$  at the top of a semi-circular hill for various incident angles.

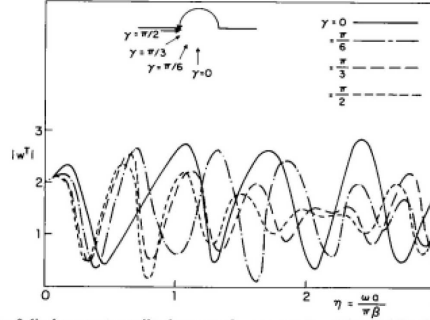


Figure 11. Graph of displacement amplitude versus frequency at position 2 (Fig. 8,  $\theta = \pi$ ) for the semicircular hill; four angles of incidence:  $\gamma = 0, \pi/6, \pi/3, \pi/2$ .

Figure 4: Sills' results for the total displacement field  $\|u\|$  at the left-hand corner of a semi-circular hill for various incident angles.

displacement is almost 2.5 times greater than that which is expected in the case of a featureless topography.... It is quite clear from these graphs that the displacement amplitude is highly dependent upon angle of incidence and frequency, as well as position along the boundary. Hence one cannot conclude on the basis of these graphs that either amplification or de-amplification will always occur at a certain position on this type of irregularity. One can conclude however, that the irregularity does have an effect, which appears profound in this case, and should be accounted for when analyzing earthquakes in regions of irregular topography."

What Sills means by 'vertical incidence' is (in our notation)  $\theta^i = 0^\circ$ , and by 'frequency' actually  $\frac{k^{[0]}h}{\pi} = \frac{\omega h}{\beta^{[0]}\pi}$ . Note that he makes *no evocation of resonances*, but rather of "rapidly varying displacement" which he attributes to "complex constructive and destructive interference" nevertheless associated with "the presence of the irregularity".

The fact that the location of the first peak in Sills' two figures does not seem to depend on the incident angle is an indication that we are actually in presence of what we previously termed the fundamental mode resonance at this frequency, this not being in contradiction with the fact that



their corner peak appears at a frequency that is lower than their summit peak (or what amounts to the same, the response at the corner is lower than at the summit, at the frequency of maximal summit response, in agreement with our prediction for the resonant response of a rectangular hill).

Let us attempt a more quantitative comparison with our own numerical results for a rectangular-shaped hill. Actually, it appeared to us to be most appropriate for this sake to choose our hill to be of height  $h = 250 \text{ m}$  and width  $w = 2h = 500 \text{ m}$  (which minimally- circumscribes Sills' semi-circular hill. Since the latter is homogeneous, lossless and composed of the same material as that of the underground, we chose  $\beta^{[2]} = \beta^{[1]} = \beta^{[0]}$  and  $\mu^{[2]} = \mu^{[1]} = \mu^{[0]}$  and somewhat arbitrarily  $\beta^{[0]} = 1629.4 \text{ ms}^{-1}$  and  $\mu^{[0]} = 6.85 \text{ MPa}$  corresponding to a density  $\rho^{[0]} = 2580.1 \text{ Kgm}^{-3}$  which is close to the Bouguer density  $2670 \text{ Kgm}^{-3}$  (itself in the range  $2650 - 2750 \text{ Kgm}^{-3}$  of granite density).

### 9.1.1 Our computed transfer functions and $1/D$ for $\theta^i = 0^\circ$

Figs. 5-8 depict our computed transfer functions  $T^{(M)}(x, y; f) = u(x, y; f)/a^i(\omega)$  and  $1/D^{(M)}(\omega)$  for incident angle  $\theta^i = 0^\circ$  and for various approximation orders  $M$ .

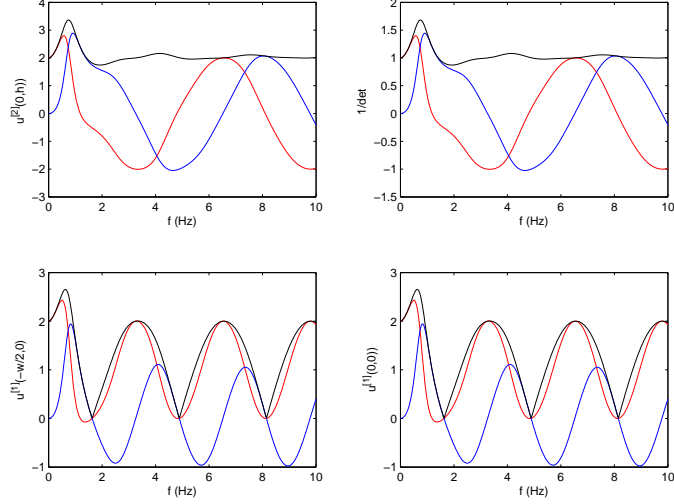


Figure 5: The lower right panel is for  $T^{(M)}(0, 0; f)$ , the lower left panel for  $T^{(M)}(-w/2, 0; f)$  and the upper left panel for  $T^{(M)}(0, h = h_2; f)$  whereas the upper right panel depicts  $1/D^{(M)}(\omega)$ , with  $D^{(M)}$  the determinant of the  $(M + 1)$ -by- $(M + 1)$  matrix equation involved in the computation of the modal coefficient vector  $\mathbf{d}^{(M)}$ . The red curves are relative to the real part, the blue curves to the imaginary part and the black curves to the absolute value.  $\beta^{[1]} = \beta^{[0]} = 1629.4 \text{ m s}^{-1}$  and  $\mu^{[1]} = \mu^{[0]} = 6.85 \text{ MPa}$ . Case  $h_1 = 250 \text{ m}$ ,  $h_2 = 0 \text{ m}$ ,  $w = 500 \text{ m}$ .  $\theta^i = 0^\circ$ ,  $\mathbf{M} = \mathbf{0}$ .

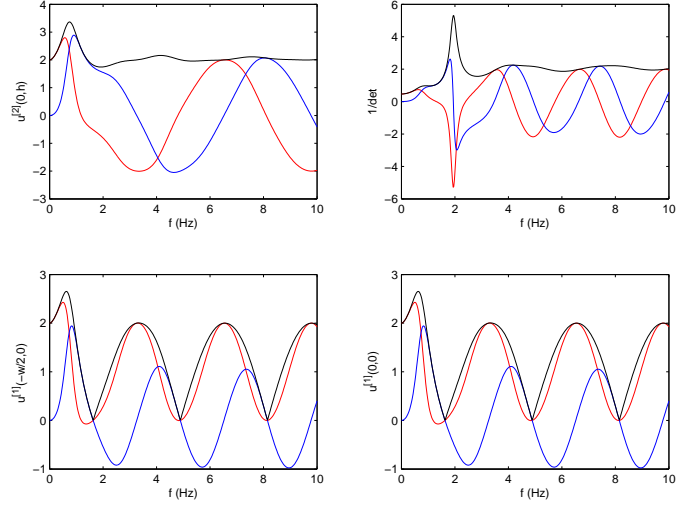


Figure 6:  $\theta^i = 0^\circ$ . Same as fig. 5 except that  $\mathbf{M} = \mathbf{1}$ .

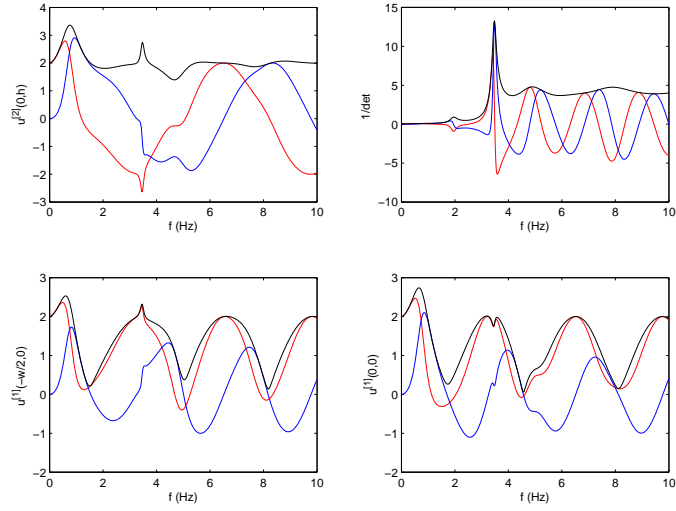


Figure 7:  $\theta^i = 0^\circ$ . Same as fig. 5 except that  $\mathbf{M} = \mathbf{2}$ .

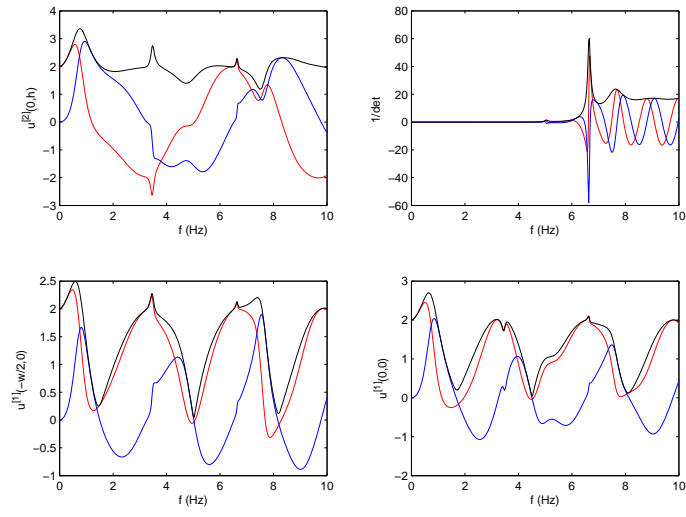


Figure 8:  $\theta^i = 0^\circ$ . Same as fig. 5 except that  $\mathbf{M} = 4$ .

### 9.1.2 Our computed transfer functions and $1/D$ for $\theta^i = 30^\circ$

Figs. 9-13 depict our computed transfer functions  $T^{(M)}(x, y; f) = u(x, y; f)/a^i(\omega)$  and  $1/D^{(M)}(\omega)$  for incident angle  $\theta^i = 30^\circ$  and for various approximation orders  $M$ .

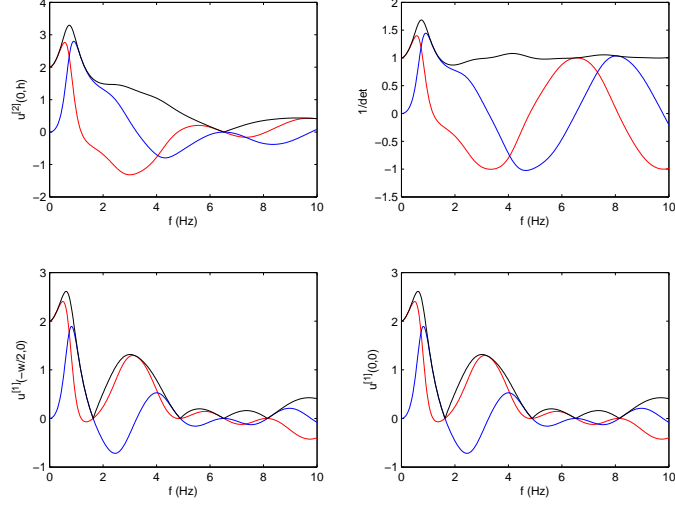


Figure 9:  $\theta^i = 30^\circ$ . Otherwise, same as fig. 5 except that  $\mathbf{M} = \mathbf{0}$ .

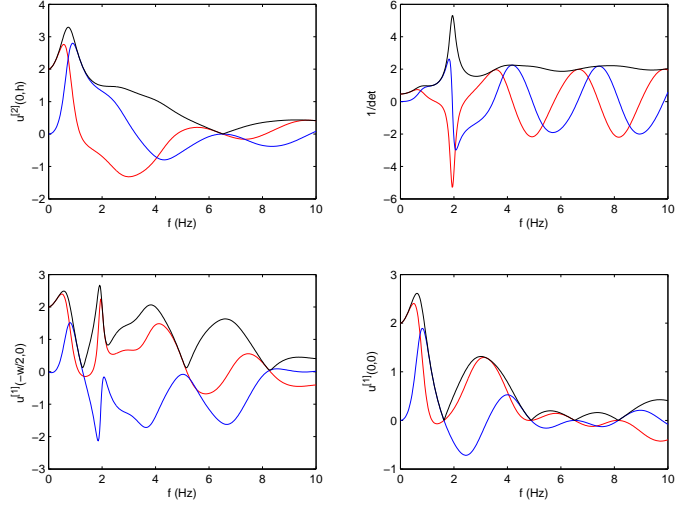


Figure 10:  $\theta^i = 30^\circ$ . Otherwise, same as fig. 5 except that  $\mathbf{M} = \mathbf{1}$ .

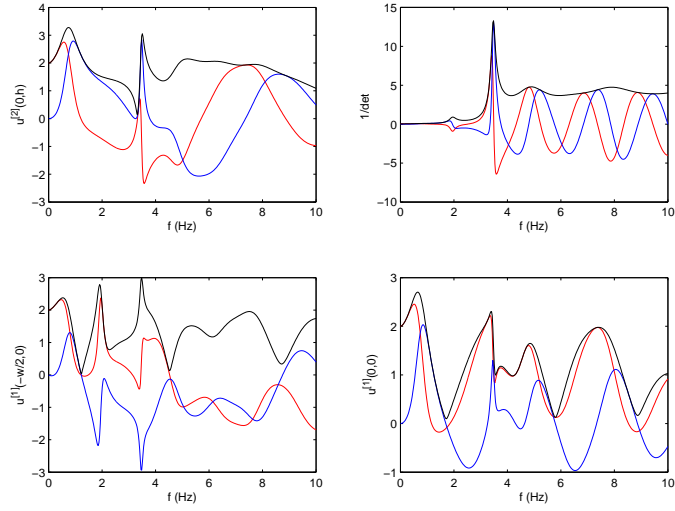


Figure 11:  $\theta^i = 30^\circ$ . Otherwise, same as fig. 5 except that  $\mathbf{M} = \mathbf{2}$ .

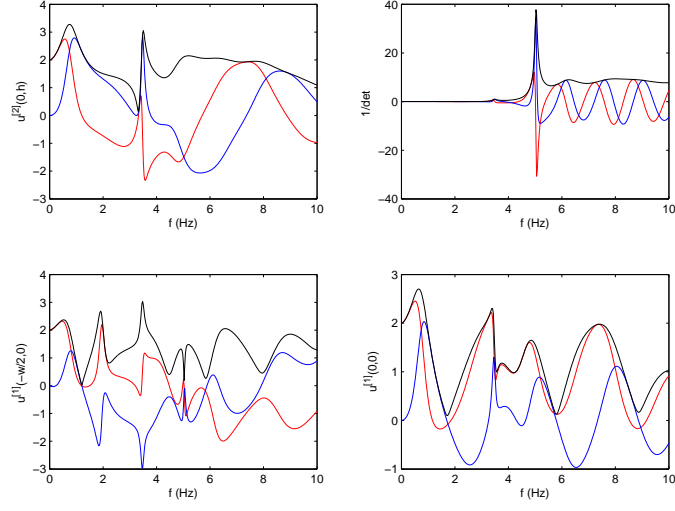


Figure 12:  $\theta^i = 30^\circ$ . Otherwise same as fig. 5 except that  $\mathbf{M} = \mathbf{3}$ .

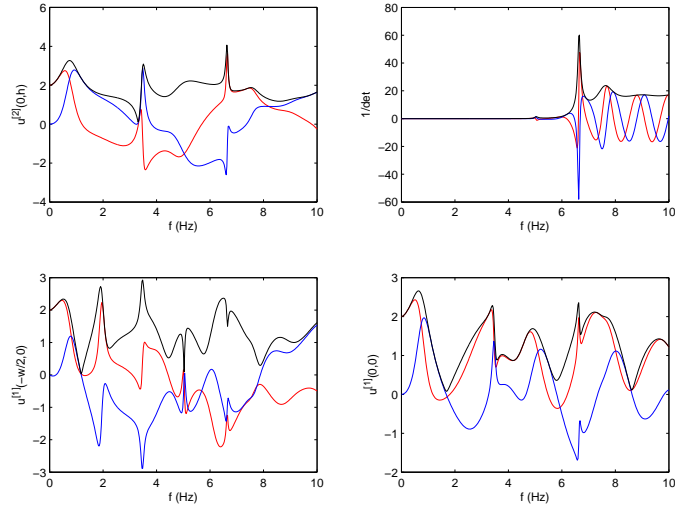


Figure 13:  $\theta^i = 30^\circ$ . Otherwise same as fig. 5 except that  $\mathbf{M} = \mathbf{4}$ .



### 9.1.3 Our computed transfer functions and $1/D$ for $\theta^i = 60^\circ$

Figs. 14-13 depict our computed transfer functions  $T^{(M)}(x, y; f) = u(x, y; f)/a^i(\omega)$  and  $1/D^{(M)}(\omega)$  for incident angle  $\theta^i = 60^\circ$  and approximation order  $M = 4$ .

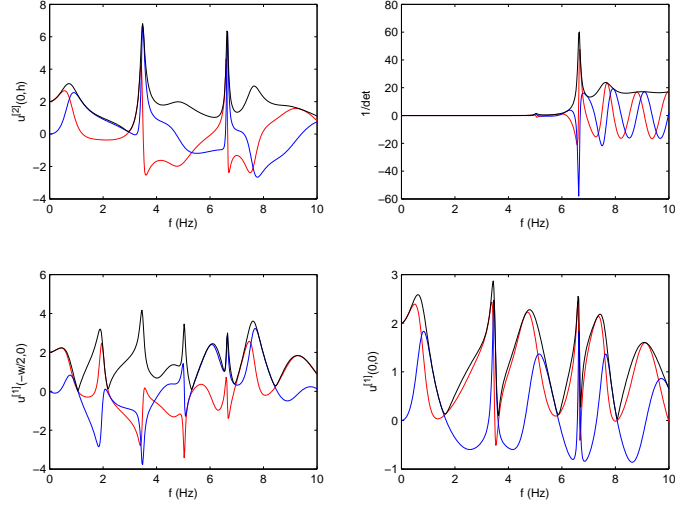


Figure 14:  $\theta^i = 60^\circ$ . Otherwise, same as fig. 5 except that  $\mathbf{M} = 4$ .

#### 9.1.4 Discussion

Note the rapid stabilization of the transfer functions as  $M$  is increased, this setting in more rapidly at low than at higher frequencies. Note the resemblance (position and height) of our first peak of the summit response to the one of Sills. This agreement is somewhat less true concerning the first peak of the left corner response, and the disagreement increases for both the summit and left corner succeeding peaks. Note that the shape of the  $\|1/D(f)\|$  (particularly evident for the first and second) peaks is lorentzian and thus evocative of resonances. Moreover, the positions of the peaks of  $\|1/D(f)\|$  in these figures do not vary with incident angle, which fact is another characteristic of surface shape resonances. We also find that the  $m$ -th peak does not appear in  $\|1/D^{(M)}(f)\|$  for  $M < m$  and its position does not vary for  $M \geq m$ . Thus, it seems reasonable to assume that Sills' peaks of summit and corner response are due to the excitation of surface shape resonances. This will be further substantiated (for our rectangular Sills-like hill) further on.

### 9.2 Beyond Sills: seismic response within the rectangular version of Sills' hill at the first five resonant frequencies

Recall that Sills' graphs relate to the response at locations exclusively *on the stress-free boundary* of the hill and ground. In fact, practically all studies (both theoretical/numerical and empirical) of seismic response of hills and mountains are of the same nature (i.e., they do not pertain to the field *within* the convex feature, which is much harder to measure than the field on the protuberance surface) and they either ignore, or do not make clear, the relation of amplified response to the occurrence of resonances. As we shall discover hereafter, a look at the field within the convex feature, at various frequencies that we are sure are resonance frequencies, will make it clear that *amplified response is indeed associated with coupling to surface shape resonances*.

The graphs (figs. 5-14) of  $\|1/D^{(4)}(f)\|$  showed that the first five resonant frequencies for this hill are: 0.7592 Hz, 1.958 Hz, 3.482 Hz, 5.030 Hz, 6.628 Hz. In figs. 15-30 we display the computed displacement field within this hill at these four frequencies for incident angles  $\theta^i = 0, 30, 60, 80^\circ$ . In the caption of each figure, we also give the corresponding first six entries of the diffraction coefficient vector  $\mathbf{d}$ . Recall that:  $\beta^{[1]} = \beta^{[0]} = 1629.4 \text{ ms}^{-1}$  and  $\mu^{[1]} = \mu^{[0]} = 6.85 \text{ MPa}$ .  $h_1 = 250 \text{ m}$ ,  $h_2 = 0 \text{ m}$ ,  $w = 500 \text{ m}$ , and we shall take  $M = 5$ .

#### 9.2.1 Displacement field graphs for $\theta^i = 0^\circ$

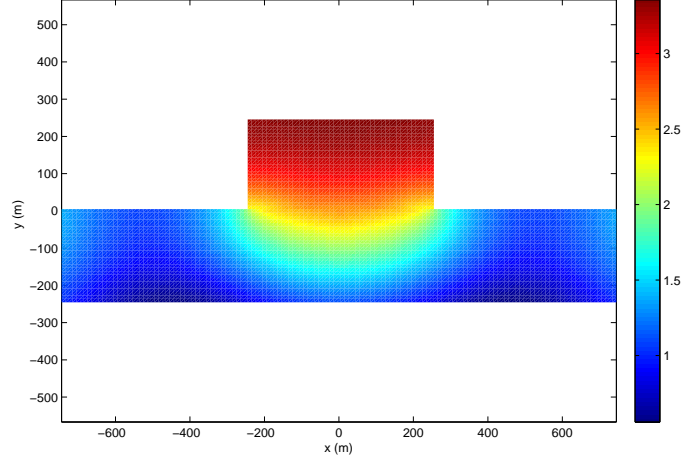


Figure 15: Map of the modulus of  $T^{(5)}(x, y; \mathbf{f} = \mathbf{0.7592 \text{ Hz}})$  for  $\theta^i = 0^\circ$ .  $\mathbf{d}^{(5)} = \{2.2835 + 2.4412i, 0.0000 - 0.0000i, -0.0072 - 0.0136i, -0.0000 + 0.0000i, -0.0001 - 0.0002i, 0.0000 - 0.0000i\}$ .

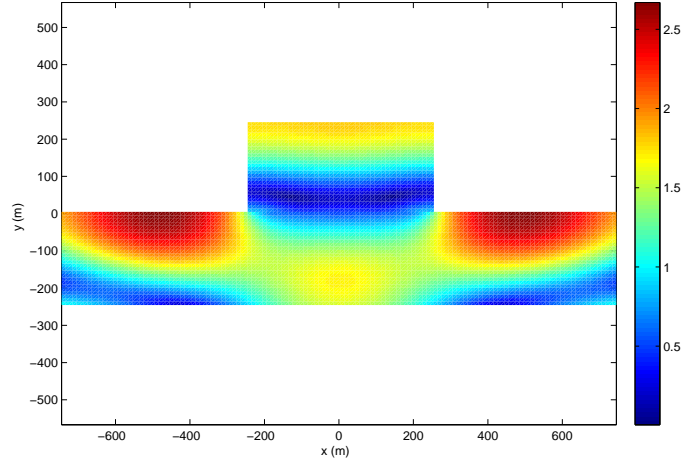


Figure 16: Map of the modulus of  $T^{(5)}(x, y; \mathbf{f} = \mathbf{1.958 \text{ Hz}})$  for  $\theta^i = 0^\circ$ .  $\mathbf{d}^{(5)} = \{-0.8614 + 1.5748i, -0.0000 + 0.0000i, 0.0575 - 0.0027i, -0.0000 - 0.0000i, 0.0004 - 0.0001i, 0.0000 - 0.0000i\}$ .

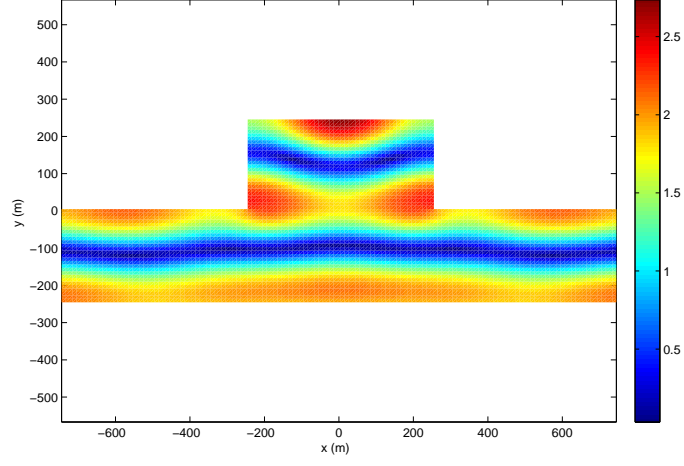


Figure 17: Map of the modulus of  $T^{(5)}(x, y; \mathbf{f} = \mathbf{3.482 \text{ Hz}})$  for  $\theta^i = 0^\circ$ .  $\mathbf{d}^{(5)} = \{-2.0516 - 0.4222i, -0.0000 - 0.0000i, 0.5326 + 0.4933i, -0.0000 - 0.0000i, -0.0003 - 0.0003i, -0.0000 - 0.0000i\}$ .

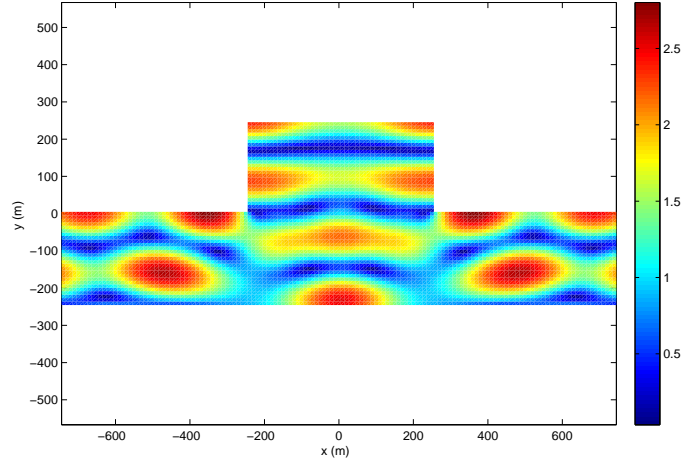


Figure 18: Map of the modulus of  $T^{(5)}(x, y; \mathbf{f} = \mathbf{5.030 \text{ Hz}})$  for  $\theta^i = 0^\circ$ .  $\mathbf{d}^{(5)} = \{0.4552 - 1.9221i, 0.0000 + 0.0000i, 0.4901 - 0.3430i, -0.0000 - 0.0000i, 0.0118 - 0.0024i, 0.0000 + 0.0000i\}$ .

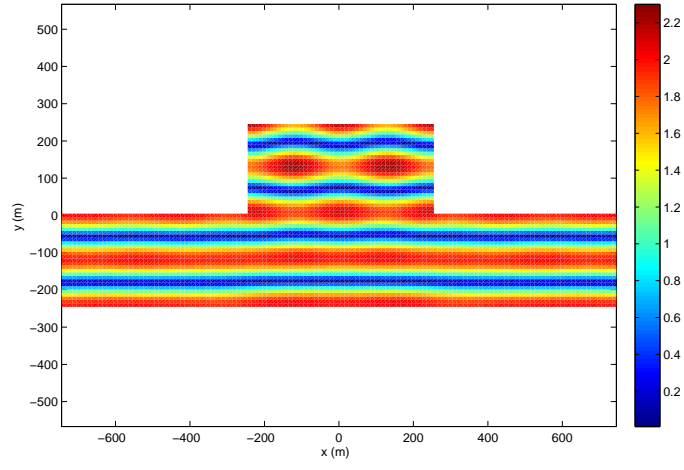


Figure 19: Map of the modulus of  $T^{(5)}(x, y; \mathbf{f} = \mathbf{6.628 \text{ Hz}})$  for  $\theta^i = 0^\circ$ .  $\mathbf{d}^{(5)} = \{2.0058 + 0.2015i, 0.0000 - 0.0000i, 0.0197 - 0.0380i, 0.0000 + 0.0000i, 0.2787 + 0.0818i, -0.0000 - 0.0000i\}$ .

These figures show that the resonant coupling to (and therefore the amplification of) the fields within the hill is rather weak at all five resonant frequencies when the incident angle is  $\theta^i = 0^\circ$ . This can be appreciated by the recollection of the fact that the value of the transfer function on the stress-free boundary of flat ground (i.e., in the absence of the protuberance) is 2.

Other features of these figures are that: 1) the field is maximal on the top, and independent of  $x$  throughout most of the protuberance, at the lowest-frequency resonance, this being in agreement with the previous discussion on the  $M = 0$  approximation, 2) the field is progressively-more inhomogeneous as the resonance frequency increases, except (see fig. 19) when something similar to the VS conditions are satisfied, 3) at all but the second and fourth of these figures, the field can be greater at locations outside of the protuberance, than within and on the top of, the protuberance. This is in agreement with some empirically-observed results [70] in environments wherein the hill is actually a building.

### 9.2.2 Displacement field graphs for $\theta^i = 30^\circ$

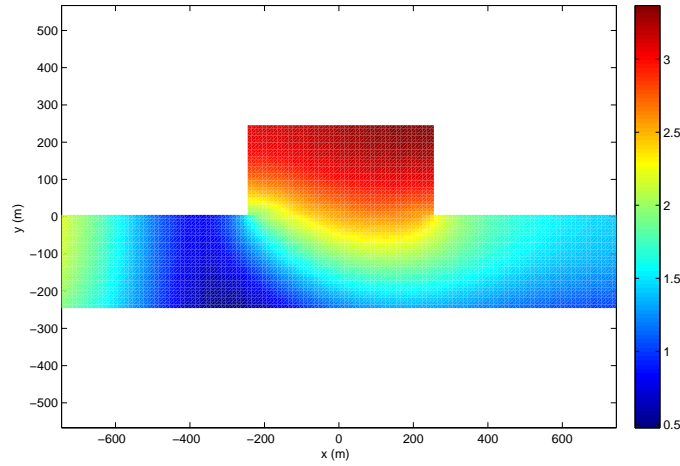


Figure 20: Map of the modulus of  $T^{(5)}(x, y; \mathbf{f} = \mathbf{0.7592 \text{ Hz}})$  for  $\theta^i = 30^\circ$ .  $\mathbf{d}^{(5)} = \{2.2254 + 2.3731i, -0.0101 - 0.1672i, -0.0097 - 0.0133i, -0.0000 - 0.0008i, -0.0001 - 0.0002i, -0.0000 - 0.0000i\}$ .

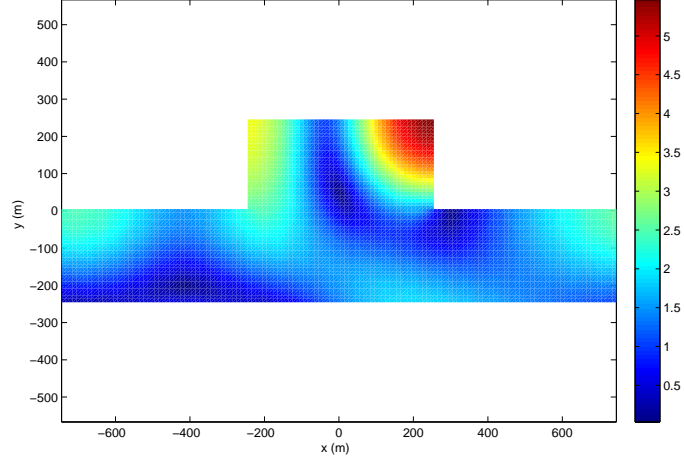


Figure 21: Map of the modulus of  $T^{(5)}(x, y; \mathbf{f} = \mathbf{1.958 \text{ Hz}})$  for  $\theta^i = 30^\circ$ .  $\mathbf{d}^{(5)} = \{-0.6914 + 1.3477i, 4.0190 - 1.4750i, 0.0195 - 0.0010i, -0.0041 - 0.0000i, 0.0001 - 0.0001i, -0.0001 + 0.0000i\}$ .

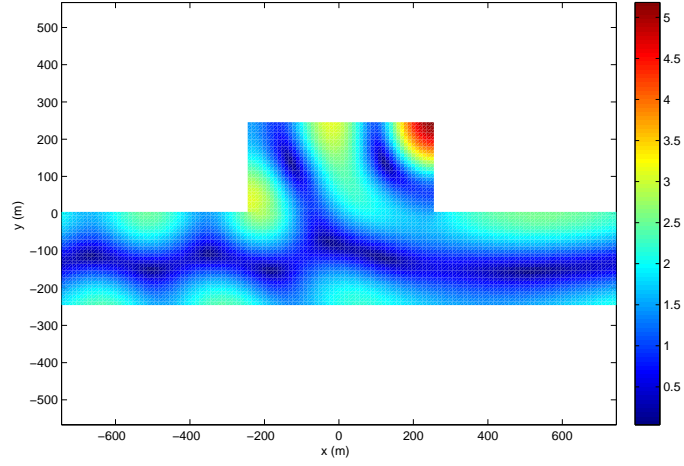


Figure 22: Map of the modulus of  $T^{(5)}(x, y; \mathbf{f} = \mathbf{3.482 \text{ Hz}})$  for  $\theta^i = 30^\circ$ .  $\mathbf{d}^{(5)} = \{-1.0119 - 0.0611i, 0.3314 + 1.9177i, -0.2862 - 2.9526i, 0.0033 - 0.0018i, -0.0007 + 0.0009i, 0.0000 - 0.0000i\}$ .

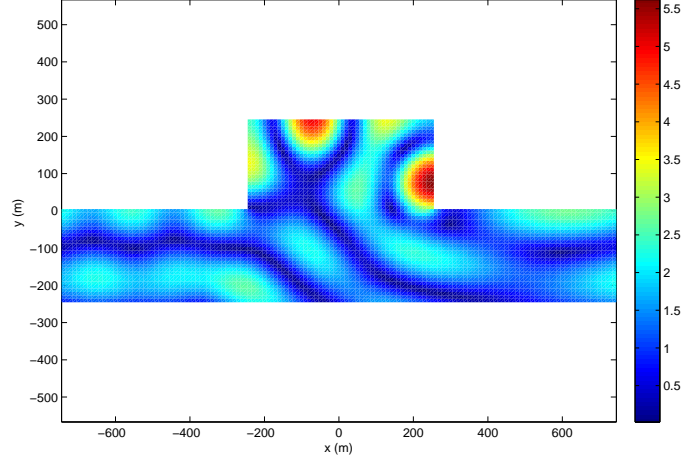


Figure 23: Map of the modulus of  $T^{(5)}(x, y; \mathbf{f} = \mathbf{5.030 \text{ Hz}})$  for  $\theta^i = 30^\circ$ .  $\mathbf{d}^{(5)} = \{0.0318 - 0.4632i, -2.4289 - 0.2308i, 1.5591 + 1.0492i, 2.3066 + 1.5719i, -0.0008 + 0.0054i, -0.0006 - 0.0002i\}$ .

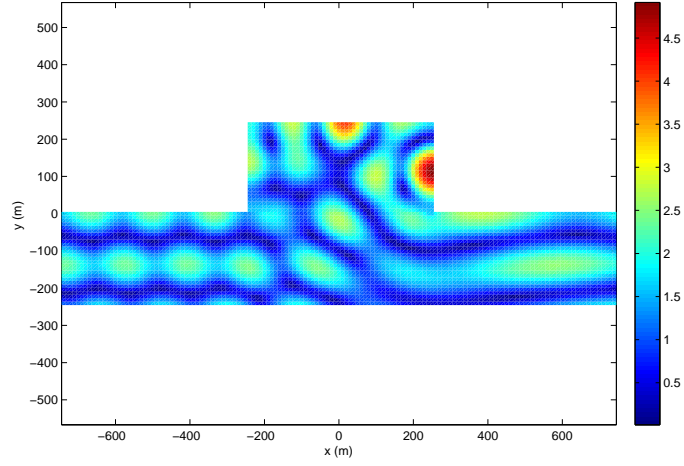


Figure 24: Map of the modulus of  $T^{(5)}(x, y; \mathbf{f} = \mathbf{6.628 \text{ Hz}})$  for  $\theta^i = 30^\circ$ .  $\mathbf{d}^{(5)} = \{0.0229 - 0.1060i, -0.3427 - 1.5837i, -1.6540 + 1.0562i, 1.2068 - 0.1370i, 1.7564 - 1.0051i, 0.0033 + 0.0049i\}$ .



These figures show that the resonant coupling to the fields at certain 'hot spots' within the hill is fairly-strong at all five resonant frequencies when the incident angle is  $\theta^i = 30^\circ$ . However, at other locations within the protuberance, the displacement field can be smaller than at certain locations in the underground. Thus, when we speak of amplified motion (with respect to the ground motion) in the protuberance at resonance, it should be understood that this amplification does not systematically occur at all locations within the protuberance and for all locations on the ground. Moreover, at the higher resonant frequencies, the field at most locations within the protuberance is much greater than that at most locations on the ground and within the underground.

### 9.2.3 Displacement field graphs for $\theta^i = 60^\circ$

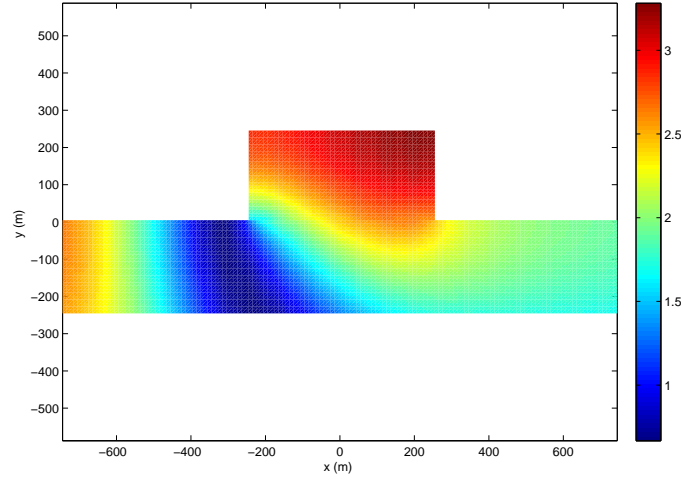


Figure 25: Map of the modulus of  $T^{(5)}(x, y; \mathbf{f} = \mathbf{0.7592 \text{ Hz}})$  for  $\theta^i = 60^\circ$ .  $\mathbf{d}^{(5)} = \{2.1117 + 2.2398i, -0.0169 - 0.2818i, -0.0145 - 0.0126i, -0.0001 - 0.0012i, -0.0002 - 0.0002i, -0.0000 - 0.0000i\}$ .

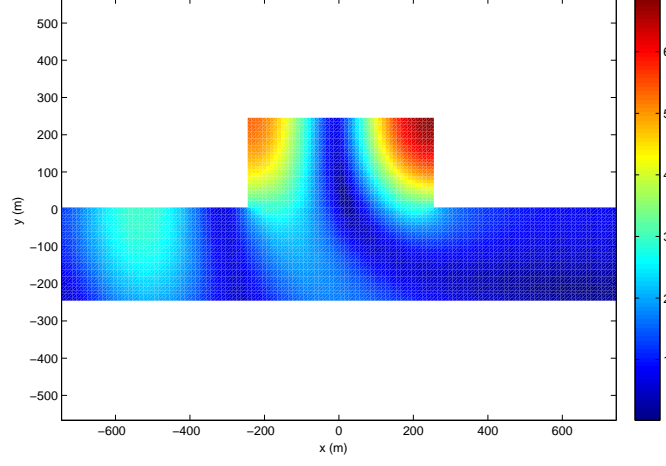


Figure 26: Map of the modulus of  $T^{(5)}(x, y; \mathbf{f} = \mathbf{1.958 \text{ Hz}})$  for  $\theta^i = 60^\circ$ .  $\mathbf{d}^{(5)} = \{-0.4013 + 0.9526i, 5.7206 - 2.1027i, -0.0441 + 0.0019i, -0.0059 + 0.0023i, -0.0002 - 0.0001i, -0.0001 + 0.0000i\}$ .

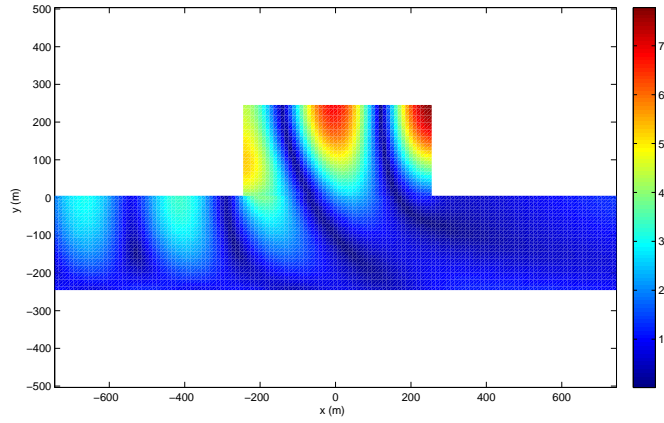


Figure 27: Map of the modulus of  $T^{(5)}(x, y; \mathbf{f} = \mathbf{3.482 \text{ Hz}})$  for  $\theta^i = 60^\circ$ .  $\mathbf{d}^{(5)} = \{0.2285 + 0.3301i, 0.4251 + 1.6318i, -1.1174 - 6.3388i, 0.0057 + 0.0276i, 0.0002 + 0.0021i, 0.0000 + 0.0002i\}$ .

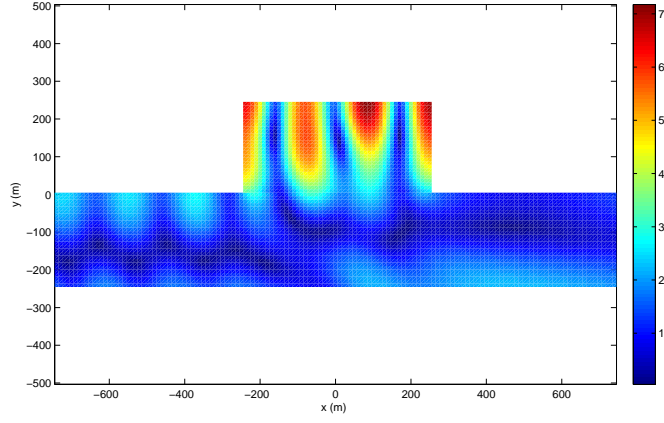


Figure 28: Map of the modulus of  $T^{(5)}(x, y; \mathbf{f} = \mathbf{5.030 \text{ Hz}})$  for  $\theta^i = 60^\circ$ .  $\mathbf{d}^{(5)} = \{-0.1428 + 0.4549i, 0.1120 + 0.0833i, 1.5944 + 1.2412i, -5.4215 + 3.4319i, 0.0099 + 0.0060i, 0.0005 - 0.0001i\}$ .

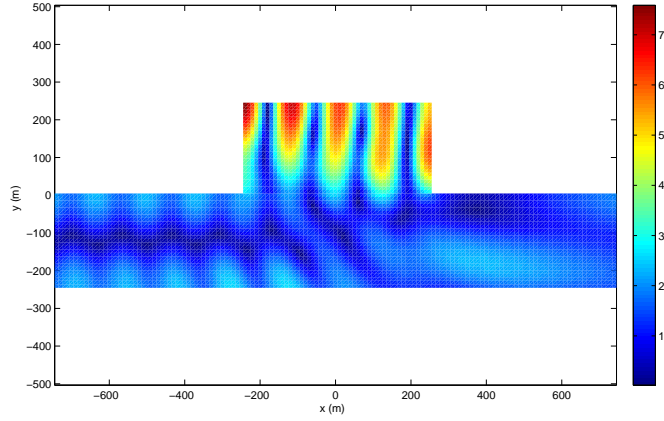


Figure 29: Map of the modulus of  $T^{(5)}(x, y; \mathbf{f} = \mathbf{6.628 \text{ Hz}})$  for  $\theta^i = 60^\circ$ .  $\mathbf{d}^{(5)} = \{-0.0414 - 0.0074i, -0.2068 + 0.5995i, -0.1802 + 0.1227i, 1.9697 - 0.3537i, 4.1149 + 4.8242i, 0.0042 - 0.0013i\}$ .

These figures show that the resonant coupling to the fields at 'hot columns' within the hill is rather strong at all five resonant frequencies when the incident angle is  $\theta^i = 60^\circ$ . Otherwise, the same comments as previously apply to this case.

#### 9.2.4 Displacement field graphs for $\theta^i = 80^\circ$

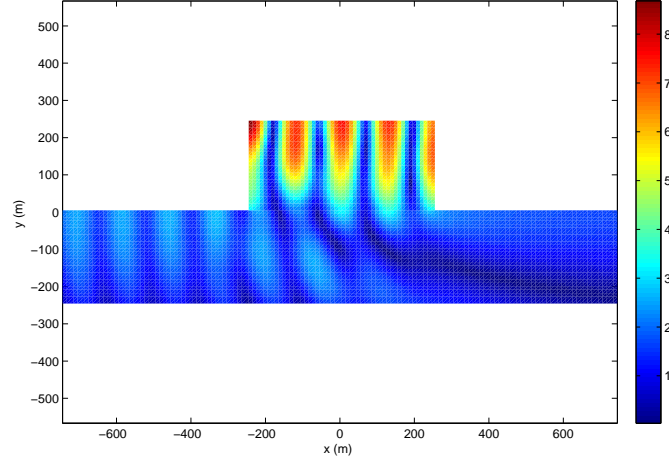


Figure 30: Map of the modulus of  $T^{(5)}(x, y; \mathbf{f} = 6.628 \text{ Hz})$  for  $\theta^i = 80^\circ$ .

This figure, and previous ones, show that the resonant coupling to the fields within the hill is usually strongest at the highest resonant frequency (but this conclusion may change, as we shall see further on, in the presence of lossy media) and when the incident angle is the largest, i.e.,  $\theta^i = 80^\circ$ . Moreover, the field within the protuberance attains values, at the resonance frequencies, that are much larger than those found by Sills for a similar hill, this being probably due to the fact that the midpoint of the top segment and the left hand bottom corner are not usually the locations at which the field is at its maximum.

## 10 Simulation of the seismic response of the Civita di Bagnoregio hill

The Civita di Bagnoregio hill [60] provides a testing ground for our rectangular ridge model, all the more so than the seismic response of a somewhat similar (to our) protuberance has been previously simulated, via a spectral element numerical scheme, by Paolucci [255].

The first problem in connection with SH wave simulations is to assign values to the shear modulus  $\mu$  (or the mass density  $\rho$ ) and the real and imaginary parts of shear wavespeed  $\beta$ . In [255], Paolucci writes, concerning his computations for the Civita di Bagnoregio hill, that the constitutive parameters of the tuff material of which the hill, as well as of the half-space basement, are supposedly-composed, are:  $\beta = 600 \text{ ms}^{-1}$  and  $\nu = 0.25$ , for the shear wavespeed and the Poisson ratio respectively. Unfortunately, he does not give the other key parameter,  $\rho$  or  $\mu$ , so that we were obliged to refer to another publication [139] treating the subject of the mechanical properties of tuff. If we suppose that this tuff is dry, the parameters given in [139] are in the ranges:  $\rho = 1270 - 1330 \text{ Kgm}^{-3}$ ,  $\beta = 1250 - 1280 \text{ ms}^{-1}$ ,  $\nu = 0.28$ ,  $\mu = 1.99 - 2.19 \text{ GPa}$ . If, on the one hand, we retain the Paolucci value for  $\beta$  and the value for  $\mu$  provided by the authors (Heap et al.) of [139] then it follows that  $\rho = 5777.8 \text{ Kgm}^{-3}$  which is clearly too large. If, on the other hand, we retain the Heap et al. values for  $\rho$  and the Paolucci value for  $\beta$  then it follows that  $\mu = 0.468 \text{ GPa}$  which appears to be somewhat small.

Thus, our first choice was:  $\beta = 600 \text{ ms}^{-1}$  and  $\mu = 0.668 \text{ GPa}$ . But this does not resolve the problem of the attenuation in the tuff. Since neither Paolucci nor Heap deal with this issue, we chose  $\beta'' = -40 \text{ ms}^{-1}$  so that  $\beta = 600 - i40 \text{ ms}^{-1}$ . Actually, with smaller attenuations, the amplifications turned out to be larger than those of Paolucci.

Our second choice appealed essentially to the mean values of the parameters provided by Heap et al.:  $\beta = 1265 \text{ ms}^{-1}$ ,  $\mu = 2.08 \text{ GPa}$ . Again, this does not resolve the attenuation issue, so we adopted the same relative attenuation as in the first choice:  $\beta'' = -84 \text{ ms}^{-1}$ , whence  $\beta = 1265 - i84 \text{ ms}^{-1}$ .

The second problem in connection with the SH seismic wave response of a structure such as a hill (assumed to be a protrusive body emerging from flat ground) is to define the shape and dimensions of the structure. Since our study has to do with ridge-like hills of rectangular shape (in the cross-section), the shape parameters are the width  $w$  and height  $h$  of the rectangle. The shape of the ridge-like Civita di Bagnoregio hill in [255] is much more complicated than a simple rectangle, but there appears to exist a nearly-rectangular region near the top whose dimensions are  $w = 275 \text{ m}$  and  $h = 50 \text{ m}$ , these being the geometrical parameters we adopted in our initial (i.e., first and second model) computations.

Last but not least, in conformity with what was assumed by Paolucci, we chose the seismic disturbance to be a normally-incident plane wave (i.e.,  $\theta^i = 0^\circ$ ), and both the basement and hill

to be occupied by the same (macroscopically-homogeneous) material so that the aforementioned parameters apply throughout the scattering configuration (except for  $\beta^{[0]''}$  which is taken to be zero).

Thus, we shall assume, for the first model, that:  $\theta^i = 0^\circ$ ,  $h_1 = 0$  m,  $h_2 = 50$  m,  $w = 275$  m,  $\mu^{[0]} = 0.668$  GPa,  $\beta^{[0]} = 600$  ms<sup>-1</sup>,  $\mu^{[2]} = 0.668$  GPa,  $\beta^{[2]} = 600 - i40$  ms<sup>-1</sup>.

## 10.1 First model results

The next step is to choose the number of terms  $M + 1$  in the modal representation of the hill. We found that the choice  $M = 8$  guaranteed that neither the first nine modal coefficients nor the displacement field changed significantly for larger  $M$  when the frequencies are near 1 Hz. These coefficients (i.e., the first nine (for the first model at  $f = 1$  Hz) are:

$\mathbf{d}^{(8)} = \{1.7924 + 1.2365i, 0.0000 - 0.0000i, -0.0112 - 0.1229i, -0.0000 + 0.0000i, -0.0025 - 0.0102i, -0.0000 - 0.0000i, -0.0005 - 0.0016i, -0.0000 + 0.0000i, -0.0001 - 0.0003i\}$  which shows that the dominant mode is the  $m = 0$  mode, the odd-order mode coefficients are unsurprisingly nil (due to the assumption of normal incidence) and the other even-order modes die out rather rapidly as  $m$  increases. The transfer functions, defined (in the same manner as in [255]) as  $T^{(M)}(x, y; f) = u^{(M)}(x, y; f)/a^i(\omega)$ , are depicted in our figs. 31-33 for  $M = 0, 2, 8$  respectively in which the lower right panel is for  $T^{(M)}(0, 0; f)$ , the lower left panel for  $T^{(M)}(-w/2, 0; f)$  and the upper left panel for  $T^{(M)}(0, h = h_2; f)$ . The upper right panel depicts  $1/D^{(M)}(\omega)$ , with  $D^{(M)}$  the determinant of the  $(M + 1)$ -by- $(M + 1)$  matrix equation involved in the computation of the modal coefficient vector  $\mathbf{d}^{(M)}$ .

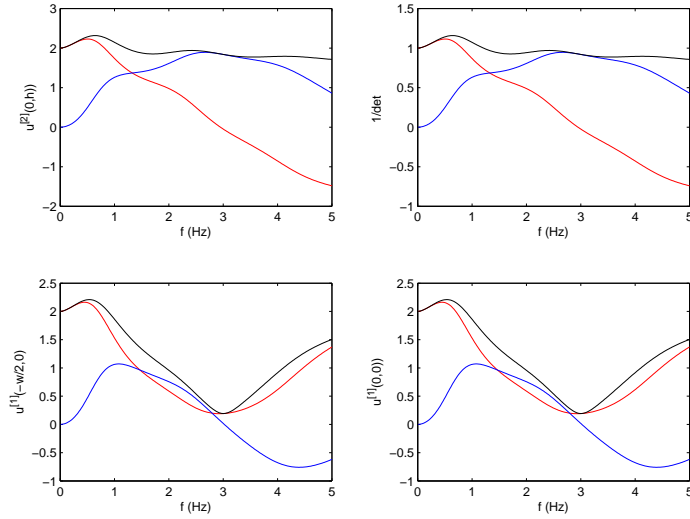


Figure 31: The lower right panel is for  $T^{(M)}(0, 0; f)$ , the lower left panel for  $T^{(M)}(-w/2, 0; f)$  and the upper left panel for  $T^{(M)}(0, h = h_2; f)$  whereas the upper right panel depicts  $1/D^{(M)}(\omega)$ . The red curves are relative to the real part, the blue curves to the imaginary part and the black curves to the absolute value. Case  $\theta^i = 0^\circ$ ,  $h_1 = 0$  m,  $h_2 = 50$  m,  $w = 275$  m,  $\mu^{[0]} = 0.668$  GPa,  $\beta^{[0]} = 600$  ms<sup>-1</sup>,  $\mu^{[2]} = 0.668$  GPa,  $\beta^{[2]} = 600 - i40$  ms<sup>-1</sup>.  $\mathbf{M} = \mathbf{0}$ .

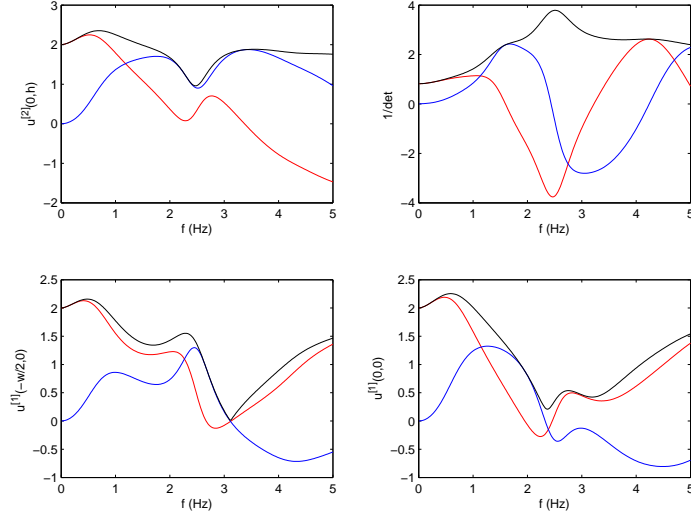


Figure 32:  $\theta^i = 0^\circ$ ,  $h_1 = 0$  m,  $h_2 = 50$  m,  $w = 275$  m,  $\mu^{[0]} = 0.668$  GPa,  $\beta^{[0]} = 600$  ms $^{-1}$ ,  $\mu^{[1]} = 0.668$  GPa,  $\beta^{[1]} = 600 - i40$  ms $^{-1}$ ,  $\mu^{[2]} = 0.668$  GPa,  $\beta^{[2]} = 600 - i40$  ms $^{-1}$ . Same as fig. 31 except that  $\mathbf{M} = \mathbf{2}$ .

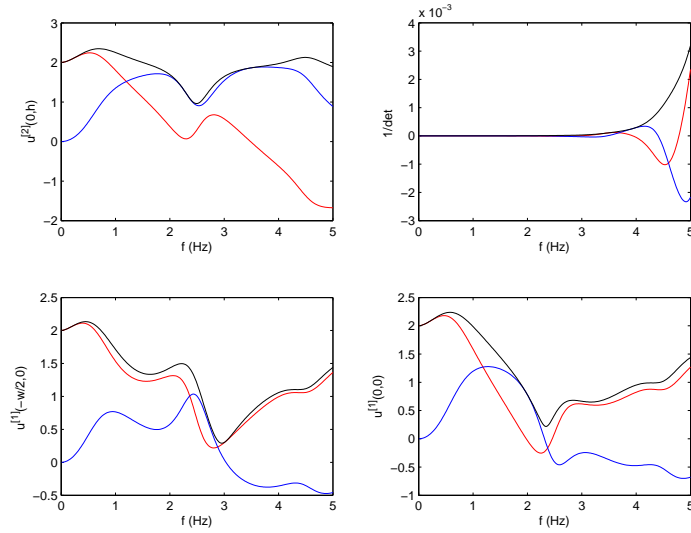


Figure 33:  $\theta^i = 0^\circ$ ,  $h_1 = 0$  m,  $h_2 = 50$  m,  $w = 275$  m,  $\mu^{[0]} = 0.668$  GPa,  $\beta^{[0]} = 600$  ms $^{-1}$ ,  $\mu^{[1]} = 0.668$  GPa,  $\beta^{[1]} = 600 - i40$  ms $^{-1}$ . Same as fig. 31 except that  $\mu^{[2]} = 0.668$  GPa,  $\beta^{[2]} = 600 - i40$  ms $^{-1}$ ,  $\mathbf{M} = \mathbf{8}$ .

In the upper right panels of figs. 31-33 we observe lorentzian behavior in  $1/D(f)$ , whose maxima indicate the frequencies of resonance (at which a mode of the basement/hill configuration is excited) and we can notice that  $f = 1 \text{ Hz}$  does not coincide with any such resonant frequency. Moreover, contrary to what was written in [255], no obviously-resonant (i.e., maximal) response (notably at the summit) appears at  $1 \text{ Hz}$ . Finally, our top transfer function has only a vague resemblance to those in fig. 5 of [255].

In spite of this, we chose to depict in our fig. 34 the graph of the displacement field along the stress-free boundary at  $f = 1 \text{ Hz}$ ,

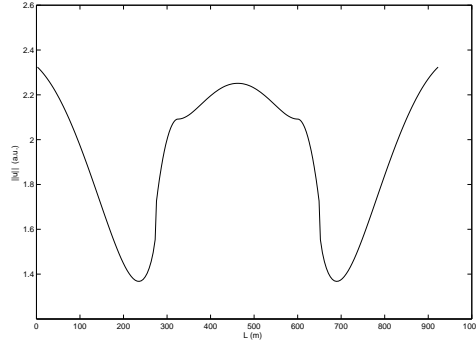


Figure 34: Normalized total displacement field  $\|u(x, y)/a^i\|$  along the stress-free boundary.  $\theta^i = 0^\circ$ ,  $h_1 = 0 \text{ m}$ ,  $h_2 = 50 \text{ m}$ ,  $w = 275 \text{ m}$ ,  $\mu^{[0]} = 0.668 \text{ GPa}$ ,  $\beta^{[0]} = 600 \text{ ms}^{-1}$ ,  $\mu^{[1]} = 0.668 \text{ GPa}$ ,  $\beta^{[1]} = 600 - i40 \text{ ms}^{-1}$ ,  $\mu^{[2]} = 0.668 \text{ GPa}$ ,  $\beta^{[2]} = 600 - i40 \text{ ms}^{-1}$ ,  $\mathbf{M} = \mathbf{8}$ .



wherein it can be observed that the field takes on values that do not exceed 2.3 (recall that this value is 2 in the absence of the hill), has the cosine-modulated shape of the zeroth-order mode on the upper face of the hill as one expects from the fact that this mode was found previously to be dominant at 1 Hz, i.e.,  $u(x, h) \approx d_0 + d_2 \cos(k_{x2}(x + w/2))$ ;  $\|d_0\| \gg \|d_2\|$ , and is even larger on portions of the ground than on the top of the hill (contrary to what is found in [255]).

## 10.2 Second model results

The parameters of the second model are:  $\theta^i = 0^\circ$ ,  $h_1 = 0$  m,  $h_2 = 50$  m,  $w = 275$  m,  $\mu^{[0]} = 2.080$  GPa,  $\beta^{[0]} = 1265$  ms<sup>-1</sup>,  $\mu^{[2]} = 2.080$  GPa,  $\beta^{[2]} = 1265 - i84$  ms<sup>-1</sup>.

Again, we found that  $M = 8$  provided stable numerical results for the modal coefficients and to be such, at  $f = 1$  Hz, that the dominant mode is again the  $m = 0$  mode, the odd-order mode coefficients are nil (due to the assumption of normal incidence) and the other even-order modes die out rapidly as  $m$  increases.

The  $M = 0, 2, 8$  transfer functions for this scattering configuration are exhibited in figs. 35-37

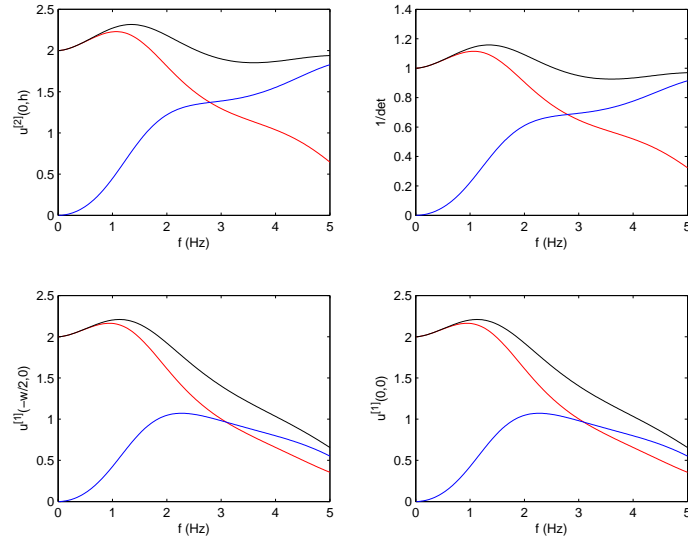


Figure 35: The lower right panel is for  $T^{(M)}(0, 0; f)$ , the lower left panel for  $T^{(M)}(-w/2, 0; f)$  and the upper left panel for  $T^{(M)}(0, h = h_2; f)$  whereas the upper right panel depicts  $1/D^{(M)}(\omega)$ , with  $D^{(M)}$  the determinant of the  $(M + 1)$ -by- $(M + 1)$  matrix equation involved in the computation of the modal coefficient vector  $\mathbf{d}^{(M)}$ . The red curves are relative to the real part, the blue curves to the imaginary part and the black curves to the absolute value.  $\theta^i = 0^\circ$ ,  $h_1 = 0$  m,  $h_2 = 50$  m,  $w = 275$  m,  $\mu^{[0]} = 2.080$  GPa,  $\beta^{[0]} = 1265$  ms<sup>-1</sup>,  $\mu^{[2]} = 2.080$  GPa,  $\beta^{[2]} = 1265 - i84$  ms<sup>-1</sup>. Same as fig. 31 and  $\mathbf{M} = \mathbf{0}$ .

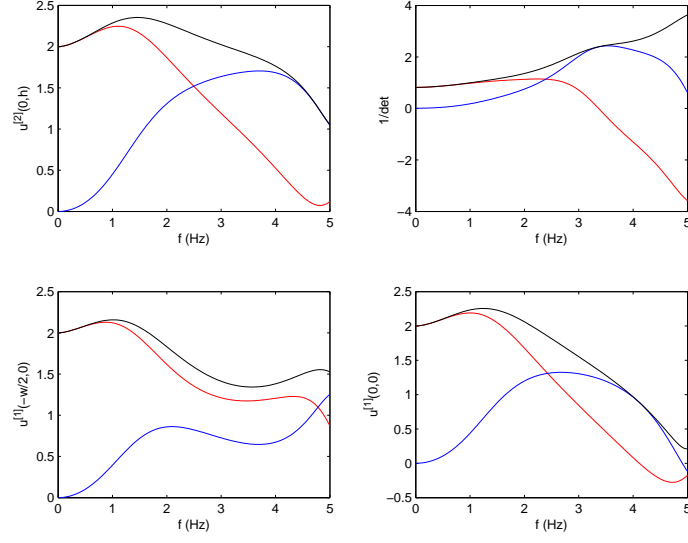


Figure 36:  $\theta^i = 0^\circ$ ,  $h_1 = 0$  m,  $h_2 = 50$  m,  $w = 275$  m,  $\mu^{[0]} = 2.080$  GPa,  $\beta^{[0]} = 1265$  ms<sup>-1</sup>,  $\mu^{[1]} = 2.080$  GPa,  $\beta^{[1]} = 1265 - i84$  ms<sup>-1</sup>,  $\mu^{[2]} = 2.080$  GPa,  $\beta^{[2]} = 1265 - i84$  ms<sup>-1</sup>. Same as fig. 35 except that  $\mathbf{M} = \mathbf{2}$ .

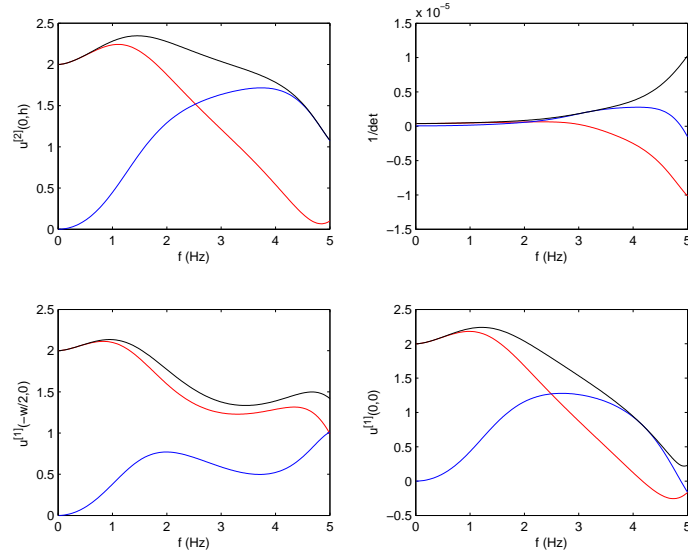


Figure 37:  $\theta^i = 0^\circ$ ,  $h_1 = 0$  m,  $h_2 = 50$  m,  $w = 275$  m,  $\mu^{[0]} = 2.080$  GPa,  $\beta^{[0]} = 1265$  ms<sup>-1</sup>,  $\mu^{[1]} = 2.080$  GPa,  $\beta^{[1]} = 1265 - i84$  ms<sup>-1</sup>,  $\mu^{[2]} = 2.080$  GPa,  $\beta^{[2]} = 1265 - i84$  ms<sup>-1</sup>. Same as fig. 35 except that  $\mathbf{M} = \mathbf{8}$ .

which, as concerns the top  $T$ , now more closely resembles (although the maximum of the top  $T$ , as well as the first maximum of  $1/D^{(M)}(\omega)$ , are now situated beyond  $1\text{ Hz}$ ) the corresponding transfer functions in fig. 5 of [255].

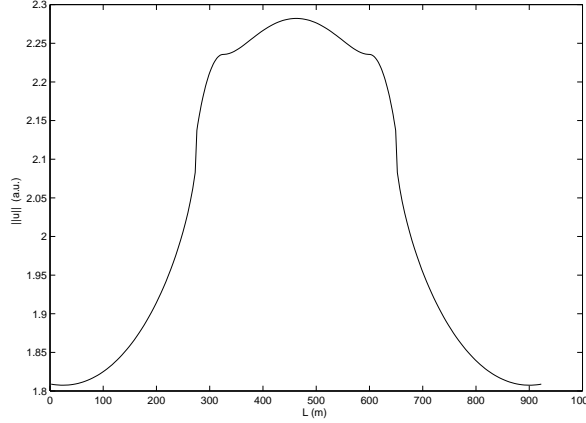


Figure 38: Normalized total displacement field  $\|u(x, y)/a^i\|$  along the stress-free boundary.  $\theta^i = 0^\circ$ ,  $h_1 = 0\text{ m}$ ,  $h_2 = 50\text{ m}$ ,  $w = 275\text{ m}$ ,  $\mu^{[0]} = 2.080\text{ GPa}$ ,  $\beta^{[0]} = 1265\text{ ms}^{-1}$ ,  $\mu^{[1]} = 2.080\text{ GPa}$ ,  $\beta^{[1]} = 1265 - i84\text{ ms}^{-1}$ ,  $\mu^{[2]} = 2.080\text{ GPa}$ ,  $\beta^{[2]} = 1265 - i84\text{ ms}^{-1}$ .  $\mathbf{M} = \mathbf{0}$ .

The displacement field on the stress-free boundary (at  $f = 1\text{ Hz}$ ) is displayed in fig. 38 wherein it can be observed that the field: 1) again takes on values that do not exceed 2.3, 2) again has the cosinus-modulated shape of the zeroth-order mode on the upper face of the hill as one expects from the fact that this mode was found previously to be dominant at  $1\text{ Hz}$ , i.e.,  $u(x, h) \approx d_0 + d_2 \cos(k_{x2}(x + w/2))$ ;  $\|d_0\| \gg \|d_2\|$ , 3) is now much smaller on the flanks at ground level than on the top of the hill as is observed to be the case in [255]). Note also that the field on the top is more constant than in the first model, this also being in agreement with what is observed in fig. 5 of [255].

To conclude this discussion, we have found that in order to obtain a result that compares favorably with the spectral element simulation of the seismic response of the somewhat irregularly-shaped hill in fig. 5 of [255], we had to choose, in our own simulation, a rectangular hill whose base (and top) is less wide and whose height is smaller than the hill of [255], and (for the second model) a shear wavespeed in the hill that is both complex (to include a fairly-substantial attenuation) and whose real part is double that of the one in [255]. This attenuation has the effect of smoothing out and reducing somewhat the height of the first broad resonance peak in the top transfer function, as well as reducing to an acceptable level the field on the top of the hill at  $f = 1\text{ Hz}$ . Our computation thus seems to substantiate the contention of Paolucci that the (actually modest) field amplification at this frequency is indeed due to a resonance (broader and whose maximum is at a higher frequency than Paolucci's) resonance at  $f = 1\text{ Hz}$ . Our results provide, in addition, the indication that this resonance is due to the excitation of the zeroth-order mode of the (rectangular) hill.

### 10.3 Alternative (third) model results

Paolucci mentions in his article that the Civita di Bagnoregio hill was the site of a major earthquake on 11 June, 1695 that caused great damage to the town located on its plateau-like summit as well as landslides along its flank(s), without notable damage having been reported in neighboring towns located beneath the hill (presumably at what we call ground level). With the relatively-modest motion of our second model, it is not easy to explain why this would cause major damage at  $1\text{ Hz}$ , especially to what one can guess (in 1695) are small buildings (4 to 8 stories) whose fundamental resonance frequencies are in the  $2.5 - 5\text{ Hz}$  range. Of course, we do not know what the dominant frequency of this earthquake was, but it cannot be excluded that it was in the  $2.5 - 5\text{ Hz}$  range rather than near  $1\text{ Hz}$ . This suggests that a not-too-radical modification of our second hill model might give rise to a resonance in the  $2.5 - 5\text{ Hz}$  range and thus explain why the buildings on the top of the hill are subjected to strong ground motion when the seismic solicitation is in this same frequency range.

Our modification consists in: a) increasing somewhat the height (this parameter is not easy to ascertain in fig.5 of [255]) of the hill to  $h = h_2 = 65\text{ m}$ , and b) hardening the underground medium without changing the hill medium so that the shear modulus and shear wavespeed in the underground are now  $8\text{ GPa}$  and  $2000\text{ ms}^{-1}$  respectively. It is not certain that the latter choice (amounting to a relatively-soft hill overlying a relatively-hard underground) is geologically-admissible, but the supposition that the underground medium be identical to the hill medium is also debatable.

Let us now see what the consequences of these changes are. The parameters of this third model are:  $\theta^i = 0^\circ$ ,  $h_1 = 0\text{ m}$ ,  $h_2 = 65\text{ m}$ ,  $w = 275\text{ m}$ ,  $\mu^{[0]} = 8\text{ GPa}$ ,  $\beta^{[0]} = 2000\text{ ms}^{-1}$ ,  $\mu^{[2]} = 2.080\text{ GPa}$ ,  $\beta^{[2]} = 1265 - i84\text{ ms}^{-1}$ .

Fig. 39 depicts the transfer functions whereby we observe that a broad maximum occurs for the top response centered at  $f = 4.2\text{ Hz}$ .

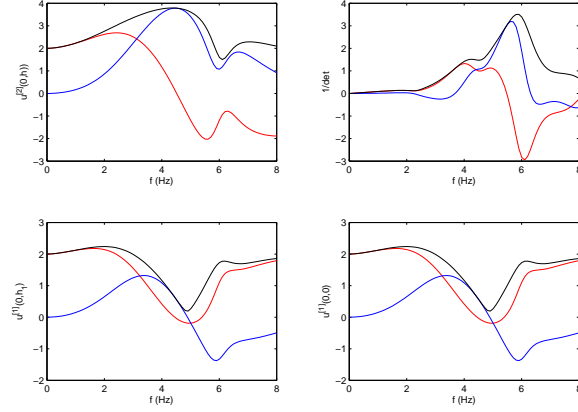


Figure 39: The lower right panel is for  $T^{(M)}(0, 0; f)$ , the lower left panel for  $T^{(M)}(-w/2, 0; f)$  and the upper left panel for  $T^{(M)}(0, h = h_2; f)$  whereas the upper right panel depicts  $1/\mathcal{D}^{(M)}(\omega)$ , with  $\mathcal{D}^{(M)}$  the determinant of the  $(M + 1)$ -by- $(M + 1)$  matrix equation involved in the computation of the modal coefficient vector  $\mathcal{F}^{(M)}$ . The red curves are relative to the real part, the blue curves to the imaginary part and the black curves to the absolute value.  $\theta^i = 0^\circ$ ,  $h_1 = 0$  m,  $h_2 = 65$  m,  $w = 275$  m,  $\mu^{[0]} = 8$  GPa,  $\beta^{[0]} = 2000$  ms $^{-1}$ ,  $\mu^{[2]} = 2.080$  GPa,  $\beta^{[2]} = 1265 - i84$  ms $^{-1}$ .  $M = 4$ . The resonances appear at:  $f = 4.2$  Hz.

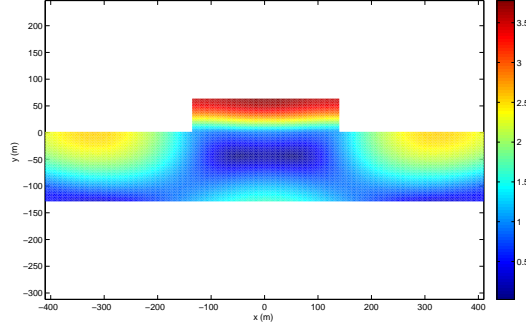


Figure 40: Map of  $\|T^{(M)}(x, y; 4.2 \text{ Hz})\|$ .  $f = 4.2 \text{ Hz}$ ,  $\theta^i = 0^\circ$ ,  $h_1 = 0 \text{ m}$ ,  $h_2 = 65 \text{ m}$ ,  $w = 275 \text{ m}$ ,  $\mu^{[0]} = 8 \text{ GPa}$ ,  $\beta^{[0]} = 2000 \text{ ms}^{-1}$ ,  $\mu^{[2]} = 2.080 \text{ GPa}$ ,  $\beta^{[2]} = \mathbf{1265 - i84 \text{ ms}^{-1}}$ .  $\mathbf{M} = 4$ .

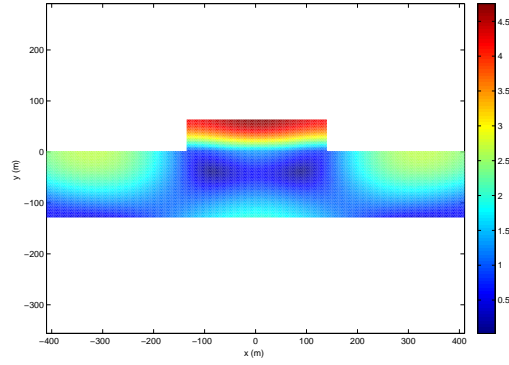


Figure 41: Map of  $\|T^{(M)}(x, y; 4.2 \text{ Hz})\|$ .  $f = 4.2 \text{ Hz}$ ,  $\theta^i = 0^\circ$ ,  $h_1 = 0 \text{ m}$ ,  $h_2 = 65 \text{ m}$ ,  $w = 275 \text{ m}$ ,  $\mu^{[0]} = 8 \text{ GPa}$ ,  $\beta^{[0]} = 2000 \text{ ms}^{-1}$ ,  $\mu^{[2]} = 2.080 \text{ GPa}$ ,  $\beta^{[2]} = \mathbf{1265 - i0 \text{ ms}^{-1}}$ .  $M = 4$ .

Fig. 40 depicts the displacement field map at this frequency wherein we observe that the top field has now increased from 2.3 to 3.7 (a.u.) over most of the plateau of the hill. If we suppress the attenuation in the hill, the displacement field map looks like fig. 41.

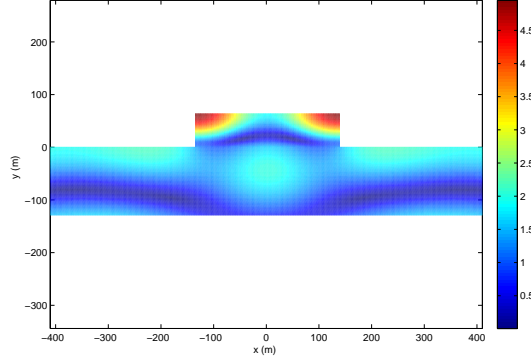


Figure 42: Map of  $\|T^{(M)}(x, y; 5.9 \text{ Hz})\|$ .  $f = 5.9 \text{ Hz}$ ,  $\theta^i = \mathbf{0}^\circ$ ,  $h_1 = 0 \text{ m}$ ,  $h_2 = 65 \text{ m}$ ,  $w = 275 \text{ m}$ ,  $\mu^{[0]} = 8 \text{ GPa}$ ,  $\beta^{[0]} = 2000 \text{ ms}^{-1}$ ,  $\mu^{[2]} = 2.080 \text{ GPa}$ ,  $\beta^{[2]} = 1265 - i84 \text{ ms}^{-1}$ .  $M = 8$ .

in which we observe that the maximum value of the field on the top increases from 3.7 to 4.7 (a.u), both these values being possibly-sufficient to account for relatively strong motion (generally measured by a quantity proportional to  $\|u\|^2$  [34, 356]) and damage to small buildings located on the crest of the Civita hill caused by a seismic wave whose dominant frequency is  $4.2 \text{ Hz}$ .

In fig. 39 we also note the presence of a strong maximum of  $1/\|\mathcal{D}\|$  at  $f = 5.9 \text{ Hz}$  which suggests the existence of a resonance at this frequency as well, with the concurrent possibility of significant amplification of the displacement field within the hill for an incident seismic wave whose dominant frequency is  $f = 5.9 \text{ Hz}$ .

Fig. 42 tells us what the field distribution looks like at this frequency. Now the field is concentrated at the upper edges, which might explain the origin of the landslides observed in 1695, and at various occasions since then, affecting the Civita hill.

This shows that, at  $f = 5.9 \text{ Hz}$ , both the  $m = 0$  and  $m = 2$  modes are being excited (i.e., resonate). Now, instead of  $u(x, h) \approx d_0 + d_2 \cos(k_{x2}(x + w/2))$ ;  $\|d_0\| \gg \|d_2\|$ , we have  $u(x, h) \approx d_0 + d_2 \cos(k_{x2}(x + w/2))$ ;  $\|d_0\| \approx \|d_2\|$  whence  $u(\pm w/2, 0) \approx d_0 + d_2$  and  $u(0, 0) \approx d_0 - d_2$ , which on account of the signs of the real and imaginary parts of  $d_0$  and  $d_2$ , accounts for the fact that the fields at the corners are maximal and the field at the center of the plateau is minimal at  $f = 5.9 \text{ Hz}$ .

A look at the coefficients of the hill modes helps to understand why the field concentrates at the upper edge.  $\mathbf{d}^{(9)} = \{-1.9083 + 2.7632i, 0.0000 - 0.0000i, -0.3842 + 1.6453i, -0.0000 - 0.0000i, 0.0195 - 0.0017i, -0.0000 - 0.0000i, 0.0017 - 0.0005i, -0.0000 - 0.0000i, 0.0002 - 0.0001i, 0.0000 + 0.0000i\}$ .

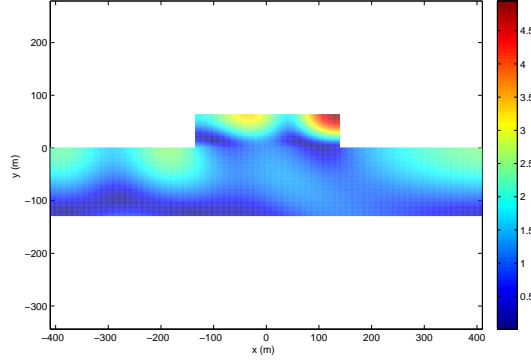


Figure 43: Map of  $\|T^{(M)}(x, y; 5.9 \text{ Hz})\|$ .  $f = 5.9 \text{ Hz}$ ,  $\theta^i = 40^\circ$ ,  $h_1 = 0 \text{ m}$ ,  $h_2 = 65 \text{ m}$ ,  $w = 275 \text{ m}$ ,  $\mu^{[0]} = 8 \text{ GPa}$ ,  $\beta^{[0]} = 2000 \text{ ms}^{-1}$ ,  $\mu^{[2]} = 2.080 \text{ GPa}$ ,  $\beta^{[2]} = 1265 - i84 \text{ ms}^{-1}$ .  $M = 8$ .  $N = 200$ .

Actually, the landslides of the Civita hill, which continue until this day, appear to affect mostly its eastern flank. This led us to hypothesize that most of the seismic disturbances in the Bagnoregio area come from the same source which is not directly (but far) beneath the hill but rather to the left (in our field map figures). If we suppose that this amounts to a seismic solicitation in the form of a plane SH wave having  $\theta^i = 40^\circ$  incidence, then the displacement field map has the appearance of fig. 43 wherein we observe that the region of the strongest motion is now concentrated at the eastern edge of the plateau, thus possibly explaining why the landslides of this topographic feature take place predominantly on its eastern flank.

## 11 On the possibility of very-strong seismic response in a hill

The previous numerical results seemed to imply that the seismic displacement response in hills, entirely-filled with a solid that is either the same as, or different from, that of the underground, is systematically inferior to about four times the flat-ground response (the latter equals 2). In this section we show, via Figs. 44-61, that this response can, in fact, be much stronger, even for a hill having a relatively-large aspect ratio  $w/h = 500 \text{ m}/150 \text{ m} = 3.333$ . *Now, we assume that the hill is entirely-filled with a solid that is different from that of the underground.*

### 11.1 Without attenuation

We first examine the case in which there are no material losses within and underneath the hill. The parameters of the configuration are:  $h_1 = 0 \text{ m}$ ,  $h_2 = 150 \text{ m}$ ,  $w = 500 \text{ m}$ ,  $\mu^{[0]} = 6.85 \text{ GPa}$ ,  $\beta^{[0]} = 1629.4 \text{ ms}^{-1}$ ,  $\mu^{[2]} = 2 \text{ GPa}$ ,  $\beta^{[2]} = 1000 - i0 \text{ ms}^{-1}$ .



### 11.1.1 Search for the first four resonant frequencies

Figs. 44-47 depict the transfer functions for  $M = 0, 1, 2, 3$  whereby we spot the resonant frequencies.

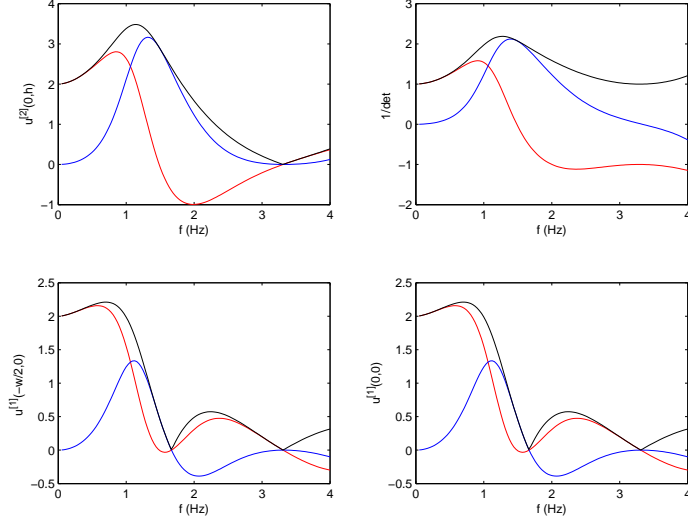


Figure 44: The lower right panel is for  $T^{(M)}(0, 0; f)$ , the lower left panel for  $T^{(M)}(-w/2, 0; f)$  and the upper left panel for  $T^{(M)}(0, h = h_2; f)$  whereas the upper right panel depicts  $1/D^{(M)}(\omega)$ , with  $D^{(M)}$  the determinant of the  $(M + 1)$ -by- $(M + 1)$  matrix equation involved in the computation of the modal coefficient vector  $\mathbf{d}^{(M)}$ . The red curves are relative to the real part, the blue curves to the imaginary part and the black curves to the absolute value.  $\theta^i = 80^\circ$ ,  $h_1 = 0$  m,  $h_2 = 150$  m,  $w = 500$  m,  $\mu^{[0]} = 6.85$  GPa,  $\beta^{[0]} = 1629.4$  ms<sup>-1</sup>,  $\mu^{[2]} = 2$  GPa,  $\beta^{[2]} = 1000 - i0$  ms<sup>-1</sup>.  $\mathbf{M} = \mathbf{0}$ .

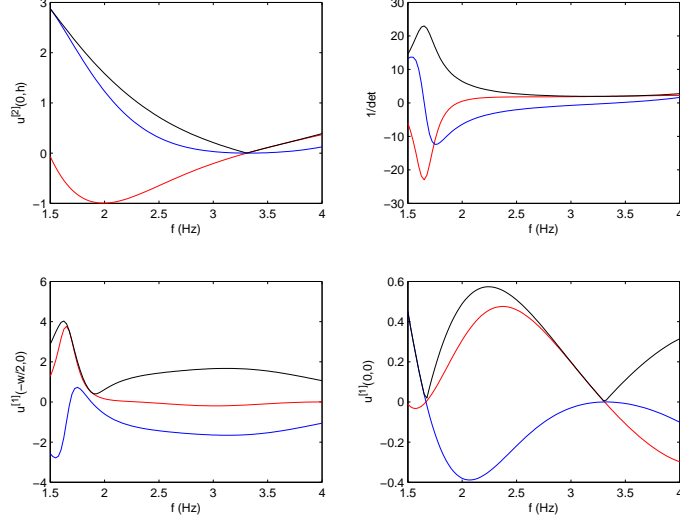


Figure 45: Same as fig. 44 except that  $\mathbf{M} = \mathbf{1}$ .

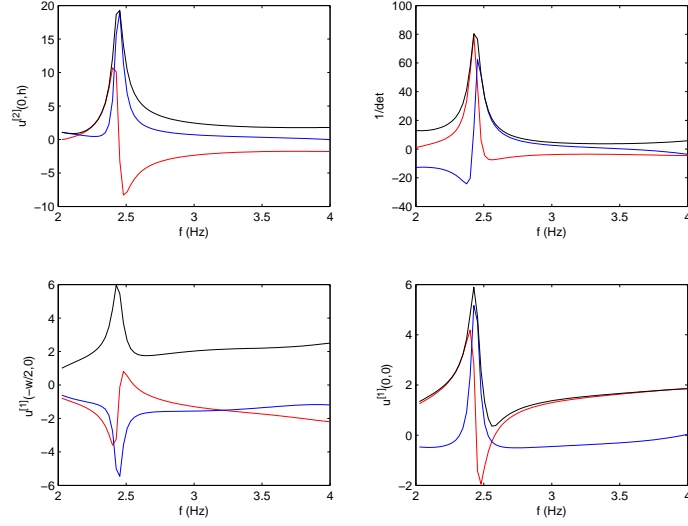


Figure 46: Same as fig. 44 except that  $\mathbf{M} = \mathbf{2}$ .

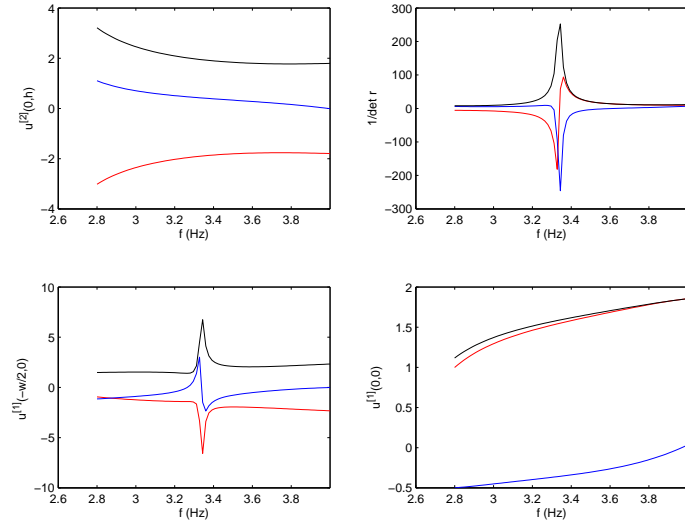


Figure 47: Same as fig. 44 except that  $\mathbf{M} = \mathbf{3}$ .

The first four resonant frequencies are thus found to be: 1.28, 1.64, 2.44, 3.337  $Hz$ . Note that in fig. 47 there appears no trace of resonant coupling to the response at the specific point  $(0, h)$ . As we shall see further on, this fact contrasts sharply with what fig. 53 reveals as to the appearance of very hot spots on the hilltop at this same frequency and incident angle. *This finding underlines the danger of guessing the response at arbitrary points on and within the hill from its response at a single point on the top its (stress-free) surface.*

### 11.1.2 Resonant coupling at $f = 2.44 \text{ Hz}$

Figs. 48-48 are field maps for three incident angles at  $f = 2.44 \text{ Hz}$ .

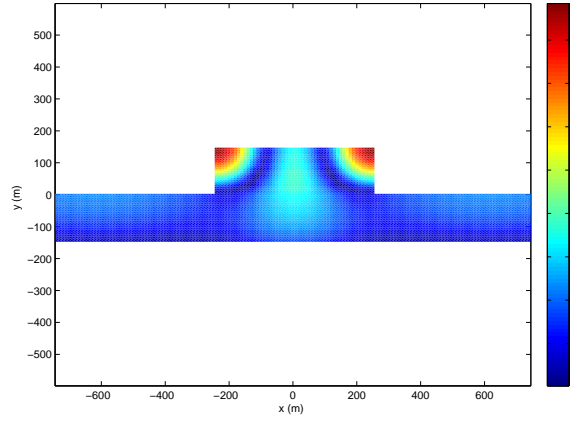


Figure 48: Map of  $T(x, y; f = 2.44 \text{ Hz})$ .  $\theta^i = \mathbf{0}^\circ$ ,  $h_1 = 0 \text{ m}$ ,  $h_2 = 150 \text{ m}$ ,  $w = 500 \text{ m}$ ,  $\mu^{[0]} = 6.85 \text{ GPa}$ ,  $\beta^{[0]} = 1629.4 \text{ ms}^{-1}$ ,  $\mu^{[2]} = 2 \text{ GPa}$ ,  $\beta^{[2]} = 1000 - i0 \text{ ms}^{-1}$ .  $M = 5$ .

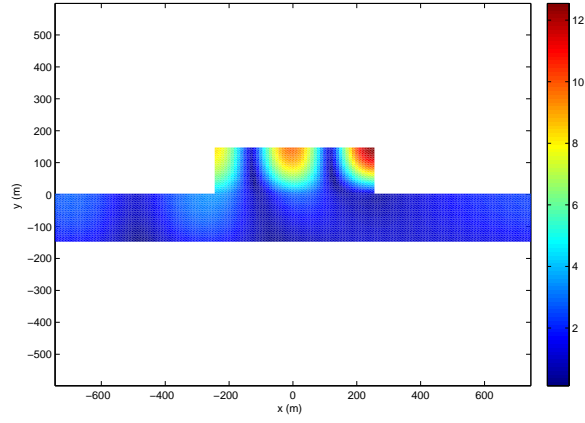


Figure 49: Same as fig. 48 except that  $\theta^i = 40^\circ$ .

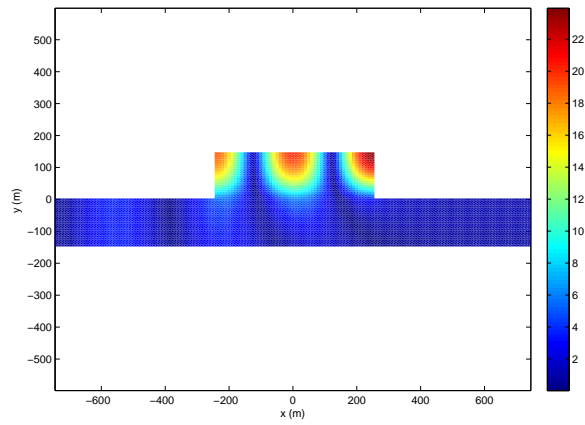


Figure 50: Same as fig. 48 except that  $\theta^i = 80^\circ$ .

Notice the strong coupling at this resonant frequency for all incident angles. However the coupling increases with  $\theta^i$  to attain a very large amount at three hot spots for  $80^\circ$  incidence (in fig. 50).

### 11.1.3 Resonant coupling at $f = 3.3374 \text{ Hz}$

Figs. 51-53 are field maps for three incident angles at  $f = 3.3374 \text{ Hz}$ .

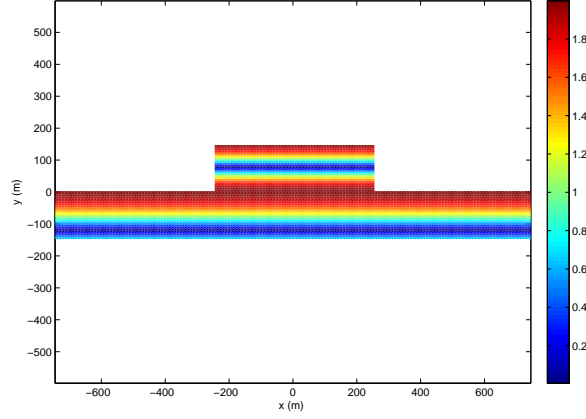


Figure 51: Map of  $T(x, y; f = 3.3374 \text{ Hz})$ .  $\theta^i = 0^\circ$ ,  $h_1 = 0 \text{ m}$ ,  $h_2 = 150 \text{ m}$ ,  $w = 500 \text{ m}$ ,  $\mu^{[0]} = 6.85 \text{ GPa}$ ,  $\beta^{[0]} = 1629.4 \text{ ms}^{-1}$ ,  $\mu^{[2]} = 2 \text{ GPa}$ ,  $\beta^{[2]} = 1000 - i0 \text{ ms}^{-1}$ .  $M = 5$ .

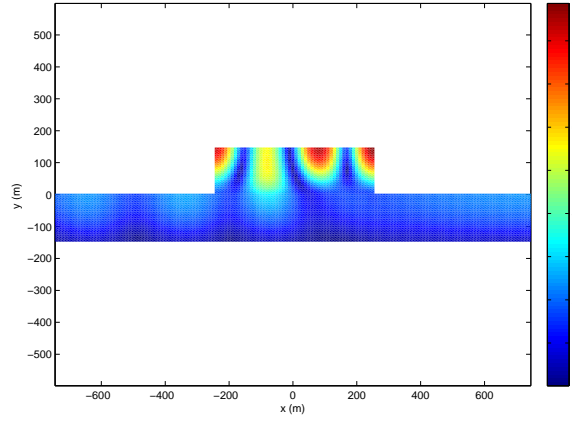


Figure 52: Same as fig. 51 except that  $\theta^i = 40^\circ$ .

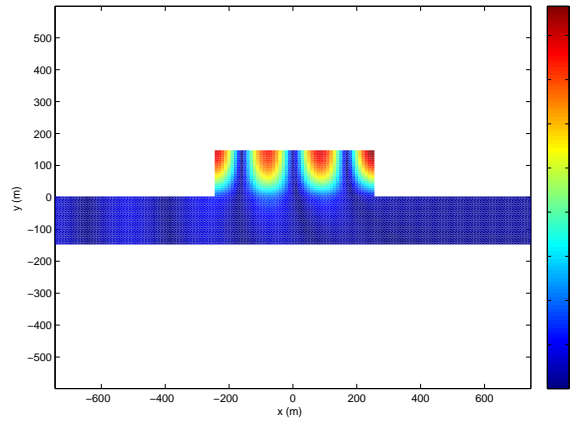


Figure 53: Same as fig. 51 except that  $\theta^i = 80^\circ$ .

Notice the very weak coupling at this resonant frequency for normal incidence. However the coupling increases with  $\theta^i$  to attain a huge amount at four hot spots for  $80^\circ$  incidence (fig. 53). Again, it is important to underline the fact, illustrated in figs. fig. 47 and 53, that *the transfer function at the midpoint of the top surface of the hill is far from being an adequate indicator of the seismic response within the hill and at other points on its boundary*. The same comments apply to the transfer function at the midpoint of the base of the hill, both of these midpoint transfer functions being often employed (see e.g., [70]) to guess what the motion is at arbitrary points within, and on, a convex surface feature such as a mountain, hill or building.

## 11.2 With attenuation

Next, we examine the case in which there are material losses within the hill. The parameters of the configuration are:  $h_1 = 0$  m,  $h_2 = 150$  m,  $w = 500$  m,  $\mu^{[0]} = 6.85$  GPa,  $\beta^{[0]} = 1629.4$  ms<sup>-1</sup>,  $\mu^{[2]} = 2$  GPa,  $\beta^{[2]} = 1000 - i20$  ms<sup>-1</sup>.

### 11.2.1 Search for the third and fourth resonant frequencies

Figs. 54-55 depict the manner of searching for the resonance frequencies.

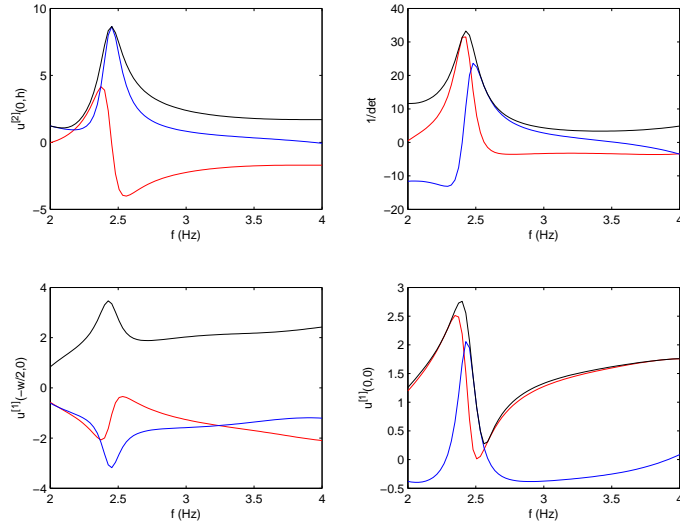


Figure 54: The lower right panel is for  $T^{(M)}(0, 0; f)$ , the lower left panel for  $T^{(M)}(-w/2, 0; f)$  and the upper left panel for  $T^{(M)}(0, h = h_2; f)$  whereas the upper right panel depicts  $1/D^{(M)}(\omega)$ , with  $D^{(M)}$  the determinant of the  $(M + 1)$ -by- $(M + 1)$  matrix equation involved in the computation of the modal coefficient vector  $\mathbf{d}^{(M)}$ . The red curves are relative to the real part, the blue curves to the imaginary part and the black curves to the absolute value.  $\theta^i = 80^\circ$ ,  $h_1 = 0$  m,  $h_2 = 150$  m,  $w = 500$  m,  $\mu^{[0]} = 6.85$  GPa,  $\beta^{[0]} = 1629.4$  ms<sup>-1</sup>,  $\mu^{[2]} = 2$  GPa,  $\beta^{[2]} = 1000 - i20$  ms<sup>-1</sup>.  $\mathbf{M} = \mathbf{2}$ .



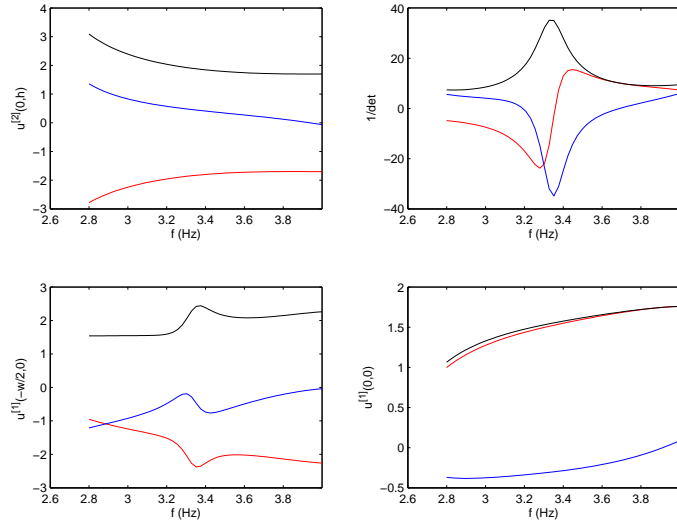


Figure 55: Same as fig. 54 except that  $M = 3$ .

The third and fourth resonance frequencies are seen to be:  $2.44 \text{ Hz}$ ,  $3.3350 \text{ Hz}$ .

### 11.2.2 Coupling at the third resonance frequency

Figs. 56-58 are field maps for three incident angles.

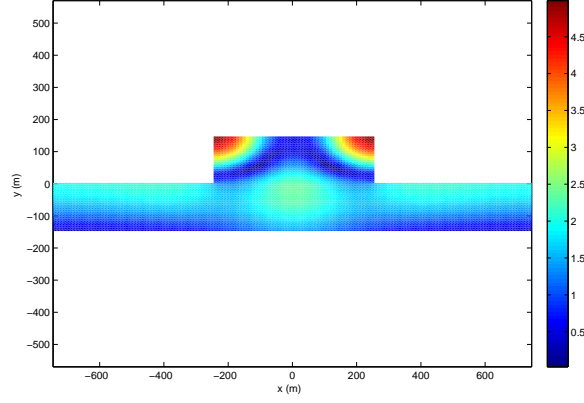


Figure 56: Map of  $T(x, y; f = 2.44 \text{ Hz})$ .  $\theta^{\mathbf{i}} = \mathbf{0}^\circ$ ,  $h_1 = 0 \text{ m}$ ,  $h_2 = 150 \text{ m}$ ,  $w = 500 \text{ m}$ ,  $\mu^{[0]} = 6.85 \text{ GPa}$ ,  $\beta^{[0]} = 1629.4 \text{ ms}^{-1}$ ,  $\mu^{[2]} = 2 \text{ GPa}$ ,  $\beta^{[2]} = 1000 - i20 \text{ ms}^{-1}$ .  $M = 5$ .

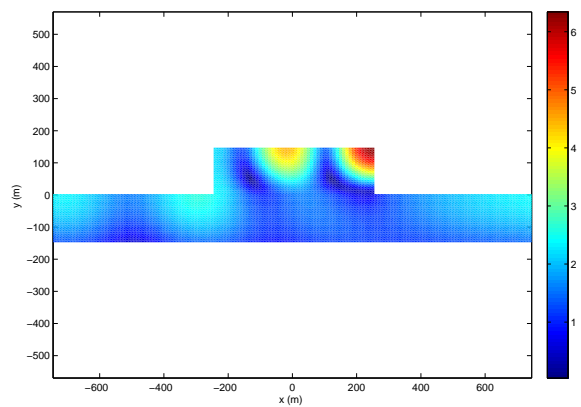


Figure 57: Same as fig. 56 except that  $\theta^i = 40^\circ$ .

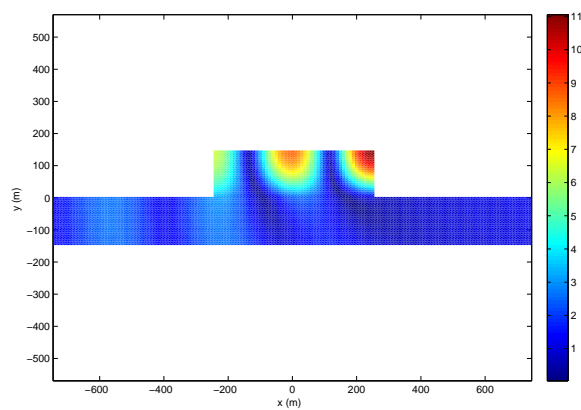


Figure 58: Same as fig. 56 except that  $\theta^i = 80^\circ$ .

The coupling efficiency again increases with incident angle and still attains considerable proportions (in fig. 58) for  $\theta^i = 80^\circ$ .

### 11.2.3 Coupling at the fourth resonant frequency

Figs. 59-61 are field maps for three incident angles.

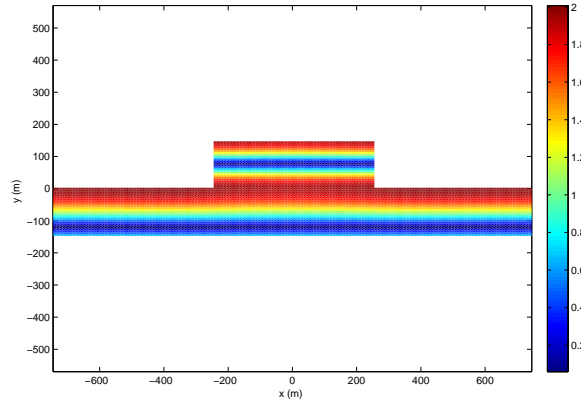


Figure 59: Map of  $T(x, y; f = 3.3350 \text{ Hz})$ .  $\theta^i = 0^\circ$ ,  $h_1 = 0 \text{ m}$ ,  $h_2 = 150 \text{ m}$ ,  $w = 500 \text{ m}$ ,  $\mu^{[0]} = 6.85 \text{ GPa}$ ,  $\beta^{[0]} = 1629.4 \text{ ms}^{-1}$ ,  $\mu^{[2]} = 2 \text{ GPa}$ ,  $\beta^{[2]} = 1000 - i20 \text{ ms}^{-1}$ .  $M = 5$ .  $N = 200$ .

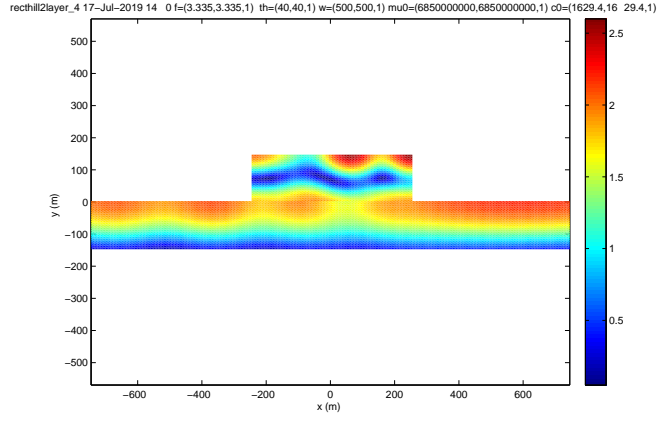


Figure 60: Same as fig. 59 except that  $\theta^i = 40^\circ$ .

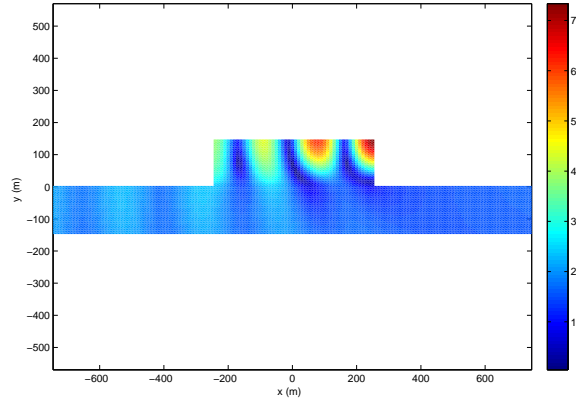


Figure 61: Same as fig. 59 except that  $\theta^i = 80^\circ$ .

*Notice that the lower frequency resonance is much less affected by material loss than the higher frequency resonance at all incident angles. This will be shown in our second contribution to be a general rule.*

Another general rule, already observable in figs. 45-47 and 54-55, is that due to the broadening of the resonance peaks in the transfer functions by the introduction of losses, the strong motion can occur over a wider frequency range than in the absence of losses in the protuberance.

Fig. 59 is an illustration of the VS case alluded to in sect. 6.4.1 (which applies, as at present, to normal incidence) since the left-hand side of the first relation in (50) is equal to  $0.1499 + i.003$  and the right hand side of the same relation equals 0.1499, this meaning, together with the fact that the second relation in (50) is satisfied exactly, that we are satisfying the conditions (for  $N = 1$ ) that define the VS case and are generating by numerical means (with a very small error) the exact VS solution of the scattering problem alluded-to in sects. 6.4.1-6.4.2. This is another illustration (in addition to the satisfaction of the conservation of flux relation [358]) of the fact that our numerical scheme is sound.

## 12 Seismic response in a small, hard-rock mountain

Empirical evidence of wavefield amplification in hard-rock [17] mountains has been published in [328]. The hard-rock mountain that we now study is higher ( $h = 1000\text{ m}$ ) and wider ( $w = 1000\text{ m}$ ) than the previously-studied hills, and the lossless solid (granite) of which it is composed, as well as of the basement, is much stiffer than those of the hills:  $\mu^{[0]} = 25\text{ GPa}$ ,  $\beta^{[0]} = 2650\text{ ms}^{-1}$ ,  $\mu^{[2]} = 25\text{ GPa}$ ,  $\beta^{[2]} = 2650\text{ ms}^{-1}$ .

### 12.1 Search for the resonances

Figs. 62-64 enable the determination of the first three resonance frequencies of the mountain by location of the maximum of  $\|1/D(f)\|$  (the function depicted in the upper right-hand panels of these figures).

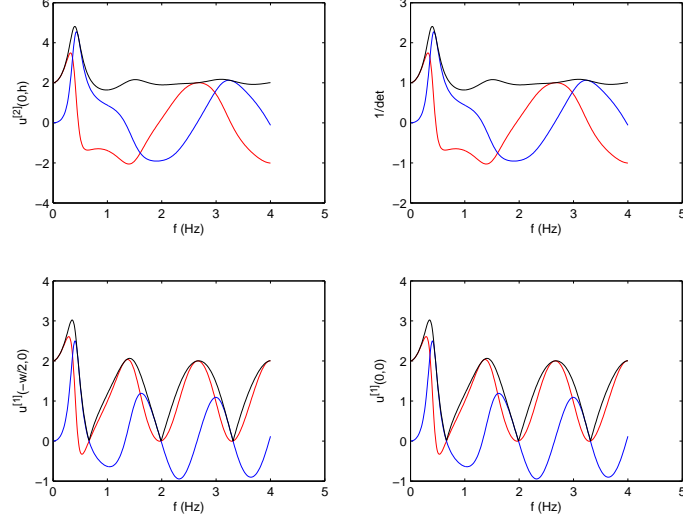


Figure 62:  $\theta^i = 80^\circ$ ,  $h_1 = 0$  m,  $h_2 = 1000$  m,  $w = 1000$  m,  $\mu^{[0]} = 25$  GPa,  $\beta^{[0]} = 2650$  ms<sup>-1</sup>,  $\mu^{[2]} = 25$  GPa,  $\beta^{[2]} = 2650 - i0$  ms<sup>-1</sup>,  $\mathbf{M} = \mathbf{0}$ . The resonance is at:  $f = 0.399$  Hz.

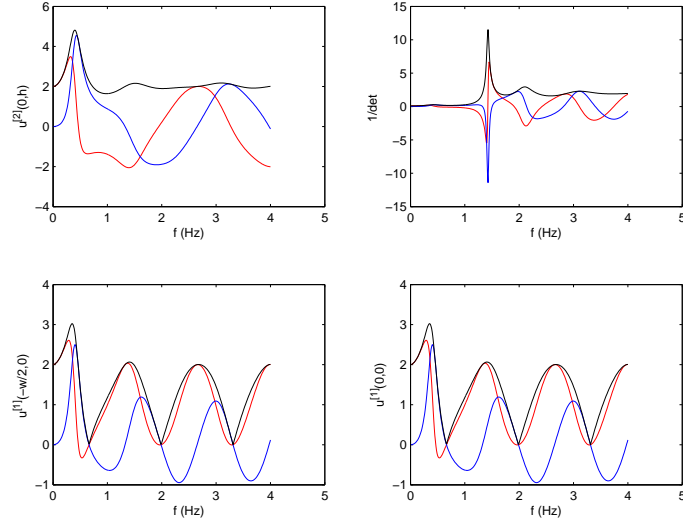


Figure 63: Same as fig. 62 except that  $\mathbf{M} = \mathbf{1}$ . The resonance is at:  $f = 1.426$  Hz.

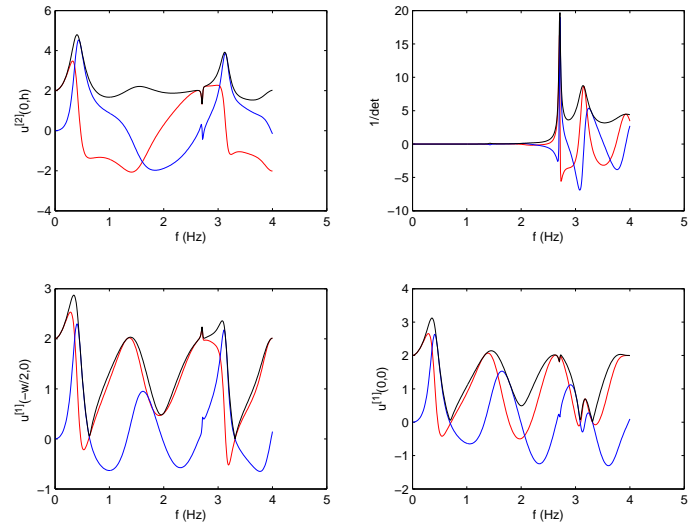


Figure 64: Same as fig. 62 except that  $\mathbf{M} = \mathbf{2}$ . The resonance is at:  $f = 2.713 \text{ Hz}$ .



## 12.2 Response within the mountain at the resonant frequencies and two angles of incidence

Figs. 65-70 constitute field maps of the mountain at several resonant frequencies.

### 12.2.1 Response at the first resonant frequency

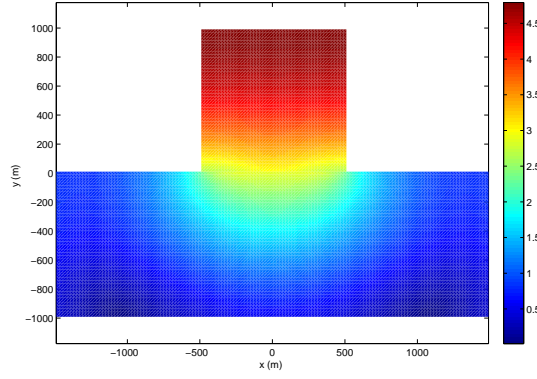


Figure 65:  $f = 0.399 \text{ Hz}$ ,  $\theta^i = 0^\circ$ ,  $h_1 = 0 \text{ m}$ ,  $h_2 = 1000 \text{ m}$ ,  $w = 1000 \text{ m}$ ,  $\mu^{[0]} = 25 \text{ GPa}$ ,  $\beta^{[0]} = 2650 \text{ ms}^{-1}$ ,  $\mu^{[2]} = 25 \text{ GPa}$ ,  $\beta^{[2]} = 2650 - i0 \text{ ms}^{-1}$ ,  $M = 3$ .

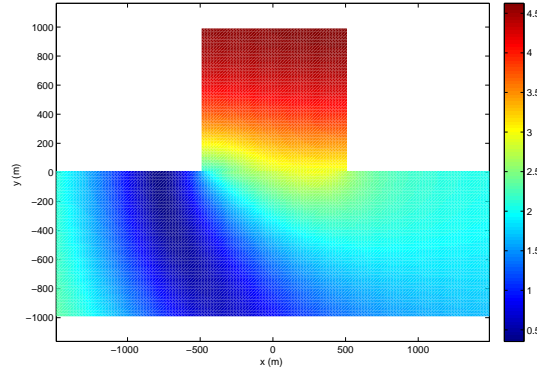


Figure 66: Same as fig. 65 except that  $\theta^i = 80^\circ$ .

### 12.2.2 Response at the second resonant frequency

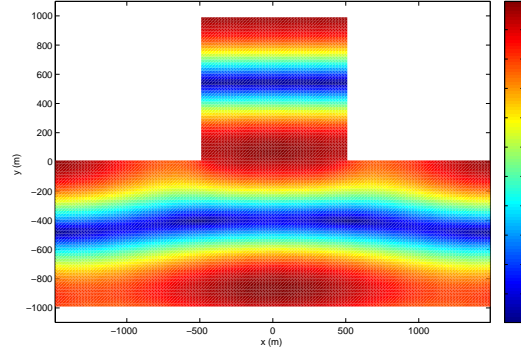


Figure 67:  $f = 1.426 \text{ Hz}$ ,  $\theta^i = \mathbf{0}^\circ$ ,  $h_1 = 0 \text{ m}$ ,  $h_2 = 1000 \text{ m}$ ,  $w = 1000 \text{ m}$ ,  $\mu^{[0]} = 25 \text{ GPa}$ ,  $\beta^{[0]} = 2650 \text{ ms}^{-1}$ ,  $\mu^{[2]} = 25 \text{ GPa}$ ,  $\beta^{[2]} = 2650 - i0 \text{ ms}^{-1}$ ,  $M = 3$

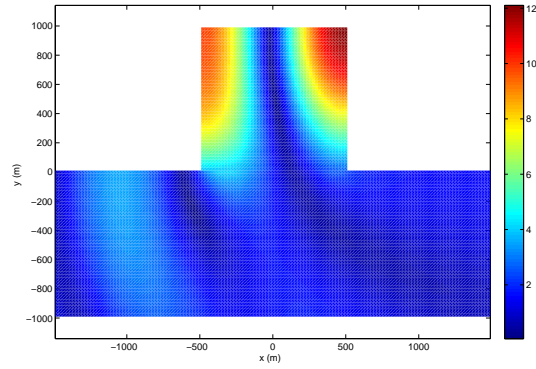


Figure 68: Same as fig. 67 except that  $\theta^i = 80^\circ$ .

### 12.2.3 Response at the third resonant frequency

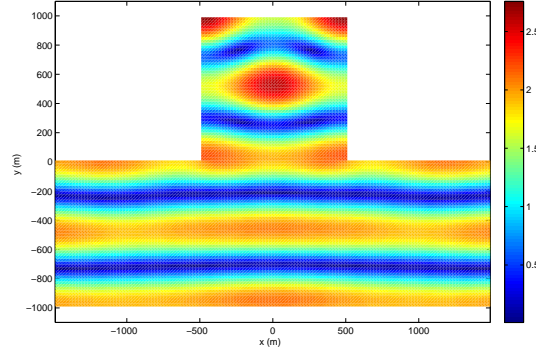


Figure 69:  $f = 2.713 \text{ Hz}$ ,  $\theta^i = \mathbf{0}^\circ$ ,  $h_1 = 0 \text{ m}$ ,  $h_2 = 1000 \text{ m}$ ,  $w = 1000 \text{ m}$ ,  $\mu^{[0]} = 25 \text{ GPa}$ ,  $\beta^{[0]} = 2650 \text{ ms}^{-1}$ ,  $\mu^{[2]} = 25 \text{ GPa}$ ,  $\beta^{[2]} = 2650 - i0 \text{ ms}^{-1}$ ,  $M = 3$ .

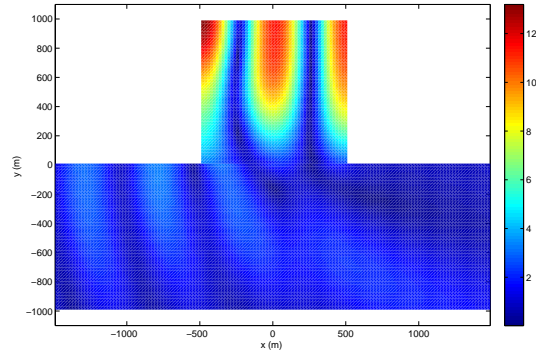


Figure 70: Same as fig. 69 except that  $\theta^i = 80^\circ$ .

These figures show that mountains respond to seismic waves in much the same manner as hills, i.e., they enable coupling to shape resonances at which frequencies the displacement field can attain significantly-large values within the mountain, especially for large incident angles of the plane-wave solicitation.

### 12.3 Response within the mountain at an off-resonant frequency

To appreciate the difference between resonant and non-resonant response, we chose, in figs. 71-72 (for two incident angles) to offer field maps of the mountain at a frequency rather far away from the previous resonant frequencies..

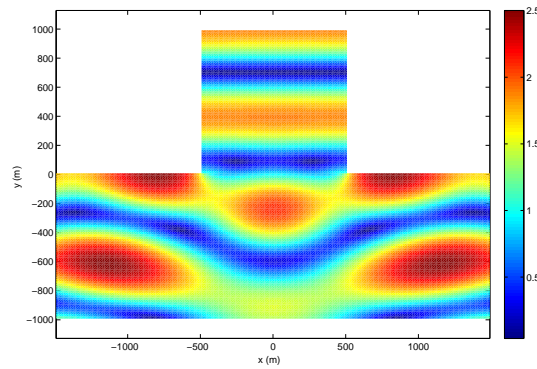


Figure 71:  $f = 2.171 \text{ Hz}$ ,  $\theta^i = 0^\circ$ ,  $h_1 = 0 \text{ m}$ ,  $h_2 = 1000 \text{ m}$ ,  $w = 1000 \text{ m}$ ,  $\mu^{[0]} = 25 \text{ GPa}$ ,  $\beta^{[0]} = 2650 \text{ ms}^{-1}$ ,  $\mu^{[2]} = 25 \text{ GPa}$ ,  $\beta^{[2]} = 2650 - i0 \text{ ms}^{-1}$ ,  $M = 4$ .

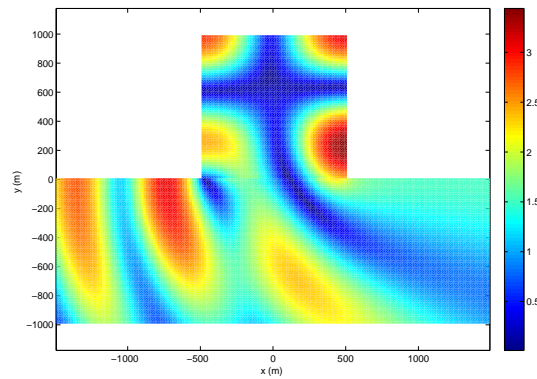


Figure 72: Same as fig. 71 except that  $\theta^i = 80^\circ$ .

These figures show that large-scale seismic response in a mountain (like that in a hill) is possible only at, or in the neighborhood of, its (shape-) resonant frequencies. Furthermore, at the higher-frequency resonant frequencies, the amplified field is highly-concentrated within the protuberance. At off-resonant frequencies, the field leaks out into the lower half space, and the modulus of the field within and outside of the protuberance is of the same (modest, i.e.,  $\sim 2$ ) order.

## 13 Conclusion

This investigation began with a rather broad evocation of the scientific literature on the problem of the response of a large variety of objects (mostly of geophysical interest) to a wavefield solicitation. The reason for having done this was to show that even though many studies treat this general problem, the ones in one field (specially the one dealing with seismics) usually ignore the results (notably of theoretical nature) obtained in another field. Moreover, the great majority of articles, particularly the recent ones, are of numerical and/or parametric nature wherein it is difficult to discern the underlying physical mechanisms giving rise to the numerical results.

In many of the recent investigations, the effort is directed to configurations that are as close to reality as possible, this being increasingly achievable due to the availability of modern numerical (boundary-integral, finite difference, finite element, spectral element,...) methods and powerful computers, but although this can have the effect of making possible the discovery of the universal nature of such phenomena as amplified response, it does not usually afford an understanding (which should be of theoretical nature) of this universality.

For this reason, our study was devoted to a quite simple, perhaps unrealistic, geophysical object: a monolayer or bilayer cylindrical hill or mountain of rectangular shape. Moreover, rather than take into account the complex reality of earthquake sources, we assumed a seismic solicitation in the form of a SH plane body wave. For those who think that real hills and mountains are of triangular rather than rectangular shape, we gave references to the many articles, including our own, that treat this problem in a manner (relying on separation-of-variables (SOV) representations of the field) quite similar to the one adopted herein for a rectangular above-ground structure (AGS). Moreover, we treated the medium in the half-infinite region below the AGS as being homogeneous, although it is well-known that realistic undergrounds are quite inhomogeneous, and often characterized by a layer-like structure, the uppermost layer being softer than the other components of the underground. It is well-known that this layering, especially the one concerning the uppermost layer, has the effect of aggravating the amplifications in the AGS, but this makes it more difficult to define, theoretically, the condition, which we qualify as 'resonant', and related conditions for efficient coupling at the resonance frequencies, that underly these amplifications (however, the interested reader can refer to Groby's thesis and publications to appreciate more completely the complexity of this problem for the seismic response of an AGS residing on a layered underground). Other sources of complexity that we have avoided are the P or SV polarizations of the 2D problems, and the 3D treatments that are now practically-routinely undertaken in numerical studies. A less common type of problem is one in which the media are nonlinear and anisotropic, but even in the more-recent studies it is rare to encounter ones that deal with these elements of reality.

Having evoked the shortcomings of our study, we now mention some of its achievements. First and foremost, we established the general theoretical framework for (surface shape) resonances and applied it to the SOV representation and solution for the chosen AGS. We were thus able to show that the said solution requires the resolution of an infinite-order linear matrix equation (similar

ones occur in a variety of domain decomposition techniques for the description of scattering by other types of objects so that the subsequent remarks are actually of quite general nature) for the wavefield in one of the subregions (i.e., its interior) of the rectangular protuberance and that the resonances occur for those shape parameters and frequency for which the determinant of the matrix equation vanishes (for lossless media and neglect of radiation damping) or is very small (for lossy media and/or account being taken of radiation damping), thus resulting in one or a few of the elements of the SOV coefficients becoming large. We also showed that this condition (for the existence of a resonance) is independent of the characteristics (other than the frequency) of the solicitation, a finding that corroborates and explains such empirically-observed (by Sills and others) independence.

We defined coupling to a resonance as the moment when not only the SOV coefficients (of what we called 'modes'), i.e., the unknowns of the matrix equation, become large, but the characteristics of the solicitation are such as to enable the field within the AGS to become large at certain points within the protuberance (which does not exclude the fact that coupling to resonances also can have a noticeable effect on the wavefield exterior to the AGS). Thus, a vanishing or very small determinant of the matrix equation is a necessary, but not sufficient condition for the field to become amplified (this amplification is what causes destruction at certain points within AGS's and BGS's during earthquakes) at resonance.

Another achievement of this study is the demonstration that it is possible to obtain an exact solution of the chosen scattering problem for normal incidence and when the frequency and geometric/constitutive parameters satisfy a certain so-called VS condition. This solution, which provides a useful testing device for evaluating subsequent numerical results, amounts to the expression of the scattered field everywhere, i.e., in the protuberance as well as in the underground, as a specularly-reflected wave, so that the total field is everywhere in the form of a standing wave.

Furthermore, under certain low frequency, narrow protuberance, normal-incidence conditions, it is possible to obtain an approximate analytical solution for the wavefield that we called the Homogeneous Shear Wall Resonance (HSWR) which is familiar to all those (starting with Trifunac's shear wall paper) who make use of the so-obtained simple formula (that depends only on the height and constitution of the protuberance) for the resonance frequencies to define what they call 'the resonance frequency of the structure', whatever be the width and shape of the structure. By refining this approximation, we were able to show that when the drastic conditions for its existence are relaxed (as is usually the case in realistic situations) the HSWR frequencies can be rather distant from their actual values and the field at resonance is also different from the HSWR prediction.

Having treated the theoretical aspects, we then undertook the numerical resolution (actually a finite-order version) of the matrix equation, tested the so-obtained solution in the VS case, and by seeing if the conservation of flux relation (refer to our previous paper this year) is, as it should be, satisfied.

Further confidence in our numerical scheme was provided by the comparison of our response results with those, supposedly-correct, of Sills. Although this author treated the case of a semi-circular cylindrical hill, his transfer functions were found to resemble ours for a rectangular hill that is closest to Sills' semi-circular hill, this being particularly evident at low frequencies. Above all, the said transfer functions were found to possess characteristic resonant behavior (amplifications at certain frequencies), not very different from those of Sills (who was unaware of their resonant nature), which fact, plus that of the independence of the frequencies of resonance (but not the coupling efficiency at resonance) with respect to the incident angle of the plane wave solicitation,

illustrates the universal nature (i.e., for all types of AGS's) of the resonant response of topographical features.

Moreover, as Sills' results are for the transfer functions at selected points on the scattering boundary of his AGS, and since the locations of interest in seismic engineering are rather in the interior of the AGS, we directed our attention to the internal field of the AGS (this did not exclude the determination of the field in the underground), notably at resonance. This enabled us to show that this field is essentially concentrated (all the more so the resonance frequency and angle of incidence are larger) within (notably near the corners and edges of) the protuberance at resonance, and is much less intense and more dispersed (into the underground) at off-resonance frequencies. All this suggests that the prediction of the seismic response of an AGS by the sole examination of the transfer function at one location (usually taken to be the midpoint of the highest portion of the protuberance) is not foolproof, since the field can, at resonance, be much larger at other points of the boundary, and within, the protuberance. Furthermore, the fact that the efficiency of coupling to the resonances appears to increase with incident angle, shows that it is dangerous to predict the seismic response of an AGS from the sole response at normal incidence. A final result was that when, as is assumed by Sills, the homogeneous medium within this particular hill is identical to that in the underground, the displacement field can attain values at certain points of the hill that are nearly four times the value of the field on flat ground (for the same underground) and larger than the amplifications on the boundary of Sills' hill.

Another, although more-hazardous, test of our numerical scheme was provided by a confrontation with the supposedly-correct (spectral element) numerical and experimental results of Paolucci for a specific hill in Italy. We encountered a difficulty with Paolucci's paper in that the constitutive parameters of the hill and the underground are not well-defined therein and the shape of the hill is only approximately rectangular (which makes it difficult to determine its most-appropriate aspect ratio). Contrary to Sills, Paolucci speaks of resonant response, notably near  $1\text{ Hz}$ , but we were unable to obtain transfer functions similar to his for what we considered our rectangular hill to be closest to his. As with Sills, Paolucci assumes the medium in the hill to be homogeneous and the same as the medium in the underground, and, from what we gathered, to be lossless, but to obtain a response similar to that of Paolucci, we had to introduce substantial losses into the medium.

Thus, the confrontation with Paolucci's results was not very satisfactory, but certain remarks, of historical nature, made by the author of this work, concerning the absence of damage to structures on the ground and damage initiated at the edge(s) of the hill (i.e., landslides), led us to associate the causes of these damages, or absence of damages, with resonances. Again, the field maps within and below the structure proved to be a useful tool for examining this issue. In this way, we showed that the field, rather far away from the  $1\text{ Hz}$  resonance, is concentrated at the two upper edges of the hill when (as is assumed by Paolucci) the incidence is normal, and at only one of these edges when the incidence is oblique. This led us to the speculation that the damage (i.e., landslides, initiated predominantly at one edge of the hill) or absence of damage (to towns on the ground outside of the hill) is due to a resonance initiated by a seismic wave of higher frequency (i.e.,  $4.2\text{ Hz}$ ) and larger angle of incidence than what was assumed by Paolucci.

This speculation was based on the perhaps-dubious assumption that an amplification of approximately 2 at an edge of the hill is sufficient to initiate a landslide, so that we were led to inquire as to whether other hills might give rise to much larger amplifications (recall that our Sills-compatible hill gave rise to amplifications about twice this amount). To do this, we concentrated our attention on a monolayer hill, whose aspect ratio was 3.33, filled with a medium that is softer than that of



the underground. We first treated the case in which the filler medium is lossless, and subsequently when it is lossy. In the lossless case we found, locations within the hill at which the resonant response attains a value of more than 40 (i.e. an amplification with respect to the flat ground field of 20) which is not very different from the empirically-obtained values of Davis and West, among others, but for mountains. This large amplification was obtained at rather high resonance frequencies and for large incident angles, and often not at the midpoint of the top portion of the boundary, which again shows that it is dangerous to predict the overall seismic response of an AGS from its response at such a point.

The next question was whether large amplifications are maintained for the case of a lossy hill. The answer turned out to be that the amplifications at resonance are attenuated all the more so the higher the frequency (they are still largest at 'hotspots' for oblique incidence).

Finally, we turned our attention to the seismic response of a mountain. Our working hypothesis was that a typical mountain: 1) is characterized by a shape which is such that its aspect ratio (i.e., the ratio of the width  $w$  to the height  $h$ , which we chose to be equal to 1) is smaller than that of a hill, and 2) by a composition that is such that the solid in the mountain is the same as in the underground and is hard rock, non lossy-like (we chose granite). We then proceeded as previously by searching for the resonance frequencies via the minima of the determinant of the matrix equation for the coefficient vector  $\mathbf{d}$  (or  $\mathcal{F}$ ) and then plotted the displacement field maps, inside and underneath the mountain, at these resonance frequencies as well as at a non-resonance frequency. The successive resonance frequencies were found to be lower than their counterparts of the hill, and the fields at these frequencies to be less-intense than for a hill, except at the large angle of incidence. Moreover, as for the hills, the field was found to be non-uniformly distributed within and underneath the protuberance, with a clear tendency for it (i.e., its modulus) to be largest near or on the top segment of the boundary, this occurring at all resonance frequencies, and at the top edges for the higher resonance frequencies and incident angle. This again means that there exist regions within the protuberance at which the field is significantly amplified at resonance and our last two figures show that such is not the case at an off-resonance frequency (i.e., at these frequencies, the field within and underneath the mountain is close to what it would be (=2) in the absence of the mountain).

All this shows that the principal (i.e., qualitative) characteristics of the seismic response of a mountain are quite similar to those of a hill, and that the occurrence of significative amplification of the displacement field in certain internal regions of both of these structures is due to the coupling of the incident wave to (surface shape) resonances.

Although we have provided a positive answer to Celebi's question (Topographical amplifications-a reality?), there still exists a host of yet unanswered questions, such as those raised by Assimaki & Jeong on the one hand and Burjanek, Fäh et al. on the other hand, concerning the relative importance of the shape and composition (notably 'weathering') of the protuberance in the amplification phenomena. Other, related, questions have to do with how the radiation damping varies with the protuberance parameters, the role of the aspect ratio and material losses of the protuberance in the level of shaking, as well as how to deal with multiple protuberances spread out on the ground. We shall address these questions in subsequent contributions, mostly in the numerical, parametric manner afforded by our domain decomposition separation of variables formulation.



## References

- [1] Abramowitz M and Segun IA, Handbook of Mathematical Functions, Dover, New York (1968).
- [2] Abubakar I, Scattering of plane elastic waves at rough surfaces. I, Math. Proc. Cambr. Phil. Soc., 58(1), 136-157 (1962).
- [3] Adams BM, Basin-edge effects from SH-wave modelling with reference to the lower Hutt valley, New Zealand, Phd thesis, University of Canterbury NZ (2000).
- [4] Adams SDM, Craster RV and Williams DP, Rayleigh waves guided by topography, Proc. Roy. Soc. 1, 463(2078), 3097-4014 (2006).
- [5] Aki K and Larner KL, Surface motion of a layered medium having an irregular interface due to incident plane SH waves, J. Geophys. Res., 75, 1921-1941 (1970).
- [6] Akhmanov SA, Seminogov VN, and Sokolov VI, Diffraction of light from a rough surface with an arbitrary "deep" profile: interaction of diffracted beams, anomalous absorption, and maximum attainable local fields, Sov. Phys. JETP 66 (5), 945-953 (1987).
- [7] Aldaikh H and Alexander NA and Ibraim E, Discrete model for dynamic structure-soil-structure interaction, 15th WCEE, Lisboa (2012).
- [8] Aldaikh H and Alexander NA, Ibraim E and Oddbjornsson O, Two dimensional numerical and experimental models for the study of structure-soil-structure interaction involving three buildings, Comput. Struct., 150, 79-91 (2015).
- [9] Aldaikh H, Alexander NA, Ibraim E and Knappett J, Shake table testing of the dynamic interaction between two and three adjacent buildings (SSSI), Soil Dynam. Earthqu. Engrg., 14, 219-232 (2016).
- [10] Alexander NA, Ibraim E and Aldaikh H. A simple discrete model for interaction of adjacent buildings during earthquakes. Comput. Struct., 124, 1-10 (2013).
- [11] Alielahi H and Rahimi M, Seismic site response induced by a sedimentary basin: 1D and 2D numerical analysis, 8th SEE, International Conf. Seismology and Earthquake Engineering, Teheran (2019).
- [12] Allen TI and Wald DJ, Topographic slope as a proxy for seismic site-conditions (VS30) and amplification around the globe, USGS Open-File Report 2007-1357 (2007).
- [13] Almuheidib AM and Toksoz MN, Finite difference elastic wave modeling with an irregular free surface using ADER scheme, J. Geophys. Engrg., 12(3), 435-447 (2015).
- [14] Amelsakhi M, Sohrabi-Bidar A and Shareghi A, Spectral assessing of topographic effect on seismic behavior of trapezoidal hill, Int. J. Struct. Construct. Engrg., 8(4), 245-252 (2014).
- [15] Anbazhagan P, Aditya P and Rashmi HN, Amplification based on shear wave velocity for seismic zonation: comparison of empirical relations and site response results for shallow engineering bedrock sites, Geomech. Engrg., 3(3), 189-206 (2011).

- [16] Anggraeni D, Modelling the impact of topography on seismic amplification at regional scale, Phd thesis, University of Twente, Enschede (2010).
- [17] Arora K, Chakraborty T and Rao KS, Constitutive model equation for various types of rock specimen subjected to uniaxial compression loading, in Recent Advances in Rock Engineering, Atlantis Press, New Delhi, 370-374 (2016).
- [18] Asano S, Reflection and refraction of elastic waves at a corrugated interface, Bull. Seism. Soc. Am., 56(1), 201-221 (1966).
- [19] Ashford SA, Sitar N, Lysmer J, and Deng N, Topographic effects on the seismic response of steep slopes, Bull. Seism. Soc. Am., 87(1), 701-709 (1997).
- [20] Ashrafuzzaman MD, Surface topography effects on seismic ground motion and correlation with building damages during the 2015 Mw 7.8 Nepal earthquake, MSc thesis, Univ. Twente, Enschede (2017).
- [21] Assimaki D, Gazetas G, Kausel E, Effects of local soil conditions on the topographic aggravation of seismic motion: parametric investigation and recorded field evidence from the 1999 Athens earthquake, Bull. Seism. Soc. Am., 95(3), 1059-1089 (2005).
- [22] Assimaki D and Jeong S, Ground-Motion Observations at Hotel Montana during the M 7.0 2010 Haiti Earthquake: Topography or Soil Amplification?, Bull. Seism. Soc. Am., 103(5), 2577-2590 (2013).
- [23] Assimaki D, Kausel E and Gazetas G, Wave propagation and soil-structure interaction on a cliff crest during the 1999 Athens Earthquake, Soil Dynam. Earthqu. Engrg., 25, 513-527 (2005).
- [24] Athanasopoulos G, Pelekis P and Leonidou E, Effects of surface topography on seismic ground response in the Egion (Greece) 15 June 10 1995 earthquake, Soil Dyn. Earthqu. Engrg., 18, 135-149 (1999).
- [25] Bakavoli MK, Haghshenas E and Ferdowsi JBB, Effect of nearby topography on amplification of seismic motion in topographic irregularities: The case of a hilly site in Tehran, 15th WCEE, Lisboa (2012).
- [26] Barani S, Massa M, Lovati S and Spallarossa D, Effects of surface topography on ground shaking prediction: implications for seismic hazard analysis and recommendations for seismic design, Geophys. J. Int., 197(3), 1551-1565 (2014).
- [27] Bard P-Y, Diffracted waves and displacement, field over two-dimensional elevated topographies, Geophys. J. R. Astr. Soc., 71, 731-760 (1982).
- [28] Bard P-Y, Effects of surface geology on ground motion: recent results and remaining issues, 10th European conference on earthquake engineering, Balkema, Amsterdam, 305-323 (1995).
- [29] Bard P-Y, Présentation générale des résultats de GEMGEP, Colloque Le risque sismique à Nice, Nice (2005).

- [30] Bard P-Y and Bouchon M, The seismic response of sediment-filled valleys. Part 1. The case of incident SH waves, *Bull. Seism. Soc. Am.*, 70(4), 1263-1286 (1980).
- [31] Bard P-Y and Bouchon M, The two dimensional resonance of sediment filled valleys, *Bull. Seism. Soc. Am.*, 75, 519-541 (1985).
- [32] Bard P-Y and Chaljub E, Effects of surface topography on seismic ground motion: recent results, remaining issues and needs, AGU 09, San Francisco (2009).
- [33] Bard P-Y, Durville JL and Meneroud JP, Influence de la topographie sur la modification des ondes sismiques, *Méditerranée*, 1.2, 113-121 (1984).
- [34] Bard P-Y, Guéguen P, Chazelas JL, Kham M and Semblat JF. Seismic hazard in urban environments: can man modify the hazard?, in 3e Congreso Nacional de Ingenieria Sismica, AEIS, Girona (2007).
- [35] Bard P-Y and Riepl-Thomas J, Wave propagation in complex geological structures and their effects on strong ground motion, *Wave motion in Earthquake Engineering*, Kausel E & Manolis G (Eds.), WIT Press, Southampton, 37-95 (2000).
- [36] Bard P-Y and Tucker BE, 1985. Underground and ridge site effects: a comparison of observation and theory, *Bull. Seism. Soc. Am.*, 75, 905-922 (1985).
- [37] Barrick DE, Low-frequency scatter from a semielliptic groove in a ground plane, *J. Opt. Soc. Am.*, 60(5), 625-634 (1970).
- [38] Beckman P and Spizzichino A, *The Scattering of Electromagnetic Waves from Rough Surfaces*, Artech, Norwood (1987).
- [39] Bertrand E, Regnier J, Vinatier F, Langlade P and Pernoud M, Effects of surface geology on seismic motion, 4th IASPEI / IAEE International Symposium, Santa Barbara (2011).
- [40] Bilham R, Millions at risk as big cities grow apace in earthquake zones, *Nature*, 401, 6755 (1999).
- [41] Bilotta E, Flora A, Lirer S and Viggiani C (Eds.), *Geotechnical Engineering for the Preservation of Monuments and Historic Sites*, CRC Press, Philadelphia, (2013).
- [42] Boore DM, A note on the effect of simple topography on seismic SH waves, *Bull. Seism. Soc. Am.*, 62, 275 -284 (1972).
- [43] Boore DM, The effect of simple topography on seismic waves: Implications for the accelerations recorded at Pacoima Dam, San Fernando Valley, California, *Bull. Seism. Soc. Am.*, 63(5), 1603-1609 (1973).
- [44] Boore DM, Larner KL and Aki K, Comparison of two independent methods for the solution of wave-scattering problems: Response of a sedimentary basin to vertically incident SH waves, *J. Geophys. Res.*, 76(2) 558-569 (1971).
- [45] Bouchon M, Effect of topography on surface motion. *Bull. Seism. Soc. Am.*, 63, 615-632 (1973).

- [46] Bouchon M and Barker JS, Seismic response of a hill: The example of Tarzana, California, *Bull. Seism. Soc. Am.*, 86(1A), 66-72 (1996).
- [47] Bouchon M, Schultz CA and Toksöz., Effect of three-dimensional topography on seismic motion, *J. Geophys. Res.*, doi.org/10.1029/95jB02629 (1996).
- [48] Bouckovalas GD and Papadimitriou AG, Numerical evaluation of slope topography effects on seismic ground motion, *Soil Dyn. Earthqu. Engrg.*, 25(7-10), 547-558 (2005).
- [49] Boutin C and Roussillon P, Assessment of the urbanization effect on seismic response. *Bull. Seism. Soc. Am.*, 94(1), 251-268 (2004).
- [50] Boutin C and Roussillon P, Wave propagation in presence of oscillators on the free surface. *Int. J. Engrg. Sci.*, 44, 180-204 (2006).
- [51] Bowden DC and Tsai VC, Earthquake ground motion amplification for surface waves, *Geophys. Res. Lett.*, 44, 121-127 (2017).
- [52] Bravo MA, Sánchez-Sesma FJ and Chavez-Perez S, , A hybrid approach to study the seismic response of soft-soil sedimentary basins, in *Engineering Seismology and Site Response*, A.S. Cakmak AS and Herrera I (Eds.), Mexico City (1989).
- [53] Bravo MA and Sánchez-Sesma FJ, Seismic response of alluvial valleys for incident P, SV and Rayleigh waves, *Soil Dynam. Earthqu. Engrg.*, 9(1), 16-19 (1990).
- [54] Brûlé S, Enoch S and Guenneau S, Role of nanophotonics in the birth of seismic megastructures, *Nanophotonics*, 8(10), 1591-1605 (2019).
- [55] Büch, Seismic response of Little Red Hill, Phd thesis, Univ. Canterbury (2008).
- [56] Burjanek J, Edwards B and Fäh, D, Empirical evidence of local seismic effects at sites with pronounced topography: a systematic approach, *Geophys. J. Int.*, 197(1), 608-619 (2014).
- [57] Burjanek J, Fäh D, Pischiutta M, Rovelli A, Calderoni G, Bard, P-Y and NERA-JEA working group, Site effects at sites with pronounced topography: overview & recommendations, *Res. Rept. EU project NERA*, doi: 10.3929/ethz-a-010222426 (2014).
- [58] Burjanek J, Gassner-Stamm G, Poggi V, Moore JR and Fah D, Ambient vibration analysis of an unstable mountain slope, *Geophys. J. Int.*, 180(2), 820-828 (2010).
- [59] Buyukaksoy A, Birbir F and Erdogan E, Scattering characteristics of a rectangular groove in a reactive surface, *IEEE Trans. Anten. Prop.*, 1450- AP-43(12) (1995).
- [60] Campanini G, Seismic vulnerability of building heritage in Aggregate: Civita Di Bagnoregio study case, *ATINER Conference Paper Series ARC2013-0557*, Athens Institute for Education and Research, Athens (2013).
- [61] Campillo M, Gariel JC, Aki K and Sanchez-Sesma FJ, Destructive strong motion in Mexico City: source, path, and site effects during great Michoacan Earthquake, *Bull. Seism. Soc. Am.*, 79(6), 1718-1735 (1989).

- [62] Cauzzi C, Kalogeras I, Melis N, Stupazzini M, Mazzieri I and Clinton J, Seismic response of the Acropolis of Athens (Greece) through recorded earthquake data and numerical simulations, 6th Intl. Conf. Earthqu. Geotech. Engrg., Christchurch (2015).
- [63] Carmona S, Sisterna C, Sabbione N, Magrini M, Palau R, Garcia L and Pincioli R, Effects of distant and large magnitude earthquakes on the tallest buildings in Buenos Aires City, 12th WCEE 2000, paper no. 2718 (2000).
- [64] Celebi M, Topographical and geological amplifications determined from strong-motion and aftershock records of the 3 March 1985 Chile earthquake, *Bull. Seism. Soc. Am.*, 77(4), 1147-1167 (1987).
- [65] Celebi M, Topographical amplifications-a reality?, 9th WCEE, Tokyo (1988).
- [66] Celebi M, Okawa I, Kashima T, Koyama S and Iiba M, Response of a tall building far from the epicenter of the 11 March 2011 M 9.0 Great East Japan earthquake and aftershocks, *Struct. Design Tall Spec. Build.*, 23, 427-441 (2014).
- [67] Celebi M, Comparison of recorded dynamic characteristics of structures and ground during strong and weak shaking, in *Increasing Seismic Safety by Combining Engineering Technologies and Seismological Data*, Mucciarelli M, Herak M, Cassidy J (Eds.), Springer, Dordrecht, 99-115 (2008).
- [68] Chang K-H, Tsaur D-H and Wang J-H, Ground motions around a semi-circular valley partially filled with an inclined alluvial layer under SH-polarized excitation, *Planets and Space*, 66, 53 (2014).
- [69] Chang K-H, Tsaur D-H and Wang J-H, Response of a shallow asymmetric V-shaped canyon to antiplane elastic waves. *Proc. Roy. Soc. A*, 471, 20140215 (2015).
- [70] Chavez-Garcia FJ and Cardenas-Soto M, The contribution of the built environment to the 'free-field' ground motion in Mexico City, *Soil Dynam. Earthqu. Engrg.*, 22, 773-780 (2002).
- [71] Chen J-T, Lee J-W, Wu C-F and Chen I-L, SH-wave diffraction by a semi-circular hill revisited: A null-field boundary integral equation method using degenerate kernels, *Soil Dyn. Earthqu. Engrg.*, 31(5-6), 729-736 (2011).
- [72] Chen Q-J, Li W-T, Effects of a group of high-rise structures on ground motions under seismic excitation, *Shock Vibration*, [dx.doi.org/10.1155/2015/821750](https://doi.org/10.1155/2015/821750) 1-25 (2015).
- [73] Chen ZW, Huang D, Wang G and Jin F, Topographic amplification on hilly terrain under oblique incident waves, *Conference: The International Commission on Large Dams 2019 Annual Meeting*, Ottawa, (2019).
- [74] Clouteau D and Aubry D, Modification of the ground motion in dense urban areas, *J. Comput. Acoust.*, 9, 1659-1675 (2001).
- [75] Clouteau D and Aubry D, Site effects on 3D elevated topography, *Trans. Built Environ. WIT Press*, 14 (1995).

- [76] Courjon D and Bainier C (Eds.), *La Champ Proche Optique* , Springer, Paris (2001).
- [77] Das PC and Gersten JI, Surface shape resonances, *Phys. Rev. B* 25, 6281 (1982).
- [78] Datta TK, Seismic response of buried pipelines: a state-of-the-art review, *Nucl. Engrg. Design*, 192(2-3), 271-284 doi.org/10.1016/S0029-5493(99)00113-2Get (1999).
- [79] Davis LL and West LR, Observed effects of topography on ground motion, *Bull. Seismol. Soc. Am.*, 63, 283-298 (1973).
- [80] Diatta A and Guenneau S, Elastodynamic cloaking and field enhancement for soft spheres, *J. Phys. D: Appl. Phys.*, 49 445101 (2016).
- [81] Diaz-Nunez P, Garcia-Martin JM, Gonzalez MU et al., On the large near-field enhancement on nanocolumnar gold substrates, *Scientif. Repts.*, 9, 13933 (2019).
- [82] Ditommaso R, Gallipoli MR, Mucciarelli M and Ponzo FC, Effect of vibrating building on "free field" ground motion: From the Bagnoli experiment to many-buildings simulation, *Proc 4th International Conference on Earthquake Geotechnical Engineering*, paper no. 1388, Springer, New York (2007).
- [83] Ditommaso R, Mucciarelli M, Gallipoli MR and Ponzo FC, Effect of a single vibrating building on freefield ground motion: numerical and experimental evidences, *Bull. Earthqu. Engrg*, 8(3), 693-703 (2010).
- [84] Donmez C, Eeri M and Pujol S, Spatial distribution of damage caused by the 1999 earthquakes in Turkey, *Earthqu. Spectra*, 21(1), 53-69 (2005).
- [85] Ducellier A and Aochi H, Interactions between topographic irregularities and seismic ground motion investigated using a hybrid FD-FE method. *Bull. Earthqu. Engrg.*, 10(3), 773-792 (2012).
- [86] Durand C, Chaljub E, Bard P-Y, Fry J-J, Kolmayer P and Tachker P, Méthodologie simplifiée pour la justification au séisme d'une digue sur fondation meuble, *Colloque CFBR: Justification des barrages: Etat de l'art et Perspectives*, Chambéry, (2019).
- [87] Durand S, Gaffet S and Jean Virieux J, Seismic diffracted waves from topography using 3-D discrete wavenumber-boundary integral equation simulation, *Geophys.*, 64(2), 572-578 (1999).
- [88] Duval A-M, Bertrand E, Vidal S and Delgado J, Détection des effets de site sismiques, Mise au point de méthodes expérimentales et application à Nice, *Bull. LCPC*, 279, 3-20 (2013).
- [89] Emert L, Poggi V, Burjanek J and Fäh D, Fundamental and higher two-dimensional resonance modes of an Alpine valley, *Geophys. J. Int.*, 198, 795-811 (2014).
- [90] Engheta N and Ziolkowski RW (Eds.), *Electromagnetic Metamaterials: Physics and Engineering Explorations*, Wiley, New York (2006).
- [91] Ewing WM, Jardetzky WS and Press F, *Elastic Waves in Layered Media*, McGraw-Hill, New York (1957).



- [92] Fajfar P, Vidic T and Fischinger M, A measure of earthquake motion capacity to damage medium- period structures, *Soil Dyn. Earthqu. Engrg.*, 9(5), 236-242 (1999).
- [93] Fano U, Some theoretical considerations on anomalous diffraction gratings *Phys. Rev.* 50(6), 573 (1936).
- [94] Fano U, The theory of anomalous diffraction gratings and of quasi-stationary waves on metallic surfaces (Sommerfeld's Waves), *J. Opt. Soc. Am.*, 31(3), 213-222 (1941).
- [95] Farahani RV, Dessalegn TM, Vaidya NR, et al., Seismic soil-structure interaction analysis of a nuclear power plant building founded on soil and in degraded concrete stiffness condition, *Nuclear Engineering and Design*, 297, 320-326 (2016).
- [96] Farias D and Rieder K-H, Atomic beam diffraction from solid surfaces, *Rep. Prog. Phys.* 61, 1575-1664 (1998).
- [97] Fedotov V, Metamaterials, in *Springer Handbook of Electronic and Photonic Materials*, Kasap S and Capper P (Eds), Springer Handbooks. Springer, Berlin (2017).
- [98] Fernandez-Ares A and Bielak J, Urban seismology: interaction between earthquake ground motion and multiple buildings in urban regions, in *ESG 2006*, Bard P-Y, Chaljub E, Cornu C, Cotton F and Guéguen P. (Eds.), LCPC, Paris, 87-96 (2006).
- [99] Firth NV, Hilton RG, Howarth JD et al., Carbon export from mountain forests enhanced by earthquake-triggered landslides over millennia, *Nature Geosci.*, 11(10), DOI: 10.1038/s41561-018-0216-3 (2018).
- [100] Fishman KL and Ahmad S, Seismic response for alluvial valleys subjected to SH, P and SV waves, *Soil Dyn. Earthqu. Engrg.*, 14(4), 249-258 (1995).
- [101] Flores J, Nodal patterns in the seismic response of sedimentary valleys, *European Phys. J. Special Topics* 145(1), 63-75 (2007).
- [102] Flores J, Novaro O and Seligman TH, Possible resonance effect in the distribution of earthquake damage in Mexico City, *Nature*, 326, 83-785 (1987).
- [103] Froude MJ and Petley DN, Global fatal landslide occurrence 2004 to 2016, *Nat. Hazards Earth Syst. Sci. Discuss.*, doi.org/10.5194/nhess-2018-49 (2018).
- [104] Furumura M, Sasatani T and Furumura T, Generation of basin-induced surface waves observed in the Tokachi Basin, Hokkaido, Japan, *J. Phys. Earth*, 45, 287-305 (1997).
- [105] Gaffet S and Bouchon M, Effects of two-dimensional topographies using the wavenumber boundary integral element method in P-SV cases. *J. Acoust. Soc. Am.*, 85, 2277-2283 (1989).
- [106] Gallipoli ME, Bianca M, Mucciarelli M, Parolai S and Picozzi M., Topographic vs. stratigraphic amplification: mismatch between code provisions and observations during the L'Aquila (Italy, 2009) sequence, *Bull. Earthqu. Engrg.*, 11(5), dpo: 10.1007/s10518-013-9446-3 (2013).
- [107] Garcia N, Goodman FO, Celli V and Hill NR, Theory of elastic scattering of atoms by a hard corrugated surface with an attractive potential, *Phys. Rev. B* 19, 1808 (1979).

- [108] García-Vidal FJ, Sánchez-Dehesa J, Dechelette A, Bustarret E, López-Ríos T, Fournier T, and Pannetier B, Localized surface plasmons in lamellar metallic gratings, *J. Lightwave Technol.*, 17(11) 2191-2195 (1999).
- [109] Garini E, Anastasopoulos I and Gazetas G, Soil, basin and soil-building-soil interaction effects on motions of Mexico City during seven earthquakes, *Géotechn.*, doi.org/10.680/geot.18.P.314 (2019).
- [110] Gatti F, Lopez-Caballero F, Clouteau D and De Abreu Correa L, Broad-band 3-D physics-based simulation of earthquake-induced wave-field at the Kashiwazaki-Kariwa Nuclear Power Plant (Japan): an all-embracing source-to-site approach, 16th European Conference on Earthquake Engineering (16ECEE), Thessaloniki (2018).
- [111] Geli L, Bard P-Y and Jullien B, The effect of topography on earthquake ground motion: A review and new results, *Bull. Seism. Soc. Am.*, 78, 42-63 (1988).
- [112] Geonmonond RS, Da Silva AGM, Rodrigues TS, De Freitas IC, Ando RA, Alves TV and Camargo HC, Addressing the effects of size-dependent absorption, scattering, and near-field enhancements in plasmonic catalysis, *ChemCatChem*, 10(16), doi.org/10.1002/cctc.201800691 (2018).
- [113] Ghergu M and Ionescu IR, Structure-soil-structure coupling in seismic excitation and "city effect", *Int. J. Engrg. Sci.*, 47: 342-354 (2009).
- [114] Giannini V, Sánchez-Gil JA and García-Ramos JV, Electromagnetic model and calculations of the surface-enhanced Raman-shifted emission from Langmuir-Blodgett films on metal nanostructures, *J. Chem. Phys.*, 127, 044702 (2007).
- [115] Glazer SN, Mine Seismology: Seismic response to the caving process: A case study from four mines, doi: 10.1007/978-3-319-95573-5 (2019).
- [116] Golub MV, Eremin AA, Shpak AN and Lammering R, Lamb wave scattering, conversion and resonances in an elastic layered waveguide with a surface-bonded rectangular block, *Appl. Acoust.*, 155(1), 442-452 (2019).
- [117] Gouasima A, Numerical simulation of seismic soil-structure interaction including site effects. 31 ièmes Rencontres de l'AUGC, ENS Cachan 2013.
- [118] Graizer V, Low-velocity zone and topography as a source of site amplification effect on Tarzana hill, California, *Soil Dyn. Earthqu. Engrg.*, 29, 324-332 (2009).
- [119] Griffith DW and Bollinger GA, The effect of Appalachian mountain topography on seismic waves. *Bull. Seism. Soc. Am.*, 69, 1081-1105 (1979).
- [120] Groby J-P, Modélisation de la propagation des ondes élastiques générées par un séisme proche ou éloigné à l'intérieur d'une ville, PhD thesis, Université de la Méditerranée-Aix-Marseille II, hal.archives-ouvertes.fr/tel-00115636 (2005).
- [121] Groby J.-P., Dazel O., Duclos A., Boeckx L. and Kelders L., Enhancing the absorption coefficient of a backed rigid frame porous layer by embedding circular periodic inclusions, *J. Acoust. Soc. Am.*, 130(6), 3771-3780 (2011).



- [122] Groby J.-P., Duclos A., Dazel O., Boeckx L. and Lauriks W., Absorption of a rigid frame porous layer with periodic circular inclusions backed by a periodic grating, *J. Acoust. Soc. Am.* 129 (5), 3035-3046 (2011).
- [123] Groby J-P, Tsogka C and Wirgin A, Simulation of seismic response in a city-like environment, *Soil Dyn. Earthqu. Engrg.*, 25, 487-504 (2005).
- [124] Groby J-P and Wirgin A, Two-dimensional ground motion at a soft viscoelastic layer/hard sub- stratum site in response to SH cylindrical seismic waves radiated by deep and shallow line sources-I. Theory. *Geophys J Int*; 163: 165-191 (2005).
- [125] Groby J-P and Wirgin A, Two-dimensional ground motion at a soft viscoelastic layer/hard sub- stratum site in response to SH cylindrical seismic waves radiated by deep and shallow line sources-II. Numerical results, *Geophys. J. Int.*, 163, 192-224 (2005).
- [126] Groby J-P and Wirgin A, Seismic motion in urban sites consisting of blocks in welded contact with a soft layer overlying a hard half-space. *Geophys. J. Int.*, 172(2), 725-758 (2008).
- [127] Guéguen P, Bard P-Y and Chavez-Garcia FJ, Site-city seismic interaction in Mexico City-like environments: an analytical study, *Bull. Seism. Soc. Am*, 92(2), 794-811 (2002).
- [128] Guéguen P and Colombi A, Experimental and numerical evidence of the clustering effect of structure on their response during an earthquake: a case study of three identical towers in the city of Grenoble, France, *Bull. Seism. Soc. Am*, 106(6), doi: 10.1785/0120160057 (2016).
- [129] Guéguen P, Semblat J-F, Bard P-Y and Chazelas J-L, Site-Ville : Approches expérimentales et numériques, *Bull. Labos. Ponts Chaussées*, 35-46 (2013).
- [130] Gunes O, Turkey's grand challenge: Disaster-proof building inventory within 20 years, *Case Stud. Construc. Mater.*, 2, 18-34 (2015).
- [131] Han F, Wang G-Z and Kang C-Y, Scattering of SH-waves on triangular hill joined by semi-cylindrical canyon, *Appl. Math. Mech. (Engl. ed.)*, 32(3), 309-326 (2011).
- [132] Hao L, Lee VW and Liang J, Anti-plane (SH) waves diffraction by an underground semi-circular cavity: analytical solution, *Earthqu. Engrg. Engrg. Vibr.*, 9, 385-396 (2010). Anti-plane (SH) waves diffraction by an underground semi-circular cavity: analytical solution
- [133] Harkrider DG, Surface waves in multilayered elastic media i. Rayleigh and Love waves from buried sources in a multilayered elastic half-space. *Bull. Seism. Soc. Am.*, 54, 627-679 (1964).
- [134] Harrison RK, Mechanisms and applications of near-field and far- field enhancement using plasmonic nanoparticles, *Phd thesis, Univ. Texas at Austin, Austin* (2012).
- [135] Hartzell S, Meremonte M, Ramirez-Guzman L and McNamara D, Ground motion in the presence of complex topography: Earthquake and ambient noise sources, *Bull. Seism. Soc. Am.*, 104(1), 451-466 (2014).
- [136] Havenith HB, Jongmans D, Faccioli E, Abdrakhmatov K and Bard P-Y, Site effect analysis around the seismically induced Ananevo rockslide, Kyrgyzstan, *Bull. Seism. Soc.Am.*, 92(8), 3190-3209 (2002).

- [137] Havenith H-B, Strom A, Jongmans D, Abdrakhmatov A, Delvaux D et al., Seismic triggering of land slides, Part A: Field evidence from the Northern Tien Shan, in *Natural Hazards and Earth System Science*, Copernicus Pub. on behalf of the EGU, 3 (1/2), 135-149 (2003).
- [138] Hayir A, Todorovska MI and Trifunac MD, Antiplane response of a dike with flexible soil-structure interface to incident SH waves, *Soil Dynam. Earthqu. Engrg.*, 21, 603-613 (2001).
- [139] Heap MJ, Baud P, Meredith PG, Vinciguerra S and Reuschl T, The permeability and elastic moduli of tuff from Campi Flegrei, Italy: implications for ground deformation modelling, *Solid Earth*, 5, 25-44 (2014).
- [140] Heuer M and Rice TM, Theory of diffuse atom scattering from isolated adatoms, *Z. Physik B*, 59(3), 299-309 (1985).
- [141] Hewitt K, Seismic risk and mountain environments: the role of surface conditions in earthquake disaster, *Mountain Res.*, 3(1, 27-44) (1983).
- [142] Hill NR and Levander AR, Resonances of low-velocity layers with lateral variations, *Bull. Seism. Soc. Am.*, 74 (2) 521-537 (1984).
- [143] Hirotani K, Ogata Y, Otake H and Iida J, Simulation analysis of earthquake response of Onagawa nuclear power plant to the 2011 off the Pacific coast of Tohoku earthquake, 15th ECEE, Lisboa (2012).
- [144] Hisada Y and Yamamoto S, One-, two-, and three-dimensional site effects in sediment-filled basins, 11th World Conf. Earthqu. Engrg., paper 2040 (1996).
- [145] Holley JR and Schnitzer O, Extraordinary transmission through a narrow slit, *Wave Motion*, 91, 102381
- [146] Housner GW, Interaction of building and ground during an earthquake, *Bull. Seism. Soc. Am.*, 47, 179-86 (1957).
- [147] Huang C-F, Acoustic wave scattering from rough sea surface and seabed, Master thesis, National Sun-Yat-Szn Univ. (1998).
- [148] Hudson JA, Humphries RF, Mason IM and Kumbhani VK, The scattering of longitudinal elastic waves at a rough surface, *J. Phys. D Appl. Phys.*, 6, 2174-2183 (1973).
- [149] Hulpke E (Ed.), *Helium Atom Scattering from Surfaces*, Springer, Berlin (2010).
- [150] Imperatore P, Iodice A and Riccio D, Transmission through layered media with rough boundaries: First-order perturbative solution, *IEEE Trans. Anten. Prop.*, 57(5), 1481-1494 (2009).
- [151] Isbilibroglu Y, Taborda R and Bielak J, Coupled soil-structure interaction and coupling effects in building clusters, in *Proc. Tenth U.S. National Conf. Earthqu. Engrg.*, Anchorage (2014).
- [152] Isbilibroglu Y, Taborda R and Bielak J, Coupled soil-structure interaction effects of building clusters during earthquakes, *Earthqu. Spectra*, 31, 1-38 (2015).

- [153] Janod F and Coutant O, Seismic response of three-dimensional topographies using a time-domain boundary element method, *Geophys. J. Int.*, 142, 603-614 (2000).
- [154] Jarenprasert S, Bazan-Zurita E and Bielak J, Seismic soil-structure interaction response of inelastic structures, *Soil Dyn. Earthqu. Engrg.*, 47, 132-143 (2013).
- [155] Jardetzky WS and Press F, Crustal structure and surface wave dispersion. III: Theoretical dispersion curves for suboceanic Rayleigh waves, *Bull. Seism. Soc. Am.*, 43, 137-144 (1953).
- [156] Jennings PC and Bielak J, Dynamics of building-soil interaction, *Bull. Seism. Soc. Am.*, 63, 9-48 (1973).
- [157] Jin L and Liang J, Dynamic soil-structure interaction with a flexible foundation embedded in a half-space: Closed-form analytical solution for incident plane SH waves, *J. Earthqu. Engrg.*, DOI: 10.1080/13632469.2019.1586802 (2019).
- [158] Jongmans D, Les phénomènes d'amplification d'ondes sismiques dus à des structures géologiques, *Ann. Soc. Geol. Belg.* 112(2), 369-379 (1989).
- [159] Kamalian M, Jafari MK, Sohrabi-Bidar A and Razmkhah A, Seismic response of 2-D semi-sine shaped hills to vertically propagating incident waves: Amplification patterns and engineering applications, *Earthqu. Spectra*, 24(2), 405-430 (2008).
- [160] Kanamori H, Jennings PC, Singh SK and Astiz L, Estimation of strong ground motions in Mexico City expected for large earthquakes in the Guerrero seismic gap, *Bull. Seism. Soc. Am.*, 83(3), 811-829 (1993).
- [161] Kawase H, The cause of the damage belt in Kobe: "The basin-edge effect", constructive interference of the direct S-Wave with the basin-induced diffracted/Rayleigh waves, *Seism. Res. Lett.*, 67(5), 25-34 (1996).
- [162] Kawase H, Site effects on strong ground motion, in *International Handbook of Earthquake & Engineering Seismology*, Lee WHK, Kanamori H, Jennings P and Kisslinge C (Eds.), Academic Press, 61, 1013-1030 (2003).
- [163] Kawase H, Seismic responses of irregular ground-four decades of development from theory to observation, 14 th World Conference on Earthquake Engineering, Beijing (2008)
- [164] Kawase H, Matsushima S, Baoyintu A, Motosaka M, Ohno S, Watanabe H, Tanaka R, Tanaka H, Ogawa J, Yamaya R and Take Y, Earthquake, geology, and tsunami, in *Preliminary Reconnaissance Report of the 2011 Tohoku-Chiho Taiheiyō-Oki Earthquake*, Architectural Institute of Japan (Ed.), Springer, Tokyo, 29-114 (2012).
- [165] Keefer DK, The importance of earthquake-induced landslides to long-term slope erosion and slope-failure hazards in seismically active regions, *Geomorphology*, 10(1-4), 265-284 (1994).
- [166] Kennett BLN, Seismic wave scattering by obstacles on interfaces, *Geophys. J. R. Astr. Soc.*, 28, 249-266, (1972)
- [167] Kennett BLN, Seismic waves in laterally inhomogeneous media, *Geophys. J. R. Astr. Soc.*, 27, 301-325 (1972).

- [168] Kennett BLN, The Seismic Wavefield, Volume I: Introduction and Theoretical Development, Cambridge U. Press, Cambridge (2001).
- [169] Kham M, Propagation d'ondes sismiques dans les bassins sédimentaires : Des effets de site à l'interaction site-ville, Phd thesis, Ecole Nationale des Ponts et Chaussees, Paris (2004).
- [170] Kham M, Semblat JF, Bard P-Y and Dangla P, Seismic site-city interaction: main governing phenomena through simplified numerical models, Bull. Seism. Soc. Am., 96(5), 1934-1951 (2006).
- [171] Khan S, Van der Meijde M, Van der Werff H and Shafique M, The impact of topography on seismic amplification during the 2005 Kashmir earthquake, , Nat. Hazards Earth Syst. Sci. Discuss., <https://doi.org/10.5194/nhess-2019-13> (2019).
- [172] Khodasevych IE, Wang L, Mitchell A and Rosengarten G, Micro- and Nanostructured Surfaces for Selective Solar Absorption doi:10.1002/adom.201500063 (2015).
- [173] Knopoff L., A matrix method for elastic wave problems, Bull. Seism. Soc. Am., 54(1), 431-438 (1964).
- [174] Kojic S and Trifunac MD, Earthquake stresses in arch dams: I. theory and antiplane excitation, J. Eng. Mech. ASCE, 117(3), 532-552 (1991).
- [175] Kojic S and Trifunac MD, Earthquake stresses in arch dams: II. excitation by SV, P and Rayleigh waves, J. Eng. Mech. ASCE, 117(3), 553-574 (1991).
- [176] Kontoe S, Zdravkovic L, Pottes DM and Menkiti CO, Case study on seismic tunnel response, Canad. Geotech. J., DOI: 10.1139/T08-087 (2008).
- [177] Kouoh-Bille L, Sanchez-Sesma F-J and Wirgin A, Réponse résonante d'une montagne cylindrique à une onde sismique SH, C. R. Acad. Sci. Paris, 312, Série II, 849-854 (1991).
- [178] Kouoh-Bille L and Wirgin A, Réponse sismique en surface d'une montagne triangulaire soumise à une onde SH, C. R. Acad. Sci. Paris, 315, Série II, 1187-1192 (1992).
- [179] Krishnan S, Ji C, Komatitsch D and Tromp J, Case studies of damage to tall steel moment-frame buildings in southern California during large San Andreas earthquakes, Bull. Seism. Soc. Am., 96, 1523- 1537 (2006).
- [180] Krowne CM and Zhang Y, Physics of Negative Refraction and Negative Index Materials, Springer, Berlin (2007).
- [181] Kumar N and Narayan JP, Effects of hilly region topography on Rayleigh wave, Conference on Infrastructure Sustainability in Hilly Regions (CISHR) (2018).
- [182] Kumar N and Narayan JP, Comparison of 3D and 2D site-city interaction effects on building response and free field motion under double resonance condition , ASCE Conf. Urbanization Challenges in Emerging Economies (2018).
- [183] Kumar N and Narayan JP, Role of shape and numbers of ridges and valleys in the insulating effects of topography on the Rayleigh wave characteristics, doi.10.1007/s00024-018-1832-y.

- [184] Kumar N and Narayan JP, Quantification of fundamental frequencies of 3D basins and structures and site-city interaction effects on responses of structures, *Pure Appl. Geophys.*, doi.org/10.1007/s00024-019-02158-8 (2019).
- [185] Kumar N and Narayan JP, Quantification of site-city interaction effects on the response of structure under double resonance condition, *Geophys. J. Intl.*, doi: 10.1093/gji/ggx397 (2017).
- [186] Kumar R, Tomar SK and Chopra A, Reflection/refraction of SH-waves at a corrugated interface between two different anisotropic and vertically heterogeneous elastic solid half-spaces, *Anziam J.*, 44, 447-460 (2003).
- [187] Lamb H, On waves in an elastic plate, *Proc. R. Soc. London, A* 93, 114-128 (1917).
- [188] Laske G and Widmer-Schmid R, Theory and observations: normal mode and surface wave observations, in *Treatise on Geophysics*, Second Edition, Elsevier, London, <http://dx.doi.org/10.1016/B978-0-444-53802-4.00003-8> (2015).
- [189] Laurendeau A, Définition du mouvement sismique "au rocher", Phd thesis, Univ. Grenoble, Grenoble (2013).
- [190] Laurenzano G, Priolo E, Gallipoli MR, Mucciarelli M and Ponzo FC, Effect of vibrating buildings on free-field motion and on adjacent structures: Bonefro (Italy) case, history. *Bull. Seism. Soc. Am.*, 100(2), 802-818 (2010).
- [191] LeBrun B, Hatzfeld D and Bard P-Y, Experimental study of the ground-motion on a large scale topographic hill a Kitherion (Greece), *J. Seismology*, 3, 1-15 (1999).
- [192] Lee MW, Proposed moduli of dry rock and their application to predicting elastic velocities of sandstones, *Scientific Investigations Report 2005-5119 UGS*, Reston (2005).
- [193] Lee VW and Amornwongpaibun A, Scattering of anti-plane (SH) waves by a semi-elliptical hill: I - shallow hill, *Soil Dyn. Earthqu. Engrg.*, 52, 116-125 (2013).
- [194] Lee VW and Amornwongpaibun A, Scattering of anti-plane (SH) waves by a semi-elliptical hill: II-deep hill, *Soil Dyn. Earthqu. Engrg.*, 52, 126-137 (2013).
- [195] Lee SJ, Chan YC, Komatitsch D, Huang BS and Tromp J, Effects of realistic surface topography on seismic ground motion in the Yangminshan region of Taiwan based on the spectral-element method and LiDAR DTM, *Bull. Seism. Soc. Am.*, 99, 681-693 (2009).
- [196] Lee VW, Liu WY, Trifunac MD and Orbovic N, Scattering and diffraction of earthquake motions in irregular elastic layers, I: Love and SH waves, *Soil Dyn. Earthqu. Engrg.*, 66, 125-134 (2014)
- [197] Lee VW, Luo H and Liang J, Antiplane (SH) waves diffraction by a semicircular cylindrical hill revisited: An improved analytic wave series solution, *J. Engrg. Mech.*, 132(10) (2006).
- [198] Le Perchec J, High-efficiency subwavelength bridge-shaped photo-absorbers based on transverse cavity modes, *Optics Lett.*, 44(21) (2019).

- [199] Le Perchec J, Light-field enhancement on thin and ultra-thin high-index dielectric slabs with rectangular nano-pits, *J. Opt. Soc. Am. B*, 36(8) (2019).
- [200] Le Perchec J, Barbara A and Qu  merais, Near-, mesoscopic and far-field regimes of a sub-wavelength Young’s double-slit, *New J. Phys.*, 13, 083025 (2011).
- [201] Levander AR and Hill NR, P-SV resonances in irregular low velocity layers, *Bull. Seism. Soc. Am.*, 75, 847-864 (1985).
- [202] Levy A and Deresiewicz H, Reflection and transmission of elastic waves in a system of corrugated layers, *Bull. Seism. Soc. Am.*, vol. 57(3) 393-419 (1967).
- [203] Li K, Hogan J, Kale MJ, Halas NJ, Nordlander P and Christopher P, Balancing near-field enhancement, absorption, and scattering for effective antenna-reactor plasmonic photocatalysis, *Nano Lett.*, 17(6), 3710-3717 (2017).
- [204] Lin C, Wang B, Teo KH and Zhang Z, Near-field enhancement of thermoradiative devices, *J. Appl. Phys.* 122, 143102, <https://doi.org/10.1063/1.5007036> (2017).
- [205] Liu G, Chen H, Liu D and Khoo BC, Surface motion of a half-space with triangular and semicircular hills under incident SH Waves, *Bull. Seism. Soc. Am.*, 100(3), 1306-1319 (2010).
- [206] Liu T, Luan Y and Zhong W, Earthquake responses of clusters of building structures caused by a near-field thrust fault, *Soil Dyn. Earthqu. Engrg.*, 42, 56- 70 (2012).
- [207] Liu XN, Hu GK, Huang GL and Sun CT, An elastic metamaterial with simultaneously negative) mass density and bulk modulus, *App. Phys. Lett.*, 98, 251907 (2011).
- [208] Lombaert G and Clouteau D, Resonant multiple wave scattering in the seismic response of a city, *Waves Rand. Complex Med.*, 16(3) 205-230 (2006).
- [209] Lombaert G and Clouteau D, Elastodynamic wave scattering by finite-sized resonant scatterers at the surface of a horizontally layered halfspace, *J. Acoust. Soc. Am.*, 125, 2041-2052 (2009).
- [210] Lopez-Rios T, Mendoza D , Garcia-Vidal FJ, Sanchez-Dehesa JS and Pannetier B, Surface shape resonances in lamellar metallic gratings, *Phys. Rev. Lett.* 81, 665 (1998).
- [211] Lopez-Rios T and Wirgin A, Role of waveguide and surface plasmon resonances in surface-enhanced Raman scattering at coldly evaporated metallic films, *Solid State Commun.*, 52(2), 197-201 (1984).
- [212] Lovati S, Ground motion amplification induced by topographic irregularities: results, open issues and future developments, *Phd thesis, Univ. Genova* (2017).
- [213] Love AEH, *Some Problems of Geodynamics*, University Press, Cambridge (1911).
- [214] Luco JE and Wong HL, Response of structures to nonvertically incident seismic waves, *Bull. Seism. Soc. Am.*, 72(1), 275-302 (1982).



- [215] Luzon F and Sanchez-Sesma FJ, Seismic response of three-dimensional topographies, *Transactions on the Built Environment*, WIT Press, 14, 247-258 (1995).
- [216] Ma S, Archuleta RJ and Page MT, Effects of large-scale surface topography on ground motions, as demonstrated by a study of the San Gabriel Mountains, Los Angeles, California, *Bull. Seism. Soc. Am.*, 97, 2066-2079 (2007).
- [217] Mal AK and Knopoff L., Transmission of Rayleigh waves past a step change in elevation, *Bull. Seism. Soc. Am.*, 56, 455-466 (1966).
- [218] Mal AK and Yin CC, Elastic waves in locally inhomogeneous layered media, in *Ground Motion and Engineering Seismology*, Cakmak AS (Ed.), Elsevier, Amsterdam, 107-122 (1987).
- [219] Manga M and Brodsky E, Seismic triggering of eruptions in the far field: Volcanoes and geysers, *Ann. Rev. Earth Planet. Sci.*, 34, 263-291 (2006).
- [220] Maradudin AA, Interaction of surface polaritons and plasmons with surface roughness, in *Surface Polaritons: Electromagnetic Waves at Surfaces and Interfaces*, Agranovich VM, Mills DL (Eds.), North-Holland, Amsterdam (1982).
- [221] Maradudin AA, Surface acoustic waves on rough surfaces, in *Recent Developments in Surface Acoustic Waves*, Parker DF and Maugin GA (Eds.), Springer series on wave phenomena, Berlin, 100-128 (1988).
- [222] Maradudin AA, Ryan P and McGurn AR, Shear horizontal acoustic surface shape resonances, *Phys. Rev. B*, 38, 3068 (1988).
- [223] Maradudin AA and Visscher WM, Electrostatic and electromagnetic surface shape resonances, *Zeitsch. Phys. B, Cond. Mat.*, 60(2-4), 215-230 (1985).
- [224] Marsh HW, Sound reflection and scattering from the sea surface, *J. Acoust. Soc. Am.*, 35, 240-244 (1963).
- [225] Massa M, Barani S and Lovati S, Overview of topographic effects based on experimental observations: meaning, causes and possible interpretations, *Geophys. J. Int.* 197, 1537-1550 (2014).
- [226] Matasovic N and Kavazanjian Jr E, Seismic response of a composite landfill cover, *J. Geotech. Geoenviron. Engrg. ASCE*, 132(4), 448-455 (2006).
- [227] Maufroy E, Caractérisation et modélisation numérique de l'effet de site topographique 3D : application à la Grande Montagne de Rustrel, Vaucluse, Phd thesis, Univ. Nice Sophia-Antipolis (2010).
- [228] Maufroy E, Cruz-Atienza VM, and Gaffet S, Robust method for assessing 3-D topographic site effects: A case study at LSBB underground laboratory, France, *Earthquake Spectra* 28(3), 1097-1115 (2012).
- [229] Maufroy E, Cruz-Atienza VM, Cotton F and Gaffet S, Frequency-scaled curvature as a proxy for topographic site-effect amplification and ground-motion variability, *Bull. Seism. Soc. Am.*, 105(1), doi: 10.1785/0120140089 (2015).

- [230] Maystre D, Survey of surface plasmon polariton history, in Plasmonics, Enoch S and Bonod N (Eds.), Springer, Berlin (2012).
- [231] Mc Ivor IK, Two-dimensional scattering of a plane compressional wave by surface imperfections, *Bull. Seism. Soc. Am.*, 59(3), 1349-1364 (1969).
- [232] Melgar D, Perez-Campos X, Ramirez-Guzman L, Spica Z, Espíndola HV, Hammond WC and Cabral-Cano E, Bend faulting at the edge of a flat slab. The 2017 Mw7.1 Puebla Morelos, Mexico earthquake, *Geophys. Res. Lett.*, 45(6) (2018).
- [233] Meslem A, Yamazaki F, Maruyama Y, D'Ayala D, Naili M and Benouar D, Effect of topographic reliefs on building damage distribution in Boumerdes City during the 2003 Algeria earthquake, 15thWCEE, Lisboa (2012).
- [234] Meza-Fajardo K, Jean-François Semblat J-F, Chaillat S and Lenti L, Seismic wave amplification in 3D alluvial basins: 3D/1D amplification ratios from fast multipole BEM simulations, *Bull. Seism. Soc. Am.* (2016).
- [235] Moczo P, Bystricky E, Kristek J, Carcione JM and Bouchon M, Hybrid modeling of P-SV seismic motion at inhomogeneous viscoelastic topographic structures, *Bull. Seism. Soc. Am.*, 87(5), 1305-1323 (1997).
- [236] Moleron M, Felix SF, Pagneux V and Richoux O, Low frequency acoustic resonances in urban courtyards *J. Acoust. Soc. Am.*, 135(1), 74-82 (2014).
- [237] Moore JR, Gischig V, Burjanek J, Loew S and Fäh D, Site effects in unstable rock slopes: Dynamic behavior of the Randa instability (Switzerland), *Bull. Seism. Soc. Am.*, 101(6), 3110-3116 (2011).
- [238] Morgan MA, Mode expansion solution for scattering by a material filled rectangular groove, *Prog. In Electromagn. Res.*, 18, 1-17 (1998).
- [239] Morse PM and Feshbach H, *Methods of Theoretical Physics*, vol. 1, McGraw-Hill, New York (1953).
- [240] Moskovits M, Surface-enhanced spectroscopy, *Rev. Mod. Phys.*, 57, 783-826 (1985).
- [241] Mostaghel N and Nowroozi AA, Earthquake response of hills, *Bull. Seism. Soc. Am.*, (1975).
- [242] Mow CC and Pao Y-H , The diffraction of elastic waves and dynamic stress concentrations, Rept. R-482-PR, Rand Corp., Santa Monica (1971).
- [243] Mucciarelli M, Effect of buildings on free-field ground motion: Introduction, in *Increasing Seismic Safety by Combining Engineering Technologies and Seismological Data*, Mucciarelli M, Herak M and Cassidy J (Eds.), Springer, Dordrecht, 139-140 (2008).
- [244] Mucciarelli M, Ditommaso R, Gallipoli MR and Ponzio FC, Effect of building-building interaction on "free-field" ground motion, in *Increasing Seismic Safety by Combining Engineering Technologies and Seismological Data*, Mucciarelli M, Herak M, and Cassidy J (Eds.), Springer, Dordrecht, 141-146 (2008).



- [245] Mwafy A, Elnashai A, Sigbjornsson R and Salama A, Significance of severe distant and moderate close earthquakes on design and behavior of tall buildings, *Struct Design Tall Special Build.*, 15(4): 391-416 (2006).
- [246] Murphy J, Moser P, Nagl A and Uberall H, A surface wave interpretation for the resonances of a dielectric sphere *IEEE Trans. Antenn. Prop.*, 28(6), 924-927 (1980).
- [247] Nechtschein S, Bard PY, Gariel JC, Meneroud JP, Dervin P, Cushing M, Gaubert C, Vidal S and Duval AM, A topographic effect study in the Nice region, *Proc. 5th Intl. Conf. Seismic Zonation*, Ouest Eds., Nantes, II, 1067-1074 (1995).
- [248] Nakagawa S, M. Kuno M, Naito Y et al., Forced vibration tests and simulation analyses of a nuclear reactor building, *Nucl. Engrg. Design*, 179(2):145-156 (1998).
- [249] Newmark NM, Blume JA and Kapur KK, Seismic design spectra for nuclear power plants, *J. Power Div., Amer. Soc. Civil Eng.*, 99(PO2), 287-303 (1973).
- [250] Ogilvy JA, *Theory of Wave Scattering from Random Rough Surfaces*, CRC Press, Boca-Raton (1991).
- [251] Ordaz M and Singh SK, Source spectra and spectral attenuation of seismic waves from Mexican earthquakes, and evidence of amplification in the hill zone of Mexico City, *Bull. Seism. Soc. Am.*, 82(1), 24-43 (1992).
- [252] Padron LA, Aznarez JJ and Maeso O, Dynamic structure-soil-structure interaction between nearby piled buildings under seismic excitation by BEM-FEM model, *Soil Dyn. Earthqu. Engrg.*, 29(6), 1084-1096 (2009).
- [253] Palmer JM, The measurement of transmission, absorption, emission, and reflection, in *Handbook of Optics*, Bass M, Van Stryland EW, Williams DR and Wolfe WL (Eds.), McGraw Hill, New York, II, 25 (1995).
- [254] Panou AA, Theodulidis N, Stylianidis K and Pazachos CB, Ambient noise horizontal-to-vertical spectral ratio in site effects estimation and correlation with seismic damage distribution in urban environment: the case of the city of Thessaloniki (Northern Greece), *Soil Dyn. Earthqu. Engrg.*, 25, 261-274 (2005).
- [255] Paolucci R, Amplification of earthquake ground motion by steep topographic irregularities, *Earthqu. Engrg. Struct. Dynam.*, 31, 1831-1853 (2002).
- [256] Papadimitriou A, Topographic aggravation of the peak seismic acceleration near two dimensional hills and slopes, *5th ICEGE*, Santiago (2011).
- [257] Parise M and Jibson RW, A seismic landslide susceptibility rating of geologic units based on analysis of characteristics of landslides triggered by the 17 January, 1994 Northridge, California earthquake, *Engrg. Geology*, 58(3-4), 251-270 (2000).
- [258] Paul A and Campillo M, Diffraction and conversion of elastic waves at a corrugated interface, *Geophys.*, 53(11), 1415-1424 (1988).

- [259] Pedersen HA, Sanchez-Sesma F-J and Campillo M, Three-dimensional scattering by two-dimensional topographies, *Bull. Seism. Soc. Am.*, 84, 1169-1183 (1994).
- [260] Pedersen H, LeBrun B, Hatzfeld D, Campillo M and Bard P-Y, Ground-motion amplitude across ridges, *Bull. Seism. Soc. Am.*, 84(6), 1786-1800 (1994).
- [261] Pendry J, Manipulating the near field with metamaterials, *Optics & Photonics News*, 9, 33-37 (2004).
- [262] Petit R., Tutorial introduction, in *Electromagnetic Theory of Gratings*, Petit R. (Ed.), Springer, Berlin (1980).
- [263] Pike E and Sabatier P, *Scattering*, Academic Press, New York (2001).
- [264] Pischietta M., Cultrera G., Caserta A., Luzi L. and Rovelli A, Topographic effects on the hill of Nocera Umbra, central Italy, *Geophys. J. Int.*, 182(2), 977-987 (2010).
- [265] Pischietta M and Rovelli A, Ground motion amplification at sites with pronounced topography: the controversial role of local geology, 33th Convegno del Gruppo Nazionale di Geofisica della Terra Solida 33 GNGTS 2014, Bologna (2014).
- [266] Poggi V, Ermert L, Burjanek J, Michel C and Fäh D, Modal analysis of 2-D sedimentary basin from frequency domain decomposition of ambient vibration array recordings, *Geophys. J. Int.*, 200, 615-626 (2015).
- [267] Psycharis I, *Ancient Monuments Under Seismic Actions: Modeling and Analysis*. doi: 10.1007/978-3-642-35344-4\_145 (2015).
- [268] Qiu F and Liu D, Antiplane response of isocles triangular hill to incident SH waves, *Earthqu. Engng. and Engng. Vibr.*, 4(1), 37-46 (2005).
- [269] Rai M, *Topographic Effects in Strong Ground Motion*, Phd thesis, Virginia Polytechnic Institute., Blacksburg (2015)
- [270] Rai M, Rodriguez-Marek A and Yong A, Topographic effects in strong ground motion, 15th WCEE, Lisboa (2012).
- [271] Rai M and Rodriguez-Marek A, Parametrization of topography for ground motion prediction-summary and findings, SMIP15 Seminar Proceeds. (2015).
- [272] Rao SM, Wilton DR and Glisson AW, Electromagnetic scattering by surfaces of arbitrary shape, *IEEE Trans. Anten. Prop.*, 30(3), 409 - 418 (1982).
- [273] Rault C, Effets de site, endommagement et érosion des pentes dans les zones épicentrales des chaînes de montagnes actives, Phd thesis, ENS, Paris (2019).
- [274] Rayleigh L, On waves propagated along plane surface of an elastic solid, *Proc. London Math. Soc.*, 17, 4-11 (1885).
- [275] Rayleigh L, On the free vibrations of an infinite plate of homogeneous isotropic elastic matter, *Proc. London Math. Soc.* 20, 225-234 (1889).

- [276] Rayleigh L, On the dynamical theory of gratings, *Proc. Roy. Soc. A*, 79 (532), 399-416 (1907).
- [277] Rayleigh L., *The Theory of Sound*, vol. II, sect. 272a, Dover, New York (1945).
- [278] Razmkhah A, Kamalian M and Sadroldini SMA, Application of boundary element method to study the seismic response of triangular hills, 14th WCEE, Beijing (2008).
- [279] Rial JA, A Note on the relationship between a sedimentary basin's basement topography and the damage pattern of earthquakes: Chaos and order, *Seism. Res. Lett.*, 68(3), 451-459 (1997).
- [280] Rice SO, Reflection of electromagnetic waves from slightly rough surfaces, in *The Theory of Electromagnetic Waves*, Kline M (Ed.), Dover, New York, 351-378 (1951).
- [281] Riga E, Makra K and Pitilakis K, Aggravation factors for seismic response of sedimentary basins: A code-oriented parametric study, <http://dx.doi.org/10.1016/j.soildyn.2016.09.048> (2016).
- [282] Ripperger J, Igel H and Wassermann J, Seismic wave simulation in the presence of real volcano topography, *J. Volcanol. Geotherm. Res.*, 128(1-3), 31-44 (2003).
- [283] Robertsson JOA, A numerical free-surface condition for elastic/viscoelastic finite-difference modeling in the presence of topography, *Geophys.*, 61(6), 1921-1934 (1996).
- [284] Roesset JM, Soil structure interaction. The early stages., *J. Appl. Sci. Engrg.*, 16(1): 1-8 (2013).
- [285] Rogers AM, Katz LJ, and Benett TJ, Topographic effect on ground motion for incident P waves: a model study, *Bull. Seism. Soc. Am.*, 64, 437-456 (1974).
- [286] Roussillon P, Interaction sol-structure et interaction site-ville: aspects fondamentaux et modélisation, Phd thesis, INSA, Lyon (2006).
- [287] Ruiz-Garcia J, Mainshock-aftershock ground motion features and their influence in building's seismic response, *J. Earthqu. Engrg.*, 16(5), 719-737 (2012).
- [288] Safak E, New approach to analyzing soil-structure systems. *Soil. Dynam. Earthqu. Engrg.* 17, 509-517 (1998).
- [289] Safak E and Harmsen S, Seismic hazard and design by using energy flux, 12th WCEE, paper 0658 (2000).
- [290] Sahar D and Narayan JP, Quantification of modification of ground motion due to urbanization in a 3D basin using viscoelastic finite-difference modelling, *Natural Hazards*, 75: 1167-1186 (2015).
- [291] Saikia CK, Dreger S and Helmberger DV, Modeling of energy amplification recorded within greater Los Angeles using irregular structure, *Bull. Seism. Soc. Am.*, 84(1), 47-61 (1994).
- [292] Sanchez-Sesma FJ and Campillo M, Diffraction of P, SV and Rayleigh waves by topographic features: a boundary integral formulation, *Bull. Seism. Soc. Am.*, 81(6), 2234-2253 (1991).

- [293] Sanchez-Sesma FJ, Campillo M and Irikura K, A note on the Rayleigh hypothesis and the Aki-Larner method, *Bull. Seism. Soc. Am.*, 79(6), 1995-1999 (1989).
- [294] Sandu T and Boldeiu G, Extinction spectra and near-field enhancement of metallic nanoparticles, *Proc. Intl. Semiconductor Conf. CAS*, doi:10.1109/SMICND.2012.6400736, 441-444 (2012).
- [295] Sarychev AK, Ivanov A, Lagarkov A and Barbillon G, Light concentration by metal-dielectric micro-resonators for SERS sensing, *Materials*, 12, 103-143 (2019).
- [296] Sawi TM and Manga M, Revisiting short-term earthquake triggered volcanism, *Bull. Volcanology*, 80(57) (2018).
- [297] Schwan L, Boutin C, Dietz M, Padron L, Bard PY, Ibraim E, Maeso O, Aznarez JJ and Taylor C, Multi-building interactions and site-city effect-An idealized experimental model, in *Experimental Research in Earthquake Engineering, E.-U. Series Concluding Workshop*, Taucer F and Apostolska R (Eds.). Springer, Heidelberg, 28, 459-476 (2015).
- [298] Schwan L, Boutin C, Padron L, Dietz M, Bard P-Y and Taylor C, Site-city interaction: Theoretical, numerical and experimental crossed-analysis, *Geophys. J. Intl.*, 205(2), 1006-1031 (2016).
- [299] Semblat JF, Modeling seismic wave propagation and amplification in 1D/2D/3D linear and nonlinear unbounded media, *Int. J. Geomech. (ASCE)*, doi:10.1061/(ASCE)GM.1943-5622.0000023 (2011).
- [300] Semblat JF, Duval A-M and Dangla P, Numerical analysis of seismic wave amplification in Nice (France) and comparisons with experiments, *Soil Dyn. Earthqu. Engrg.*, 19(5), 347-362 (2000).
- [301] Semblat JF, Kham M and Bard P-Y, Seismic-wave propagation in alluvial basins and influence of site-city interaction, *Bull. Seism. Soc. Am.*, 98, 2665-2678 (2008).
- [302] Semblat J-F, Kham M, Guéguen P, Bard P-Y and Duval AM, Site-city interaction through modifications of site effects, *arXiv:0908.2718v1* (2009).
- [303] Semblat JF, Kham M, Parara E, Bard P-Y, Pitilakis K, Makra K and Raptakis D, Site effects: basin geometry versus soil layering, *Soil Dyn. Earthqu. Engrg.*, 25(7-10), 529-538 (2005).
- [304] Sepulveda SA, Murphy W, Jibson RW and Petley DN, Seismically induced rock slope failures resulting from topographic amplification of strong ground motions: The case of Pacoima Canyon, Calif., *Engrg. Geology*, 80, 336-348 (2005).
- [305] Shafique M, Anggraeni D, Bakker W and Van der Meijde M, Modeling the impact of topography on seismic amplification at regional scale, *Geophys. Res. Abstr.*, 12, EGU2010-8452-1 2010, EGU General Assembly (2010).
- [306] Sills LB, Scattering of horizontally-polarized shear waves by surface irregularities, *Geophys. J. Int.*, 54(2), 319-348 (1978).

- [307] Sincraian MV and Oliveira CS, A 2-D sensitivity study of the dynamic behavior of a volcanic hill in the Azores Islands: Comparison with 1-D and 3-D models, *Pure Appl. Geophys.*, 158, 2431-2450 (2001).
- [308] Smith, WD, The application of finite element analysis to body wave propagation problems, *Geophys. J. R. Astr. Soc.*, 42, 747-768 (1975).
- [309] Spudich P, Hellweg M and Lee WHK, Directional topographic site response at Tarzana observed in aftershocks of the 1994 Northridge, California, earthquake: implications for main-shock motions, *Bull. Seism. Soc. Am.*, 86(1B), S193-S208 (1996).
- [310] Stoneley R, Dispersion of waves in a double superficial layer, *Monthly Notices Roy. Astron. Soc. Geophys. Suppl.*, 1, 527-531 (1928).
- [311] Stoneley R and Tillotson E, The effect of a double surface layer on Love waves, *Monthly Notices Roy. Astron. Soc. Geophys. Suppl.*, 1, 521-527 (1928).
- [312] Taborda R, Three dimensional nonlinear soil and site-city effects in urban regions, Phd thesis, Carnegie Mellon Univ., Pittsburgh (2010).
- [313] Taborda R and Bielak J, Large-scale earthquake simulation: computational seismology and complex engineering systems, *Computing Sci. Engrg.*, 7-8, 14-26 (2011).
- [314] Taborda R and Bielak J, Full 3D integration of site-city effects in regional scale earthquake simulations, in *Proc. 8th International Conference on Structural Dynamics, EURODDYN 2011*, De Roeck G, Degrande G, Lombaert G and Müller G (Eds.), Leuven (2011).
- [315] Tertulliani A, Leschiutta I, Bordoni P and Milana G, Damage Distribution in L'Aquila City (Central Italy) during the 6 April 2009 Earthquake, *Bull. Seism. Soc. Am.*, 102(4),
- [316] Thomas R, Kumar J, Swathi S and Thomas KG, Optical effects near metal nanostructures: towards surface-enhanced spectroscopy, *Current Sci.*, 102(1), 85-96 (2012).
- [317] Todorovska MI, Ivanovic SS and Trifunac MD, Wave propagation in a seven-story reinforced concrete building I. Theoretical models, *Soil Dyn. Earthqu. Engrg.*, 21, 211-223 (2001).
- [318] Todorovska MI and Trifunac M, The system damping, the system frequency and the system response peak amplitudes during in-plane building-soil interaction, *Earthqu. Engrg. Struct. Dynam.*, 21(2), 127-144 (1992).
- [319] Toshinawa T and Ohmachi T, Love-wave propagation in a three-dimensional sedimentary basin, *Bull. Seism. Soc. Am.*, 82(4), 1661-1677 (1992).
- [320] Trifunac MD, Interaction of a shear wall with the soil for incident plane SH waves, *Bull. Seism. Soc. Am.*, 62(1), 63-83 (1972).
- [321] Trifunac, MD and Brady AG, A study of the duration of strong earthquake ground motion, *Bull. Seism. Soc. Am.*, 65, 581-626 (1975).
- [322] Tripe, R, Kontoe, S and Wong TKC, Slope topography effects on ground motion in the presence of deep soil layers, *Soil Dyn. Earthqu. Engrg.*, 50, 72-84 (2013).

- [323] Tromp J and Dahlen FA, Variational principles for surface wave propagation on a laterally heterogeneous Earth-111. Potential representation, *Geophys. J. Int.*, 112, 195-209 (1993).
- [324] Tsaur D-H and Chang K-H, Electromagnetic plane-wave scattering from a sectorial groove in a perfectly conducting plane, *Cent. Eur. J. Phys.*, 7(1), 160-167 (2009).
- [325] Tsaur D-H and Chang K-H, Scattering and focusing of SH waves by a convex circular-arc topography, *Geophys. J. Int.*, 177, 222-234 (2009).
- [326] Tsaur D-H, Chang K-H and Hsu M-S, An analytical approach for the scattering of SH waves by a symmetrical V-shaped canyon: deep case, *Geophys. J. Int.*, 183, 1501-1511 (2010).
- [327] Tsogka C, Modélisation mathématique et numérique de la propagation des ondes élastiques tridimensionnelles dans des milieux fissurés, Phd thesis, Univ. Paris IX Dauphine, tel-01529535 (1999).
- [328] Tucker BE, King JL, Hatzfeld D and Nersesov IL, Observations of hard-rock site effects, *Bull. Seism. Soc. Am.*, 74(1), 1,121-136, (1984).
- [329] Tyagunov S, Vorogushyn S, Muñoz-Jimenez TC, Parolai S and Fleming K, Multi-hazard fragility analysis for fluvial dikes in earthquake- and flood-prone areas, *Nat. Hazards Earth Syst. Sci.*, 18, 2345-2354 (2018).
- [330] Uenishi K, The town effect: dynamic interaction between a group of structures and waves in the ground, *Rock Mech. Rock Engrg.*, 43, 811-819 (2010).
- [331] Uberall H (Ed.), *Acoustic Resonance Scattering*, Gordon and Breach, Philadelphia (1992).
- [332] Uberall H, Duclos J, El Hocine Khelil M, Maze G, Ripoche J et al., Scattering pole resonances: Relation to external and internal surface waves, *J. Acoust. Soc. Am.*, 99, 2594 (1996).
- [333] Ulysse S, Boisson D, Prépetit C and Havenith H-B, Site effect assessment of the Gros-Morne Hill area in Port-au-Prince, Haiti, Part B: Mapping and modelling results, *Geosciences*, 8, 233 (2018).
- [334] Vai R, Castillo-Covarrubias JM, Sanchez-Sesma FJ, Komatitsch D and Vilotte J-P, Elastic wave propagation in an irregularly layered medium, *Soil Dyn. Earthqu. Engrg.*, 18, 11-18 (1999).
- [335] Valdi MHT, Atrechian MR, Shalkoohy AJ and Balasbaneh AT, Numerical study of seismic response of trapezoidal alluvial valleys against vertically propagating incident waves, *J. Engrg. Res.*, 7(4), 37-57 (2019).
- [336] Varone C, Lenti L, Martino S and Semblat JF, Site-city interaction in a recent urbanized area: preliminary results for the case study of Rome (Italy), 5th IASPEI / IAEE International Symposium: Effects of Surface Geology on Seismic Motion (2016).
- [337] Veksler ND, *Resonance Acoustic Spectroscopy*, Springer, Berlin (1993)



- [338] Verhaeghe M-F and Wirgin A, Propagation of acoustic or electromagnetic waves in an inhomogeneous sea-type medium with rough frontiers, in AGARD Conf. Proceed. on Electromagnetics of the Sea, 77, Halley P. (Ed.), Neuilly/Seine (1970).
- [339] Viktorov IA, Rayleigh and Lamb Waves: Physical Theory and Applications, Plenum, New York (1967).
- [340] Virieux J, Etienne V, Cruz-Atienza V, Brossier R, Chaljub E, et al., Modelling seismic wave propagation for geophysical imaging. Seismic Waves - Research and Analysis, Masaki Kanao M (Ed.), 253-304 (2012).
- [341] Volk O, Shani-Kadmiel S, Gvirtzman Z and Tsesarsky M, 3D Effects of sedimentary wedges and subsurface canyons: ground-motion amplification in the israeli coastal plain, Bull. Seism. Soc. Am., 107(3), (2017).
- [342] Volkov D and Zheltukhin S, Preferred frequencies for coupling of seismic waves and vibrating tall buildings, arXiv:1403.3290v2 [math.AP] (2014).
- [343] Wang G, Du C, Huang D, Jin F, Koo RCH and Kwan JSH, Parametric models for 3D topographic amplification of ground motions considering subsurface soils, Soil Dyn. Earthqu. Engrg., 115, 41-54 (2018).
- [344] Wang L, Luo Y and Xu Y, Numerical investigation of Rayleigh-wave propagation on topography surface, J. Appl. Geophys., 86, 88-97 (2012).
- [345] Wei A, Kim B, Sadtler B and Tripp SL, Tunable surface-enhanced Raman scattering from large gold nanoparticle arrays, Chem. Phys. Chem., 2(12), 743-745 (2001).
- [346] Wirgin A, Considérations théoriques sur la diffraction par réflexion sur des surfaces quasiment planes, applications à la diffraction par des réseaux, C. R. Acad. Sc. Paris, 259, 1486-1488 (1964).
- [347] Wirgin A, Diffraction d'une onde plane par un réseau sinusoidal, C. R. Acad. Sci. Paris, 261, 2061-2064 (1965).
- [348] Wirgin A, On the theory of scattering from rough lamellar surfaces, Alta Freq., 38, 327-331 (1969).
- [349] Wirgin A, Resonance scattering of electromagnetic waves from a rectangular groove on a metallic mirror, Opt. Commun., 7(1), 70-75 (1973).
- [350] Wirgin A, Application de la méthode des ondes planes à l'étude des problèmes direct et inverse de diffraction d'ondes sur des surfaces molles comportant un relief non périodique, C. R. Acad. Sc. Paris II, 294, 17-19 (1982).
- [351] Wirgin A, Love waves in a slab with rough boundaries, in Recent Developments in Surface Acoustic Waves, Parker DF and Maugin GA (Eds.), Springer series on wave phenomena, Berlin, 145-155 (1988).
- [352] Wirgin A, Amplification résonante du tremblement d'une chaîne de montagnes cylindriques soumise à une onde SH, C. R. Acad. Sci. II, 309, 311-313 (1989).

- [353] Wirgin A, Amplification résonante du mouvement du sol sur une montagne cylindrique isolée soumise à une onde sismique SH, C. R. Acad. Sci. II, 311, 651-655 (1990).
- [354] Wirgin A, Resonant response of a soft semi-circular cylindrical basin to an SH seismic wave, Bull. Seism. Soc. Am., 85(1), 285-299 (1995).
- [355] Wirgin A, Acoustical imaging : classical and emerging methods for applications in macro-physics, in Scattering, Pike R and Sabatier P (Eds.), Academic, San Diego, 95-120 (2002).
- [356] Wirgin A, Layer model description of the SH seismic response in anisotropically-idealized cities, <https://doi.org/10.1080/17455030.2018.1517950> (2018).
- [357] Wirgin A, Incorporation of macroscopic heterogeneity within a porous layer to enhance its acoustic absorptance, arXiv:1810.02101v1, physics.app-ph (2018).
- [358] Wirgin A, A conservation law for testing methods of prediction of the seismic wave response of a protuberance emerging from flat ground, arXiv:2001.07687v1 (2020).
- [359] Wirgin A, A conservation law for a sedimentary basin submitted to a seismic wave, arXiv:1911.1425v1 (2019).
- [360] Wirgin A and Bard P-Y, Effects of buildings on the duration and amplitude of ground motion in Mexico City, Bull. Seism. Soc. Am., 86, 914-920 (1996).
- [361] Wirgin A and Groby J-P, Amplification and increased duration of earthquake motion on uneven stress-free ground, <https://hal.ccsd.cnrs.fr/ccsd-00076746>, <http://fr.arxiv.org/abs/physics/0605239> (2006).
- [362] Wirgin A and Groby J-P, Amplification and increased duration of earthquake motion on uneven stress-free ground, in ESG 2006, Bard P-Y, Chaljub E, Cornu C, Cotton F and Guéguen P. (Eds.), LCPC, Paris, 559-568 (2006).
- [363] Wirgin A and Kouoh-Bille L, Ground amplification in the neighborhood of a group of mutually parallel triangular ridge mountains subjected to shear horizontal seismic waves, J.Phys. IV, Colloque C1, suppl. J. Phys. 111, C1729-C1732 (1992).
- [364] Wirgin A and Kouoh-Bille L, Amplification du mouvement du sol au voisinage d'un groupe de montagnes de profil rectangulaire ou triangulaire soumis à une onde sismique SH, in Génie Parasismique et Aspects Vibratoires dans le Génie Civil, 3ème Colloque National AFPS, Saint-Rémy-les Chevreuse (1993).
- [365] Wirgin A and Lopez-Rios T, Can surface-enhanced Raman scattering be caused by waveguide resonances?, Opt. Commun., 48(6), 416-420 (1984).
- [366] Wirgin A and Maradudin AA, Resonant enhancement of the electric field in the grooves of bare metallic gratings exposed to s-polarized light, Phys. Rev. B, 31, 5573-5576 (1985).
- [367] Wirgin A and Maradudin AA, Resonant response of a bare metallic grating to s- polarized light, Prog. Surf. Sci., 22, 1-99 (1986).



- [368] Witarto W, Wang SJ, Yang CY, Nie X, Mo YL, Chang KC, Tang Y and Kassawara R, Seismic isolation of small modular reactors using metamaterials, *AIP Advances*, 8, 045307 (2018).
- [369] Wojcik GL, Resonance zones on the surface of a dipping layer due to plane SH seismic input, NSF (ASRA Directorate) Grant No. PFR 78-15049 (1979).
- [370] Wolf JP and Song C, To radiate or not to radiate, *Earthqu. Engrg. Struct. Dynam.*, 25(12), 1421-1432 (1996).
- [371] Wong HL, Effect of surface topography on the diffraction of P, SV, and Rayleigh waves, *Bull. Seism. Soc. Am.*, 72(4) 1167-1183 (1982).
- [372] Wong HL and Trifunac MD, Surface motion of a semi-elliptical alluvial valley for incident plane SH waves, *Bull. Seism. Soc. Am.* 64, 1389-1408 (1974).
- [373] Wong HL and Trifunac MD, Two-dimensional, antiplane, building-soil-building interaction for two or more buildings and for incident plane SH waves, *Bull. Seism. Soc. Am.*, 65(6), 1863-1885 (1975).
- [374] Wong HL, Trifunac MD and Westermo BD, Effects of surface or subsurface irregularities in the amplitude of monochromatic waves, *Bull. Seism. Soc. Am.*, 67, 353-368 (1977).
- [375] Yang Z, Song Y, , Li X, Jiang G and Yang Y, Scattering of plane SH waves by an isosceles trapezoidal hill, *Wave Motion* 92, 102415 (2020).
- [376] Yang Z, Xu H, Hei B and Zhang J, Antiplane response of two scalene triangular hills and a semi-cylindrical canyon by incident SH-waves, *Earthqu. Engrg. Engrg. Vibr.*, Volume 13(4), 569-581 (2014).
- [377] Yoshimura S, Kobayashi K, Akiba H, Suzuki S and Ogino M, Seismic response analysis of full-scale boiling water reactor using three-dimensional finite element method, *J. Nucl. Sci. Technol.*, 52(4), 546-567
- [378] Yuan X and Men FL, Scattering of plane SH waves by a semi-cylindrical hill, *Earthqu. Eng. Struct. Dyn.*, 21, 1091-1098 (1992).
- [379] Zania V, Tsompanakis Y and Psarropoulos PN, Efficient numerical simulation of waste landfills' seismic response, in *Numerical Methods in Geotechnical Engineering*, Schweiger HF (Ed.), Taylor & Francis, London, 223-230 (2006).
- [380] Zahradnik J, Moczo P and Hron F, Testing four elastic finite-difference schemes for behavior at discontinuities, *Bull. Seism. Soc. Am.*, 83(1), 107-129 (1993).
- [381] Zeng Y, Xu Y, Deng K, Zeng Z, Yang H, Muzamil M and Du Q, Low-frequency broadband seismic metamaterial using I-shaped pillars in a half-space, *J. Appl. Phys.*, 123, 214901 (2018).
- [382] Zhang RR, Snieder R, Gargaba L and Seibi A, Modeling of seismic wave motion in high-rise buildings. *Probab. Engineer. Mech.*, 26, 520-527 (2011).
- [383] Zhou H and Chen X, A new approach to simulate scattering of SH waves by an irregular topography, *Geophys. J. Int.*, 164, 449-459 (2006).

- [384] Zhu C, Improving one-dimensional ground response analysis by incorporating basin effects, Phd thesis, Queenslant University of Technology (2018).
- [385] Zhu C, Riga E, Pitilakis K, Zhang J and David Thambiratnam D, (2018): Seismic Aggravation in Shallow Basins in Addition to One-dimensional Site Amplification, J. Earthqu. Engrg., DOI: 10.1080/13632469.2018.1472679 (2018).
- [386] Zhu C and Thambiratnam D, Interaction of geometry and mechanical property of trapezoidal sedimentary basins with incident SH waves, Bull Earthq Eng DOI 10.1007/s10518-016-9938-z (2016).
- [387] Zhu C, Thambiratnam D and Gallage C, Inherent characteristics of 2D alluvial formations subjected to in-plane motion, J. Earthqu. Engrg. (in press).
- [388] Zhu C, Thambiratnam D and Zhang J, Response of sedimentary basin to obliquely incident SH waves. Bull. Earthqu. Engrg., DOI 10.1007/s10518-015-9856-5 (2015).
- [389] Zhu K, Nuclear reactor seismic analysis considering soil-structure interaction, MSc thesis, KTH, Stockholm (2018).
- [390] Zhu K, Shi YL, Lu M and Xie F, Dynamic mechanisms of earthquake-triggered landslides, Science China, 56(10), 1769-1779 (2013).
- [391] Zhu H-R, Zhu R-C and Miao G-P, A time domain investigation on the hydrodynamic resonance phenomena of 3-D multiple floating structures, J. Hydrodynam., 20(5), 611-616 (2008).